Cognitive Sustainability

The journal is indexed by:

[Library of Hungarian Scientific Works](#)

[Repository of the Library of Hungarian Academy of Science](#)

[Google Scholar](#)

[Sherpa Romeo](#)

[RePEc (Research Papers in Economics)](#)

[Directory of Open Access Journals](#)

[Crossref](#)

[Semantic Scholar](#)

[ERIH PLUS](#)

[Index Copernicus International](#)

[Dimensions](#)

[Scilit](#)

[Lens](#)

Comprehensive overview of sustainable food packaging material alternatives

Vuk Aliz,
https://orcid.org/0000-0001-7099-0765
University of Debrecen, Doctoral School of Management and Business, University of Debrecen, Faculty of Economics and Business
Debrecen, Hungary
vuk.aliz@econ.unideb.hu,

Bauerné Gáthy Andrea
https://orcid.org/0000-0002-9515-3290
University of Debrecen, Doctoral School of Management and Business, University of Debrecen, Faculty of Economics and Business
Debrecen, Hungary
bauerne.gathy.andrea@econ.unideb.hu

Abstract

The proliferation of plastic packaging materials and their accumulation as significant amounts of waste raises serious ecological concerns affecting humanity and the natural environment. New alternative packaging materials, including biodegradable and sustainable options, are being explored to address these concerns. This paper aims to provide a comprehensive overview of the literature on alternative packaging materials. This study covers biodegradable plastics, sustainable alternatives (Cellulose, Bamboo) and emerging packaging forms (edible packaging, nano-cellulose). SWOT analysis and cross-tabulation have been used to facilitate a comparative assessment of alternatives with plastic. The results show that recycling plastics or the production of bioplastics has not proven to be an effective solution. The environmental impact of sustainable and biodegradable packaging remains unclear. In addition, new materials (edible packaging materials, nano-cellulose fibres) are currently being tested that could reduce environmental impacts and waste. No alternative can fully replace plastic packaging, but new initiatives are promising.

1. Introduction

The most common packaging material today is plastic, which has become an indispensable part of our daily lives. Plastics are used in almost every sector and industry, yet the packaging industry accounts for the largest percentage of all plastics used (Shafqat et al., 2020). As most of this packaging is single-use plastic, it often ends up in landfills in large quantities. Single-use plastic packaging accounts for almost half of the world's plastic waste, and the packaging industry generates around 30% of municipal solid waste (Kumar et al., 2016). The resistance of such wastes to biodegradation has created critical ecological crises. We cannot forget that plastic packaging can play a crucial role, and there is general agreement that many types of food need some form of packaging to protect them from environmental harm, extend shelf life and reduce food waste (Firoozi Nejad et al., 2021).

Packaging has been one of the economy's fastest-growing sectors for over a decade (Majeed et al., 2013). The most common factors that drive companies to develop new packaging are:

- the desire to refresh the product at the maturity stage of its market life cycle;
- growing environmental awareness and related external pressure to change packaging.

On the other hand, changes in product positioning, such as:

- improving packaging when the product is targeted at a different market segment;
- measures taken to respond to competition or to discriminate against competitors;
- strategic changes to the way the product is displayed on store shelves;
- scaling up production to enter new markets;
- to achieve greater consistency of the product with other products in the company;
- introducing quality changes in the product;
- introducing technical (technological) improvements to the packaging of the product (Wyrwa and Barska, 2017).

At the end of the 20th century, the concept of environmental packaging design was born. This is a way of thinking where packaging is seen as a necessary element between the product and the environment, helping to prevent their interaction. So, it protects the product from environmental stresses and, at the same time, protects the environment from the harmful effects of the product. However, this positive effect only exists when the product is in the packaging—the production of packaging material and the fact that it becomes waste after use is already environmentally damaging. Environmental packaging design aims to ensure that the packaging material performs its function with the least possible environmental impact throughout its life cycle (Tiefbrunner, 2002). The environmental regulation of packaging sets out as a general requirement for reducing environmental impacts ('reduce, reuse, recycle'). Recyclable packaging includes glass (all colours), paper, aluminium foil, takeaway containers, aluminium cans, tin and steel cans, PET, and HDPE (Marshall, 2007).

This study aims to explore the current trends in plastic packaging alternatives. The systematic literature review (the result in the appendix, Table 3) highlighted alternatives already known as food packaging materials and new options that may emerge. In the following, the alternatives presented in the literature and the new options are described in detail. In the conclusion, a SWOT analysis will be used to compare the alternatives with plastic to facilitate comparison. A cross-tabulation analysis will show how these materials have been investigated so far.

2. Alternative plastic packaging

Polyethylene terephthalate (PET) is one of the most commonly used plastics, and it is widely used as a raw material in manufacturing products such as blown bottles for soft drinks and containers for food and other consumer goods. PET bottles have replaced glass bottles as containers for storing beverages due to their light weight and ease of handling and storage. In 2007, PET beverages' annual global consumption was around 10 million tons, representing approximately 250 million bottles. This number is increasing by around 15% per year, while the percentage of recycled or taken-back bottles is very low (Frigione, 2010). Two decades ago, most (around 70%) of the packaging waste generated in the European Union (EU) was landfilled. By 2019, this has changed completely, with nearly two-thirds of packaging waste recycled. In 1998, the share of recovered material in recovered plastic packaging waste was 11% on average. Twenty years later, recycled plastic packaging material has almost quadrupled (43%) (OECD, 2022). Despite the significant progress, the road to a near-zero carbon economy is still long and winding. In recent years, the environmental impact of packaging waste, particularly plastic packaging (white pollution), has been a major concern for legislators, the media and the public (Barletta et al., 2019). Increased environmental concerns about using certain synthetic packaging and coatings and consumer demands for better quality and longer shelf-life have increased interest in research into alternative packaging materials.

2.1. Biodegradable PET and Reusable PET

Recycling waste PET polymer and producing biodegradable PET-based blends effectively reduces resource use while protecting the environment (Torres-Huerta et al., 2014). One solution to reduce packaging waste in the environment is to make the packaging biodegradable. Some plastics are biodegradable under certain conditions. Compostable plastics decompose in industrial compost, where temperature, humidity and other environmental factors promote decomposition. However, many compostable plastics do not biodegrade in nature, the marine environment, or backyard compost bins. Under the right conditions, even products made from these plastics will degrade when mixed with organic materials in an industrial

composting facility. Some substances, such as polyhydroxyalkanoate (PHA), degrade in the sea. However, their material properties, including strength, barrier (water vapour, oxygen), and temperature resistance, are unsuitable to replace conventional plastics in consumer goods packaging when protection, shelf life and food safety are considered (Clark, 2018). In their work, Vea et al. (2021) investigated the whole life cycle of PHA and reported that the biodegradation kinetics of PHA-based plastics in the environment are very uncertain. They highlight that it is not known how surface treatment may affect biodegradation kinetics under landfill conditions. The biodegradable polymer chitosan is a biopolymer that can form semi-permeable films. In recent years, efforts have been made to develop and use chitosan films in food packaging (Torres-Huerta et al., 2014). In their research, Taufik et al. (2020) investigated whether the environmental benefits consumers perceive through recyclable and compostable bio-based plastic packaging align with how these packages are disposed of. It has been found that only compostable bio-based packaging is perceived by consumers as offering more environmental benefits than fossil-based plastic packaging, but is still being mishandled. Overall, their results suggest that compostability can be a distinguishing feature and that bio-based plastic packaging materials can be differentiated from their fossil-based counterparts (Taufik et al., 2020).

Bio-based and fossil-based refer to the manufacturing process of food packaging. Recyclability, biodegradability, and compostability refer to end-of-life options. Biodegradable plastics are completely biodegradable packaging (i.e., by living microorganisms) within 180 days. Compostable packaging is a subset of biodegradable plastics that decompose into water, biomass and gases in less than three months under composting conditions (ideally industrial conditions). Thus, a compostable product is always biodegradable, while a biodegradable product is not necessarily compostable. Many biodegradable plastics require industrial composting facilities, and if compostable/biodegradable packaging is improperly disposed of (e.g. landfill), it can lead to significant greenhouse gas emissions (Koeing-Lewis et al., 2022).

2.2. Bioplastic

Most bioplastics are first-generation materials from carbohydrate-rich crops (maise, sugar cane, Ricinus, potatoes, wheat) that could be modified for food or animal feed. Second-generation bioplastics are produced from feedstocks that are not suitable for food or feed, i.e. non-food crops ('wood cellulose', short rotation crops: poplar, willow, miscanthus) and waste materials from the processing of first biomass (food waste, wood sawdust) (Brizga et al., 2020). By definition, a bioplastic is a plastic that is bio-based and/or biodegradable. It is distinguished from biodegradable plastics, which are completely degradable through biological activity (i.e. the action of microorganisms such as bacteria, archaea, fungi and algae). Under aerobic conditions, the final products are biomass, CO_2 and water; under anaerobic conditions, the final products are biomass, CO_2, methane and water. Bio-based plastics are derived whole or in part from biomass. We can talk about oxo-degradable plastics, i.e. plastics that contain additives that accelerate their degradation under heat or UV radiation, typically in the presence of oxygen. The potential for biodegradation of such plastics to CO_2 and water is uncertain and subject to considerable debate, and residual microplastics will likely remain in the environment for longer periods. There is also degradable plastic, which is often synonymous with oxo-degradable plastic, but the term does not have a specific meaning, and there is no guiding standard. It refers to the fact that the plastic is degradable but does not give any information about the end products or how it degrades (Dilkes-Hoffman et al., 2019). Bioplastic has three subcategories and can be (1) "fossil-based and biodegradable", (2) "bio-based and biodegradable", or (3) "bio-based and non-biodegradable". The latter two categories can also be combined with the term bio-based plastics (Vea et al., 2021). The biodegradable properties of some bioplastics offer an opportunity to address this social and environmental challenge. They provide a solution for packaging uses by diverting plastics from landfills without accumulating in the environment, especially in the sea. However, such biodegradable and bio-based alternatives do not necessarily improve the overall environmental impact, especially when considering functional aspects of packaging such as end-of-life management, handling for transport and retail, and waste reduction, including increasing shelf-life (Kakadellis and Harris, 2020). According to Chen et al. (2016), biofuels and bioplastics are often seen as sustainable solutions to environmental problems such as climate change, fossil fuel depletion and acidification. However, both are criticised for being economically costly, competing with other socially useful goods such as food, and offering limited environmental benefits compared to their fossil counterparts. Their research shows PET bottles made from wood and biomass have 21% less global climate change potential and require 22% less fossil fuel than their fossil-based counterparts. In contrast, they perform worse in other categories, such as ecotoxicity and ozone depletion.

Depending on the biomass feedstock, extraction and preprocessing are likely to be more emissions-intensive than the corresponding fossil refinery processes, as preprocessing involves significant emissions from the use of fertilisers and the significant chemical and energy inputs required to break down the retreating biomass (Chen et al., 2016).

The third generation refers to microorganisms' direct production of plastic (or monomers). However, these bioplastics are still in the development stage. Bioplastics are not only an economic challenge. The production of these polymers also poses a significant threat to the environment, especially if their production volume is increased. Biomaterials can replace petroleum-based materials directly through the substitution of petroleum-derived chemical feedstocks with feedstocks from biorefineries and indirectly through the increased use of bio-based materials to replace petroleum-based materials, such as natural fibres for packaging and insulation materials as substitutes for synthetic foams, which have been widely used so far. Regarding material properties for packaging, almost complete replacement of petrochemical plastics by bioplastics (not all biodegradable) is technically feasible. To reduce the environmental impact of bioplastics, technological improvements need, such as

- improving yields and reducing the use of agrochemicals in the production of raw materials,
- a shift to second and third-generation feedstocks,
- improving energy efficiency and the use of renewable energy in biorefineries,
- the higher conversion efficiency of biorefineries and
- further improving end-of-life management (Brizga et al., 2020).

Vural Gursel et al. (2021) present a life-cycle assessment of bio-based polyethene terephthalate (PET) bottles from cradle to grave and compare them with petrochemical PET bottles in 13 environmental impact categories. In addition to bio-based PET bottles made from Brazilian sugar cane, two alternative hypothetical bio-based product systems were considered: a European crop market mix of wheat straw and maise and a European crop market mix of wheat and sugar beet. They found that bio-based PET bottles performed worse overall than conventional petrochemical PET bottles and only performed better (around 10%) in abiotic depletion (fossil fuels). Similar performance was observed for climate change. Using European crops to produce ethanol instead of Brazilian sugar cane resulted in poorer environmental performance, as they produced lower yields than Brazilian sugar cane. When wheat straw was considered as the biomass feedstock for ethanol production, similar environmental performance to petrochemical PET bottles was observed (Vural Gursel et al., 2021). In their work, Brizga et al. (2020) report that biobased materials save on average 55 ± 34 GJ/t and 127 ± 79 GJ/ha of non-renewable energy and 3 ± 1 tCO2e/t and 8 ± 5 tCO2e/ha of greenhouse gas emissions compared to conventional materials. Globally, bioplastics could save 241–316 MtCO2e per year by replacing 65.8% of all conventional plastics. However, the results of the Global Warming Potential (GWP) assessment of bioplastics can be significantly affected by the chosen accounting method for biogenic carbon. They highlight that other important determinants of the climate impact of plastics are premature material degradation over their lifetime, the extent to which materials are recycled, and the proportion of fossil or biogenic carbon in the product. Kakadellis and Harris (2020), in a comprehensive summary of life cycle assessment studies of bioplastics, report that bioplastics and plastics have similar GWP impacts, with values ranging from 0.70 to 11.02 kgCO2-eq/kg polymer.

The production of biodegradable packaging materials, in whole or in part, using biopolymers is not exclusive, but it is a possible process to replace plastics in food packaging partially. Because of their properties, which differ from those of plastics, their field of application is still limited. Their use reduces packaging waste by allowing such materials to be recycled into the natural cycle under appropriate conditions (composting). A precondition for this is establishing selective waste collection and creating appropriate composting sites (Beczner et al., 1997). Naturally, renewable biopolymers can be used as barrier coatings on paper packaging materials. These biopolymer coatings can retard unwanted moisture transfer in food, are good oxygen and oil barriers, are biodegradable and could potentially replace current synthetic paper and board coatings (Khwaldia et al., 2010).

2.2.1. Polylactic acid (PLA) packaging

Polylactide (PLA), a biodegradable aliphatic polyester, has been widely studied for all its applications, from food packaging to car interiors. One of the advantages of PLA is that the raw material, lactic acid, can come from renewable sources, making PLA very attractive for packaging and considered green packaging. Although the cost of PLA is relatively higher compared to petroleum-based packaging materials, it is predicted that the price will fall following the commercial

success of the process (Ahmed and Varshney, 2011). PLA is a thermoplastic polymer dehydrated and polymerised from fermented products of corn starch. It is widely used in packaging but is expensive and has strict degradation requirements (Chen et al., 2022). Recently, the price per kilogram of bioplastics has fallen significantly. For example, the price of PLA, which was $6,000/ton in the 1990s, fell to $1984.14/ton by 2010.

Furthermore, the rise in oil price has brought the price of bio-based plastics in line with the price of oil-based thermoplastics. In terms of energy, producing biopolymer-based plastics requires less energy than their conventional counterparts. For example, 1 kg of PLA requires only 27.2 MJ of fossil fuel-based energy. In contrast, polypropylene and high-density polyethene require 85.9 and 73.7 MJ/kg, respectively. Thus, it can be concluded that biofuels successfully address concerns about cost, energy consumption, sustainability, and recycling processes compared to their synthetic counterparts (Abdul Khalil et al., 2016). Annual production of PLA is estimated at 140,000 tons, and PLA and its composites are expected to have the potential to replace petroleum-based products.

PLA has desirable properties such as good transparency and processability, glossy appearance, and rigidity. PLA shows better thermal processability than other biopolymers; therefore, different processing techniques, such as cast film, blown film, fibre spinning, and injection moulding, can produce PLA films. There are numerous examples of PLA-coated/laminated paper being used commercially for food products, such as stand-up pouches for dry fruit, trays moulded from Cellulose, and paper cups for cold liquids (Tyagi et al., 2021; Holler et al., 2023). This is also confirmed in a study by Raghuvanshi et al. (2023). They found that PLA-based nanocomposites are 100% compostable and environmentally friendly, with very low impact on the environment and human health. PLA-based nanocomposites also extend the shelf-life of packaged fruit and prove to be much more efficient than PET-based composites. Therefore, it is concluded that polylactic acid could be an excellent alternative to petrochemical-based packaging materials for use as a filler and is recommended as a safe and environmentally friendly solution. Moreover, Ingrao et al. (2015) showed that PLA has a marginally better environmental performance than plastic. Their GWP results are 4.826 $kgCO_2eq$ for PLA compared to 5.11 $kgCO_2eq$ for plastic. However, the CO_2 emissions from granulate production are slightly higher for PLA (2.65 $kgCO_2eq$) than for plastic (2.59 $kgCO_2eq$). Two main reasons have been highlighted: the cultivation of feedstock (maise) and transport. Firoozi Nejad et al. (2021) showed that PLA has a 49% lower carbon footprint than PET or polyethene.

3. Sustainable packaging – natural materials

Several organisations have tried to create 'sustainable packaging' sets, such as the Sustainable Packaging Alliance (SPA) in Australia and the Sustainable Packaging Coalition (SPC) in the US. Some companies have tried to reduce the "waste footprint" of packaging (Lewis et al., 2007), as packaging accounts for 20–40% of the product's waste footprint (Ingrao et al., 2015). In one case, a carbon tax was introduced to reduce the waste footprint of food packaging. Carbon emissions from food shopping are estimated to account for around 30% of total household greenhouse gas emissions in developed economies, with supermarkets accounting for a large share of food spending. As a result, there is a growing recognition that effective sustainability policy requires direct consumer involvement and that divergent consumer choices within stores can lead to significant reductions in the carbon footprint of food packaging (Panzone et al., 2021). Four principles of sustainable packaging have been formulated: the packaging system provides real value (efficient); the packaging system is designed to be used; the packaging materials are continuously cyclical, and material degradation is minimised; the packaging elements used in the system, including materials, coatings, inks, pigments and other additives, do not pose a risk to people or ecosystems (clean) (Lewis et al., 2007). The amount of packaging required for a product can be reduced by making the product lighter. This requires companies to measure the ratio between the amount of packaging material used and the product delivered. The reduction in the amount of materials used in packaging elements results from design or material innovation. For example, in 2006, Unilever introduced a three times more concentrated detergent than conventional detergents (Dharmadhikari, 2012).

3.1. Cellulose packaging

Cellulose fibres have been known as traditional food packaging materials for centuries, but high-performance plastic-based solutions have gradually replaced them. Typically, cheaper and lightweight plastics have enabled the development of new packaging types and packaging conversion processes, contributing to the efficient preservation and distribution of fresh and processed foods, thereby reducing food wastage. Commercial plastic packaging materials, such as polypropylene (PP), polyethene (PE) or polyethene terephthalate (PET), can be easily converted and effectively recycled in their pure form.

Combined in multilayer structures, they can have very high barrier properties, but they are much more difficult to handle in recycling processes. Without effective management systems, plastic packaging often increases the amount of waste. Plastic materials do not degrade easily in nature because they were originally designed to last. In countries where sustainable waste management systems are not widely available, waste accumulates in landfills, rivers and oceans, becoming a major environmental concern (Schenker et al., 2021). In response to concerns about the sustainability of plastic packaging and the impact of plastic pollution on our environment, large companies have started to replace plastic packaging with fibre-based solutions. Most cellulose fibre materials have favourable end-of-life properties, given that they are generally recyclable with well-established recycling infrastructure in most countries. Consumers understand the importance of recycling and apply it by sorting and recycling these materials (e.g. 85% of packaging paper and cardboard is recycled in Europe). In addition, some cellulose fibre materials have long been known to biodegrade in soil (Béguin and Aubert, 1994) and marine environments (Hofsten and Edberg, 1972). Cellulose fibre materials are widely available from certified sources and can be accessed responsibly without deforestation or ecosystem degradation. Finally, for the above reasons, many cellulose fibre materials are positively valued by consumers, which enables sustainability communication and makes these materials valuable to stakeholders in the supply chain, such as brand owners, retailers or consumers. However, cellulosic materials are not considered superior to plastics in terms of functionality and often require more weight for the same function, which can lead to similar or even greater environmental impacts than plastic packaging (Schenker et al., 2021). Cellulose fibre packaging materials have been used in the food industry for centuries and are largely made from wood or wood fibre (Johansson et al., 2012).

Cellulose fibre packaging materials, such as paper, cardboard and moulded Cellulose, are part of the broader cellulose-based packaging (which includes regenerated cellulose films, cellulose derivatives and composite materials where the fibres are embedded in a polymer matrix). Fibre-based packaging materials can be divided into flexible (paper) and rigid (paper board, moulded cellulose, corrugated board) categories, with further designations largely related to their application and historical use. The focus is on innovative materials that have the potential to replace hard-to-recycle fossil-based plastics in terms of packaging functionality while preserving the intrinsic reproducibility of traditional cellulose fibre materials.

Plastics can be shaped into various three-dimensional objects without size or shape restrictions. On the contrary, fibre-based packaging materials are often supplied as a sheet or roll of material that can only be converted into a three-dimensional object by glueing and/or folding. Fiber containers and bags are also difficult to close tightly. There is a marked difference between all fossil-based plastics and all cellulose fibre-based materials: plastics have a total load of 3-5 kg $CO_2eq_{/kg}$, while Cellulose fibre-based materials have a total load of less than 1.5 kg CO_2eq/kg. This does not necessarily mean that all fibre-based packaging offers better environmental performance than plastic-based alternatives, as the amount of fibre needed for a given protection may be more than the amount needed. Cellulose fibre-based materials are fairly widely recyclable, but their environmental performance would not change significantly if incinerated with energy recovery. Similarly, no results have been shown for organic recycling (composting or bioremediation), as packaging materials are not widely accepted in organic recycling schemes today (Schenker et al., 2021).

In the past, paper and other fibre-based materials have been largely recognised as a major source of industrial pollution and the destruction of forests of high conservation value. Over the past 40 years, the wood and paper industry has completely changed its image by tightening pollution controls in most countries developing transparent and responsible forest procurement systems. Scandinavian and Central European countries are known for forestry practices that maintain full forest cover and promote biodiversity while ensuring high yields (Rossi et al., 2018). Therefore, the eco-design of Cellulose fibre-based packaging should focus on identifying solutions that minimise weight gain compared to plastic-based packaging (Schenker et al., 2021).

However, it must be recognised that there is a possibility that a widespread and poorly designed switch to cellulose fibre materials could have negative environmental consequences. This could be due to increased deforestation in countries with weak environmental legislation, increasing land competition. Although the land-use impacts of fibre-based cellulosic materials have not been calculated, it is clear that they will be much greater than those of their fossil-based plastic counterparts, which use almost no land outside of the oil wellfield and factory infrastructure used for refining. However, increased land use does not necessarily have to harm the environment, especially given that well-managed forests preserve biodiversity from natural ecosystems (Rossi et al., 2018).

To avoid significant biodiversity impacts from increased land use of fibre-based wood cellulose, a strong, responsible forest products sourcing strategy should be implemented within companies that seek to increase the proportion of fibre-based wood cellulose packaging. In addition, indirect pressure on the soil can be reduced or avoided altogether if a broader sustainability strategy complements the cellulose fibre packaging strategy. Reducing food loss and waste or increasing the proportion of plant proteins in a company's portfolio can significantly reduce a food company's land use impacts while contributing to additional climate and other environmental benefits. Combining a fibre-based cellulose packaging strategy with a broader sustainability strategy will ensure that no carbon leakage occurs and that the packaging strategy delivers sustainability benefits beyond climate change and narrow packaging value chains (Schenker et al., 2021).

4. Additional types of packaging

4.1. Bamboo packaging

In China, an environmentally friendly pot manufacturing technology was developed using bamboo fibre as the raw material for pots, with only 3 wt% tapioca starch added as an adhesive/filler. This technology outperforms traditional pulp moulding, which is polluting, energy-intensive, and has significant environmental benefits. Bamboo resources are abundant globally; bamboo cultivation covers over 36 million hectares worldwide (Chen et al., 2022). Bamboo grows to a usable size in 3–5 years and is managed sustainably with proper pruning for better growth. A high-quality natural raw material that can be used for tableware and packaging. Using green bamboo pulp fibre to make disposable, environmentally friendly tableware has significant advantages regarding resource availability, material properties and environmental protection. The resulting products have huge market potential and significant social, environmental and economic value (Singh et al., 2023).

4.2. Nanocellulosic fiber

Various methods to improve the properties of biopolymer-based films have been proposed for their successful practical application. One of the most commonly used methods is the addition of nanomaterials, in particular, cellulose nanofibers. Due to its nano size, it interacts with the material at the atomic, molecular or macromolecular level, thus influencing the functional behaviour of biopolymer films. Cellulose nanofibers derived from natural resources are recognised as the most abundant and renewable polymeric material and a key source of sustainable materials on an industrial scale. Because of their attractive properties such as biocompatibility, biodegradability and chemical stability, cellulosic materials have been used as raw materials in the production of paper, pharmaceuticals and textiles for more than 150 years (Cherian et al., 2022; Mary et al., 2022).

In recent years, nano cellulosic materials have attracted researchers' interest in maximising packaging materials' mechanical and barrier properties. Using cellulose nanofibers in packaging minimises the cost of packaged products as they are widely available and inexpensive. Cellulose nanofibers are also good for the environment thanks to their recyclability and reusability. The effective design of cellulose nanofibers for sustainable packaging involves their qualitative and quantitative operation throughout the product life cycle. In addition, the design of nano-cellulose materials provides a better experience for the end-user and enables efficient manufacturing systems. Cellulose fibres are traditionally used in packaging categories such as dry foods, frozen or liquid foods, beverages and fresh foods.

The most commonly used cellulose-based food packaging is cellophane, also known as regenerated cellulose film. Several cellulose derivatives, such as carboxymethyl cellulose, methylcellulose, ethyl cellulose, hydroxypropyl cellulose, hydroxyethyl cellulose and cellulose acetate, are used to produce cellulose-based films. Cellulose acetate and cellulose triacetate are also widely used as rigid packaging film, as are other derivatives, due to their low gas and moisture barrier properties. Cellulose nanofibers are derived from natural resources (wood or plants) and are, therefore, almost inexhaustible, renewable and globally abundant. Moreover, cellulose nanofibers do not interfere with the human food chain and do not need petrochemical ingredients for their production. Therefore, nano-cellulose fibres are used in many applications. The packaging sector could be one of the areas where cellulose nanofibers can be used for sustainable and environmentally friendly packaging (Abdul Khalil et al., 2016; Gervasoni et al., 2023). Using starch-based bio-packaging with nano-cellulose fillers as an alternative to synthetic plastics (Mahardika et al., 2023), (Perera et al., 2023).

4.3. Edible packaging

Nowadays, edible films have become a major area of research in food packaging, as they play a role in reducing the problem of plastic pollution (Adhikary et al., 2023). Researchers have recently focused on edible food packaging made from starch. Edible packaging is considered a sustainable and biodegradable alternative for active food packaging and optimises food quality compared to traditional packaging. The benefits of edible packaging are recognised in terms of the packaging's ability to maintain food quality, extend shelf life, reduce waste and contribute to the economy of packaging materials. The development and application of edible films is one of the most promising areas in food science, as they are versatile, can be made from a wide range of materials and can carry various active ingredients such as antioxidants and/or antimicrobial agents (Rangaraj et al., 2021; Petkoska et al., 2021). Starch has been a potential candidate for this venture, where starch from both conventional and non-traditional sources is used to produce starch-based edible food packaging (Tyagi et al., 2021). A polysaccharide-based edible film has recently been used in the meat industry to prevent moisture loss and improve texture (Petkoska et al., 2021). Overall, innovation in edible packaging has the potential to become an everyday part of consumers' lives. However, edible packaging is unlikely to solve the problem of plastic waste pollution, but it can make a significant contribution (Rangaraj et al., 2021).

5. Conclusions

The alternative packaging materials in use, as detailed in the previous chapters, are analysed using a SWOT analysis (Table 1). This chart shows alternative packaging materials' strengths, weaknesses, opportunities and threats. This makes it easier to compare them with plastic packaging.

Table 1. Results of the SWOT analysis
Source: own editing

	Strengths	Weaknesses	Opportunities	Threats
Biodegredable PET	decomposition, reducing resource use	not suitable for replacing plastic	semi-permeable film in food packaging	improper consumer treatment
Bioplastic	made from plant biomass, oxygen and oil barrier, biodegradable	uncertain decomposition into Carbon dioxide and water	can be used as a closing statement, technically can replace plastic	not necessarily improve the environmental impact, ecomnomically costly, competing food
PLA	renewable raw material, good transparency	high cost	price decreases, requires less energy, potential substitude, better thermal processability	the changeover does not necessarily mean less environmental impact
Cellulose	widely available, less environmental impact, recyclability, biodegradable	not easily shaped, more material needed, non-functional in many cases	consumers recycle, enable sustainable communication	badly planned switchover would have environmental consequences

The following conclusions can be drawn from the table. Biodegradable PET's strengths lie in its reduction of resource use and degradation in industrial composters. Its weakness is that it is not a suitable alternative to traditional plastic regarding protection, shelf life, and food safety. However, it has the potential to form semi-permeable films and can also be used in food packaging. Meanwhile, there is a risk that consumers will handle it incorrectly, i.e. not dispose of it properly. **Bioplastic**'s strengths lie in that first-generation bioplastics are made from carbohydrate-rich crops, while the second generation is made from non-food crops or waste from biomass processing. They have good oxygen and oil barrier properties and are biodegradable. Its weakness is that its biodegradability to carbon dioxide and water is uncertain. It has a wide range of potentials, such as its biodegradable property offering the possibility to address social and environmental challenges; it could provide a solution for packaging applications; the production of biodegradable packaging materials using biopolymers is a possible process; it can be used as a barrier coating on paper packaging materials and a complete replacement of petrochemical plastics is technically feasible. Their risks are that they do not necessarily improve the overall environmental impact; they are economically costly; they compete with food using the same raw materials; they offer limited environmental

benefits, and their scope is limited. The advantage of **PLA** is that its raw material can come from renewable sources, and its material is characterised by good transparency and processability. Its weakness is that it can be produced at a higher cost than plastic. Potential benefits include lower cost over time, less energy required to produce it, making it a potential substitute for plastic, and improved thermal processability. The threats do not necessarily improve environmental performance in the whole life cycle. The advantages of **Cellulose include its reduced environmental impact, beneficial end-of-life properties, recyclability,** biodegradability, and wide availability. It has the weakness that the lower environmental load is only valid for the same mass; in many cases, it is not functional; it does not have the property of being easily malleable or even difficult to close tightly. Opportunities include being recycled and positively valued by consumers, which enables sustainability communication and, therefore, becomes valuable to the parties in the supply chain. There is a risk that its environmental performance would not change significantly if it were burned for energy recovery, and a large-scale, poorly planned switch to wood cellulose could have negative environmental consequences.

This suggests that none of these options is a perfect alternative to plastic, but there are some promising alternatives. The advantage of **Bamboo** is that it is a rich source, takes 3–5 years to grow and is a high-quality natural material. It has the potential to outperform Cellulose. It has environmental benefits; it can be used to make disposable and environmentally friendly containers and has huge market potential. The use of **nano cellulosic fibre minimises costs and is environmentally friendly. I**ts design provides a better experience for the end user and enables efficient manufacturing systems. **Edible packaging** is a sustainable and biodegradable alternative that maintains food quality, extends shelf life and reduces waste. Innovation has the potential to become part of consumers' everyday lives, but there is still much resistance. These materials are mainly still experimental, but all have potential.

To complement this, we have produced a cross-table (Table 2) listing the raw materials tested from certain perspectives, showing what else might need to be tested before they can be used:

Table 2. Cross-table of the different packaging materials studied

Factors studied	Biodegradable PET packaging	Bioplastic packaging	PLA	Cellulose packaging	Bamboo packaging	Nanocellulosic fiber	Edible packaging
Reducing the use of resources	X		X		X	X	
Mechanical protection of food		X	X		X	X	
Increasing food shelf-life			X				X
Food safety							X
Dealing with social and environmental challenges	X	X		X		X	X
Reducing packaging waste	X	X		X	X	X	X
Energy-efficient			X				
Positive end-of-life properties				X	X	X	
Degradable in soil and marine environments				X	X	X	
Life-cycle assessment	X	X	X	X			

Source: own editing

The criteria shown in the table have been compiled based on the studies processed in the literature analysis. Then, we checked which packaging materials had already been tested against these criteria. In most aspects, information was available for Nanocellulosic fibre. Increasing the shelf life of the food and mechanical protection were the aspects that came up in most cases. The least frequently mentioned aspects were soil and water degradability and positive end-of-life properties. However, these aspects could reduce the amount of waste that accumulates. In several cases, a material has been reported to reduce packaging waste and the amount of material used, but surprisingly, food packaging reduces food loss rather than waste. On this basis, it can be said that there is a lot of research potential in this field, and there are still unexplored

components in the use of different materials. So far, only four of the packaging materials presented have been subjected to a life cycle analysis. No new alternatives have been investigated. Future research should include a comprehensive assessment of potential sustainable alternative packaging materials regarding their environmental impact over the whole life cycle.

Overall, long-established food packaging materials have gradually been replaced by plastic. The negative consequences of this widespread use of plastic packaging have changed how alternatives are used to replace it. There have been several attempts, such as reusing or biodegradability of plastics production of bioplastics. However, they have not proved to be a sufficient or good alternative. Sustainable and biodegradable packaging materials are also gaining space, but their positive impact on the environment is not fully understood, and their usability is limited. However, there are also promising new materials in the experimental phase, such as edible packaging or nanocellulosic fibres. Their use helps to reduce the environmental impact and the volume of waste. Each packaging material presented has advantages and disadvantages, and several possibilities exist. However, at the moment, none of them can properly replace plastic.

Appendix

Table 3. Results of the systematic literature analysis

Article	Packaging type	Methods
Abdul Khalil et al., 2016	Cellulosic nanofiber	Review
Adhikary et al., 2023	Polysaccharide-based packaging	Review
Ahmed and Varsney, 2011	Polylactide (PLA)	Review
Beczner et al., 1997	Biopolymer	Overview study
Béguin and Aubert, 1994	Cellulose	Overview study
Brizga et al., 2020	Bioplastic	Potential environmental consequences of substitution
Chen et al., 2016	100% bio-based polyethene terephthalate (PET) bottles, fully fossil-based and partially bio-based PET bottles	Comparative environmental Life Cycle Analysis (LCA)
Chen et al., 2022	Bamboo fibre, polylactic acid (PLA)	Investigated by exploring how the properties of their microstructures affect their mechanical properties
Cherian et al., 2022	Nano-cellulose based coatings	Discusses aspects, challenges and future perspectives of nanocellulose-based coatings
Clark, 2018	Biobased and Renewable Plastics	Review
Dilkes-Hoffman et al., 2019	Bioplastics	Online survey of Australian consumers
Gervasoni et al., 2023	Active food packaging based on cellulose nanocomposites	Review
Hofsten and Edberg, 1972	Cellulose fibers	The rate of degradation in aquatic environments
Holler et al., 2023	Polylactic acid (PLA), bio-polyethylene (Green-PE)	The effect on the oxidative stability of sunflower oil was investigated
Ingrao et al., 2015	Polylactic acid (PLA)	Discusses application of Carbon Footprint (CF)
Johansson et al., 2012	Renewable fibres, bio-based materials	Review
Kakadellis and Harris, 2020	Biodegradable plastic	A systematic review based on life-cycle assessments (LCAs)
Khwaldia et al., 2010	Biopolymer coatings	Existing and potential applications are discussed
Koeing-Lewis et al., 2022	Compostable bio-based food packaging, fossil-based plastic	Analysis of implicit attitudes
Mahardika et al., 2023	Nano-cellulose	Mini review
Mary et al., 2022	Starch-based material	Overview
Perera et al., 2023	Nano-cellulose and metal oxide-based composite	Review
Petkoska et al., 2021	Edible packaging	Review
Raghuvanshi et al., 2023	Bionanocomposite films for intelligent food packaging	Review
Rangaraj et al., 2021	Edible active packaging films	Review
Schenker et al., 2021	Cellulosic fiber-based materials	Describes the climate change impacts of using Cellulose
Singh et al., 2023	Nano-cellulose	Extract nano-cellulose from bamboo fibre by chemical treatment and mechanical grinding.
Taufik et al., 2020	Bio-based plastics	Lab-in-the-field study
Torres-Huerta et al., 2014	PET/PLA, PET/chitosan blends	Synthesis, miscibility, and degradation in real soil environment
Tyagi et al., 2021	Barrier coatings	Review
Vea et al., 2021	Polyhydroxyalkanoate (PHA)-based plastics	Life cycle assessment (LCA) to assess environmental performance
Vural Gursel et al., 2021	Bio-based polyethylene terephthalate	Life cycle assessment
Wyrwa and Barska, 2017	Active packaging	Discuss of application

Source: own editing

References

Abdul Khalil, H. P. S., Davoudpour, Y., Saurabh, C. K., Hossain, M. S., Adnan, A. S., Dungani, R., Paridah, M. T., Islam Sarker, M. Z., Fazita, M. R. N., Syakir, M. I., Haafiz, M. K. M. (2016). A review on nanocellulosic fibres as new material for sustainable packaging: Process and applications. *Renewable and Sustainable Energy Reviews*. 64, 823–836. DOI: https:/doi.org/10.1016/j.rser.2016.06.072

Adhikary, N. D., Bains, A., Sridhar, K., Kaushik, R., Chawla, P., Sharma, M. (2023). Recent advances in plant-based polysaccharide ternary complexes for biodegradable packaging. *International Journal of Biological Macromolecules*. 253, 126725. DOI: https://doi.org/10.1016/j.ijbiomac.2023.126725

Ahmed, J., Varshney, S. K. (2011). Polylactides – Chemistry, properties and green packaging technology: A review. *International Journal of Food Properties*. 14(1), 37–58. DOI: https://doi.org/10.1080/10942910903125284

Barletta, M., Aversa, C., Puopolo, M., Vesco, S. (2019). Extrusion blow molding of environmentally friendly bottles in biodegradable polyesters blends. *Polymer Testing*. 77. DOI: https://doi.org/10.1016/j.polymertesting.2019.05.001

Beczner, J., Perédi, J., Haidekker, B., Kertész, B., Lajos, J., Vásárhelyiné, P. K., Kardos Györgyné. (1997). A biológiai úton lebomló csomagolóanyagok előállítási és felhasználási lehetőségének vizsgálata itthon és külföldön *Springer Science and Business Media LLC*. URL: https://mek.oszk.hu/09800/09809/pdf/zold_belepo_05.pdf

Béguin, P., Aubert, J. (1994). The biological degradation of Cellulose. *FEMS Microbiology Reviews*. 13(1), 25–58. DOI: https://doi.org/10.1111/j.1574-6976.1994.tb00033.x

Brizga, J., Hubacek, K., Feng, K. (2020). The unintended side effects of bioplastics: Carbon, land, and water footprints. *One Earth*. 3(1), 45–53. DOI: https://doi.org/10.1016/j.oneear.2020.06.016

Chen, L., Pelton, R. E. O., Smith, T. M. (2016). Comparative life cycle assessment of fossil and bio-based polyethylene terephthalate (PET) bottles. *Journal of Cleaner Production*. 137, 667–676. DOI: https://doi.org/10.1016/j.jclepro.2016.07.094

Chen, X., Chen, F., Wang, G., Ma, X., Wang, J., Deng, J. (2022). Eco-friendly, disposable bamboo fiber dishware: Static and dynamic mechanical properties and creep behavior. *Industrial Crops and Products*. 187, 115305. DOI: https://doi.org/10.1016/j.indcrop.2022.115305

Cherian, R. M., Tharayil, A., Varghese, R. T., Antony, T., Kargarzadeh, H., Chirayil, C. J., Thomas, S. (2022). A review on the emerging applications of nano-cellulose as advanced coatings. *Carbohydrate Polymers*. 282, 119123. DOI: https://doi.org/10.1016/j.carbpol.2022.119123

Clark, D. I. (2018). Food packaging and sustainability: A manufacturer's view. *Reference Module in Food Sciences*. Elsevier. DOI: https://doi.org/10.1016/B978-0-08-100596-5.22587-0

Dharmadhikari, S. (2012). Eco-friendly packaging in supply chain. *IUP Journal of Supply Chain Management*. 9(2), 7–18. URL: https://www.proquest.com/scholarly-journals/eco-friendly-packaging-supply-chain/docview/1434427712/se-2?accountid=15756

Dilkes-Hoffman, L., Ashworth, P., Laycock, B., Pratt, S., Lant, P. (2019). Public attitudes towards bioplastics – knowledge, perception and end-of-life management. *Resources, Conservation and Recycling*. 151, 104479. DOI: https://doi.org/10.1016/j.resconrec.2019.104479

European Parliament and Council Directive 94/62/EC of 20 December 1994 on packaging and packaging waste. URL: https://eur-lex.europa.eu/legal-content/EN/TXT/?uri=celex%3A31994L0062 (accessed on 13. 06. 2024)

Firoozi Nejad, B., Smyth, B., Bolaji, I., Mehta, N., Billham, M., Cunningham, E. (2021). Carbon and energy footprints of high-value food trays and lidding films made of common bio-based and conventional packaging materials. *Cleaner Environmental Systems*. 3, 100058. DOI: https://doi.org/10.1016/j.cesys.2021.100058

Frigione, M. (2010). Recycling of PET bottles as fine aggregate in concrete. *Waste Management (Elmsford)*. 30(6), 1101–1106. DOI: https://doi.org/10.1016/j.wasman.2010.01.030

Gervasoni, L. F., Gervasoni, K., de Oliveira Silva, K., Ferraz Mendes, M. E., Maddela, N. R., Prasad, R., Winkelstroter, L. K. (2023). Postbiotics in active food packaging: The contribution of cellulose nanocomposites. *Sustainable Chemistry and Pharmacy*. 36, 101280. DOI: https://doi.org/10.1016/j.scp.2023.101280

Hofsten, B. V., Edberg, N. (1972). Estimating the rate of degradation of cellulose fibers in water. *Oikos*. 23(1), 29–34. DOI: https://doi.org/doi.org/10.2307/3543924

Holler, M., Alberdi-Cedeño, J., Auñon-Lopez, A., Pointner, T., Martínez-Yusta, A., König, J., Pignitter, M. (2023). Polylactic acid as a promising sustainable plastic packaging for edible oils. *Food Packaging and Shelf Life*. 36, 101051. DOI: https://doi.org/10.1016/j.fpsl.2023.101051

Ingrao, C., Tricase, C., Cholewa-Wójcik, A., Kawecka, A., Rana, R., Siracusa, V. (2015). Polylactic acid trays for fresh-food packaging: A carbon footprint assessment. *The Science of the Total Environment*. 537, 385–398. DOI: https://doi.org/10.1016/j.scitotenv.2015.08.023

Johansson, C., Bras, J., Mondragon, I., Nechita, P., Plackett, D., Šimon, P., Svetec, D. G., Virtanen, S., Baschetti, M. G., Breen, C., Clegg, F., Aucejo, S. (2012). Renewable fibers and bio-based materials for packaging applications: A review of recent developments. *BioResources*. 7(2), 2506–2552. DOI: https://doi.org/10.15376/biores.7.2.2506-2552

Kakadellis, S., Harris, Z. M. (2020). Don't scrap the waste: The need for broader system boundaries in bioplastic food packaging life-cycle assessment – A critical review. *Journal of Cleaner Production*. 274, 122831. DOI: https://doi.org/10.1016/j.jclepro.2020.122831

Khwaldia, K., Arab-Tehrany, E., Desobry, S. (2010). Biopolymer coatings on paper packaging materials. *Comprehensive Reviews in Food Science and Food Safety*. 9(1), 82–91. DOI: https://doi.org/10.1111/j.1541-4337.2009.00095.x

Koenig-Lewis, N., Grazzini, L., Palmer, A. (2022). Cakes in plastic: A study of implicit associations of compostable bio-based versus plastic food packaging. *Resources, Conservation and Recycling*, 178, 105977. DOI: https://doi.org/10.1016/j.resconrec.2021.105977

Kumar, G. M. Irshad, A. Raghunath, B. V., Rajarajan, G. (2016). Waste management in food packaging industry. In: Prashanthi, M., Sundaram, R. (eds) *Integrated Waste Management in India*. Springer International Publishing. 265–277. DOI: https://doi.org/10.1007/978-3-319-27228-3_24

Karli Verghese, Helen Lewis, Leanne Fitzpatrick (2012). Packaging for Sustainability. Springer London. DOI: https://doi.org/10.1007/978-0-85729-988-8 URL: https://link.springer.com/book/10.1007/978-0-85729-988-8 p384

Rangaraj, V. M., Rambabu, K., Banat, F., Mittal, V. (2021). Natural antioxidants-based edible active food packaging: An overview of current advancements. *Food Bioscience*. 43, 101251. DOI: https://doi.org/10.1016/j.fbio.2021.101251

Mahardika, M., Amelia, D., Azril, Syafri, E. (2023). Applications of nano-cellulose and its composites in bio packaging-based starch. *Materials Today: Proceedings*. 74, 415–418. DOI: https://doi.org/10.1016/j.matpr.2022.11.138

Majeed, K., Jawaid, M., Hassan, A., Abu Bakar, A., Abdul Khalil, H. P. S., Salema, A. A., Inuwa, I. (2013). Potential materials for food packaging from nanoclay/natural fibres filled hybrid composites. *Materials & Design* (1980–2015). 46, 391–410. DOI: https://doi.org/10.1016/j.matdes.2012.10.044

Marshall, J. (2007). Packaging unwrapped. *NewScientist*. 194(2598), 37–41. DOI: https://doi.org/10.1016/S0262-4079(07)60869-0

Mary, S. K., Koshy, R. R., Rehghunadhan, A.., Thomas, S., Pothan, L. A. (2022). A review of recent advances in starch-based materials: Bio-nanocomposites, pH sensitive films, aerogels and carbon dots. *Carbohydrate Polymer Technologies and Applications*. 3, 100190. DOI: https://doi.org/10.1016/j.carpta.2022.100190

OECD. (2022). Global Plastics Outlook: Economic Drivers, Environmental Impacts and Policy Options. DOI: https://doi.org/10.1787/de747aef-en URL: https://www.oecd.org/en/publications/global-plastics-outlook_de747aef-en/full-report.html

Panzone, L. A., Ulph, A., Zizzo, D. J., Hilton, D., Clear, A. (2021). The impact of environmental recall and carbon taxation on the carbon footprint of supermarket shopping. *Elsevier BV*. DOI: https://doi.org/10.1016/j.jeem.2018.06.002

Perera, K. Y., Pradhan, D., Rafferty, A., Jaiswal, A. K., Jaiswal, S. (2023). A comprehensive review on metal oxide-nanocellulose composites in sustainable active and intelligent food packaging. *Food Chemistry Advances*. 3, 100436. DOI: https://doi.org/10.1016/j.focha.2023.100436

Petkoska, A. T., Daniloski, D., D'Cunha, N. M., Naumovski, N., Broach, A. T. (2021). Edible packaging: Sustainable solutions and novel trends in food packaging. *Food Research International*. 140, 109981. DOI: https://doi.org/10.1016/j.foodres.2020.109981

Raghuvanshi, S., Khan, H., Saroha, V., Sharma, H., Gupta, H. S., Kadam, A., Dutt, D. (2023). Recent advances in biomacromolecule-based nanocomposite films for intelligent food packaging. A review. *International Journal of Biological Macromolecules*. 253, 127420. DOI: https://doi.org/10.1016/j.ijbiomac.2023.127420

Rossi, V., Lehesvirta, T., Schenker, U., Lundquist, L., Koski, O., Gueye, S., Taylor, R., Humbert, S. (2018). Capturing the potential biodiversity effects of forestry practices in life cycle assessment. *The International Journal of Life Cycle Assessment*. 23(6), 1192–1200. DOI: https://doi.org/10.1007/s11367-017-1352-5

Schenker, U., Chardot, J., Missoum, K., Vishtal, A., Bras, J. (2021). Short communication on the role of cellulosic fiber-based packaging in reduction of climate change impacts. *Carbohydrate Polymers*, 254, 117248. DOI: https://doi.org/10.1016/j.carbpol.2020.117248

Shafqat, A., Tahir, A., Mahmood, A., Tabinda, A. B., Yasar, A., Pugazhendhi, A. (2020). A review on environmental significance carbon foot prints of starch based bio-plastic: A substitute of conventional plastics. *Biocatalysis and Agricultural Biotechnology*. 27, 8. DOI: https://doi.org/10.1016/j.bcab.2020.101540

Singh, H., Kumar Verma, A., Kumar Trivedi, A., Gupta, M. K. (2023). Characterisation of nano-cellulose isolated from bamboo fibers. *Materials Today: Proceedings*, DOI: https://doi.org/10.1016/j.matpr.2023.02.300

Taufik, D., Reinders, M. J., Molenveld, K., Onwezen, M. C. (2020). The paradox between the environmental appeal of bio-based plastic packaging for consumers and their disposal behaviour. *Elsevier BV*. DOI: https://doi.org/10.1016/j.scitotenv.2019.135820

Tiefbrunner, A. (2002). Packaing and Environmental Protection [in Hungarian: Csomagolás és környezetvédelem]. *Paper-Press Association [in Hungarian: Papír-Press Egyesülés]*.

Torres-Huerta, A. M., Palma-Ramírez, D., Domínguez-Crespo, M. A., Del Angel-López, D., de la Fuente, D. (2014). Comparative assessment of miscibility and degradability on PET/PLA and PET/chitosan blends. *European Polymer Journal*. 61, 285–299. DOI: https://doi.org/10.1016/j.eurpolymj.2014.10.016

Tyagi, P., Salem, K. S., Hubbe, M. A., Pal, L. (2021). Advances in barrier coatings and film technologies for achieving sustainable packaging of food products: A review. *Trends in Food Science & Technology*. 115, 461–485. DOI: https://doi.org/10.1016/j.tifs.2021.06.036

Vea, E. B., Fabbri, S., Spierling, S., Owsianiak, M. (2021). Inclusion of multiple climate tipping as a new impact category in life cycle assessment of polyhydroxyalkanoate (PHA)-based plastics. *Science of the Total Environment*. 788, 147544. DOI: https://doi.org/10.1016/j.scitotenv.2021.147544

Vural Gursel, I., Moretti, C., Hamelin, L., Jakobsen, L. G., Steingrimsdottir, M. M., Junginger, M., Høibye, L., Shen, L. (2021). Comparative cradle-to-grave life cycle assessment of bio-based and petrochemical PET bottles. *Elsevier BV*. DOI: https://doi.org/10.1016/j.scitotenv.2021.148642

Wyrwa, J., Barska, A. (2017). Innovations in the food packaging market: Active packaging. *Springer Science and Business Media LLC*. DOI: https://doi.org/10.1007/s00217-017-2878-2

Structural response of Autoclave due to vibrations and optimisation of its supports by spring elements

Aleksandar Jovanovic

https://orcid.org/0009-0009-6539-1325
Mont-R, Dubravska 2d, Meljak
Belgrade, Serbia
a.jovanovic@mont-r.rs

Lazar Jeremic

https://orcid.org/0000-0002-9568-2766
Innovation Centre of the Faculty of Mechanical Engineering, Kraljice Marije 16
Belgrade, Serbia
ljeremic@mas.bg.ac.rs

Branislav Djordjevic

https://orcid.org/0000-0001-8595-6930
Innovation Centre of the Faculty of Mechanical Engineering, Kraljice Marije 16
Belgrade, Serbia
brdjordjevic@mas.bg.ac.rs

Simon Sedmak

https://orcid.org/0000-0002-2674-541X
Innovation Centre of the Faculty of Mechanical Engineering, Kraljice Marije 16
Belgrade, Serbia
simon.sedmak@yahoo.com

Dorin Radu

https://orcid.org/0000-0001-5043-2723
Transilvania University of Brașov, Faculty of Civil Engineering
Brașov, Romania
dorin.radu@unitbv.ro

Abstract

This paper will present a novel approach to supporting a piece of process equipment subjected to long-term exploitation conditions, with the main goal of improving its reliability and safety. Optimising the supports of the process equipment (in this particular case, 16 autoclaves used for coal drying) began by measuring the load at the support points. It was followed by an analysis based on good engineering practice to develop a new technical solution. The old support solution represented a rigid connection between the autoclave envelope and the supporting structure. Meanwhile, the new approach introduced spring supports, thus providing flexible connections between the Autoclave and the structure. This flexibility ensures that the load on the vessel's shell is reduced significantly and that stress distribution at the support points is uniform. Simultaneously, the load distribution in the structure's support zone is significantly more favourable. The economic benefit of such an approach and a reflection on sustainability are also discussed.

Keywords

autoclave, structural response, supports, vibrations, spring elements;

1. Introduction

Depending on its type and working parameters, pressure equipment can be exposed to different conditions during the in-service period. These exploitation conditions can lead to the most dangerous type of failure, i.e. brittle fracture, which results in significant material damages and down-time for the whole installation (Lancaster, 2005; Sedmak et al., 2009; Benac et al., 2016; Benac, 2002; Filipović et al., 2007). Both scientific and engineering practices provide an increasing number of probabilistic methods used for the assessment of failure and equipment (or material) reliability (Mastilovic et al., 2024; Popović et al., 2024; Kirin et al., 2020; Sedmak et al., 2023; Chavoshi et al., 2021; Ruggieri, 2024). These methods can, to a certain extent, predict a safe work life within a given time interval. It should be emphasised that it is necessary to recognise all risks for each of these probabilistic methods in order to adequately apply them (Horváth-Kálmán et al., 2023; Jovanović et al., 2023). Integrity and reliability assessment also includes classic engineering methods, such as non-destructive testing (Kurz et al., 2013; Jarić et al., 2024a, 2024b), which can provide insight into the current damage state but not what caused it. One of the major aspects to consider during downtime of pressure vessel equipment and during monitoring and reconstruction is the economic impact. Recently, all of these aspects were recognised, and all fit into a discipline of cognitive sustainability, representing an interdisciplinary approach that helps determine the sustainability of a proposed solution or process (Zöldy et al., 2022).

Damage to process equipment is often caused by a static load to which such equipment is subjected or by aggressive mediums, which may cause erosion and/or degradation of pressure vessel walls. This was the case with the coal drying Autoclave in question, which was the subject of numerous studies regarding its reconstruction and repairs, such as cases presented by Ilić and Radić (2003), Maneski et al. (2008) and Jovanović et al. (2022). Dynamic loading represents the second most dangerous cause of long-term damage to the material (Németh et al., 2020; Stosiak et al., 2022; Towoju et al., 2023; Leshchinskii et al., 2024; Sedmak et al., 2019; Di Nicola et al., 2024; John et al., 2024) is often less considered in overall structural response on pressure vessel equipment. Dynamic loading caused by vibrations in very "stiff" supports can lead to failure of the whole Autoclave, resulting in downtime, all for a rather "banal" reason – damage of the autoclave support, which (at first glance) does not play any role in the technological process of drying of coal. The fact that there are supports to keep the Autoclave in place and ensure its safe operation is often neglected.

As previously mentioned, the way this pressure equipment was supported could greatly impact its work life when it is subjected to variable load while having an inappropriate technical solution for its support. The original and initial solution for autoclave supports included a stiff connection between the vessels and the load-bearing steel structure. In this example, regarding these specific autoclaves, a very important fact was neglected during their design: autoclaves are equipment subjected to periodic filling and emptying (due to their use – coal drying). Since this represents dynamic loading, such equipment cannot be considered a classic pressure vessel (subjected to internal pressure and/or dilatations due to temperature changes). In this particular case, 16 autoclaves have suffered a significant number of failures while in use due to cracks occurring in the support zone of the Autoclave. This would then result in unplanned production downtimes and additional costs for repairs. All aforementioned factors affect the sustainability of the whole facility, which must guarantee a reliable, safe and constant process of coal drying.

In order to restore pressure equipment functionality, it is necessary to consider all the unfavourable effects that caused it to fail in the first place. Since a common cause of autoclave failure was through-thickness cracks in the support zone, it was concluded that the sole reason lies in the inadequate connection between the Autoclave and the load-bearing structure. Thus, there was a need to assess the overall structural response, with special attention devoted to dynamic loading caused by vibrations.

In order to reach proper conclusions about the cause, a static analysis was performed, along with measuring amplitudes (dynamic loading) during autoclave operation. The measurements and thorough analyses provided the solution that the fixed connection (typically used for pressure vessels) should be replaced with a flexible connection (spring supports), which can absorb impact loads caused by filling, emptying and inadequate operation of this equipment. In this way, favourable load distribution in pressure equipment walls and load-bearing structures can be achieved, resulting in less downtime for the whole facility and less need for repair. A techno-economic analysis along with a cost comparison of the traditional solution (which involves a repair welding procedure of fixed connections) and the new solution (that includes mounting of spring

elements) of the Autoclave was conducted as well, with a purpose of direct indication of the economic and sustainable benefit of the new approach. A thorough analysis of the proposed support solution is offered. It should be emphasised that the analysis of spring supports and the overall structural response of autoclaves was conducted during their operating mode (i.e. under real exploitation conditions) due to time constraints for prototyping and the demands of the energy supply industry.

2. Load Measurements

The fixed connections of the autoclave supporting system exercise unfavourable stress on the shell around them. This state could initiate fatigue cracks, one of the problems observed during previous reconstruction. The technical solution for autoclave support suggested 20 years ago that fixed (rigid) elements proved to be inappropriate for long-term exposure to various loads imposed by working conditions (more about this problem basis can be found in Ilić and Radić (2003), Maneski et al. (2008) and Jovanović et al. (2022)). In order to find an appropriate solution for supporting the Autoclave, the whole analysis was preceded by load measurements in autoclaves subjected to real exploitation conditions. The proposed solution involves placing four spring-damping elements between the support feet of the Autoclave and the steel support (i.e. steel structure) around the Autoclave. The drawing of the Autoclave, its major elements, and the proposed technical support solution are presented in Fig. 1.
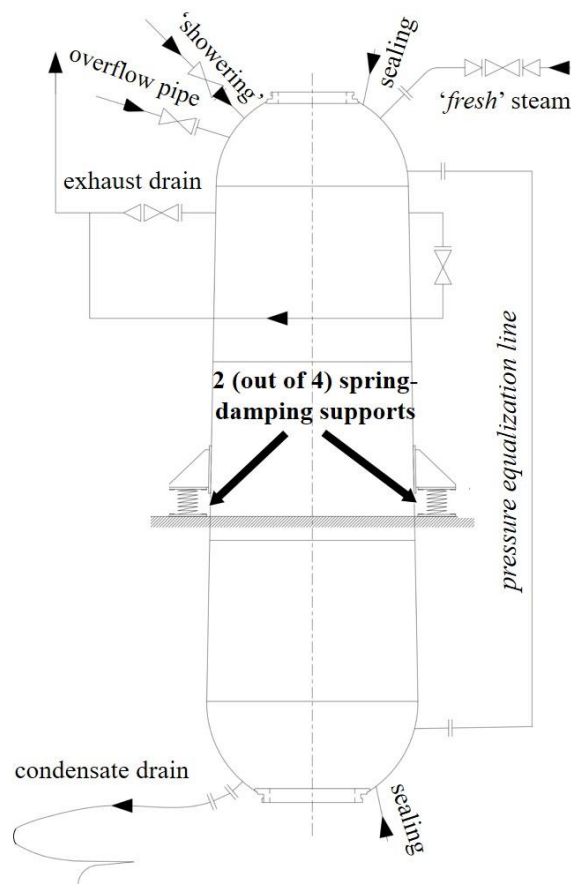
Figure 1. Illustration of the technical solution for Autoclave support with spring-damping supports

Both static and dynamic loads and their influence on overall structural integrity were analysed. Static load analysis was performed first. Magnitudes of static loads to which pressure equipment was subjected were:

- Empty Autoclave (with heat insulation and pipelines) – 410 kN;
- Autoclave filled with raw coal (lignite) – 745 kN;
- Autoclave with coal after drying – 580 kN;
- Autoclave with maximum load (e.g. during a hydro test) – 985 kN.

Measuring dynamic loads during the exploitation of autoclaves was performed using the MEDA software package (version: R2016-1), made by IRIS (Wölfel Engineering). The measurement of dynamic loads in the original supports using a sensor made by the Wölfel Monitoring System model VS-1D. The layout of measuring locations before and after support replacement is shown in Fig. 2. Locations where sensors were installed on the original autoclave supports are shown in Fig. 3.
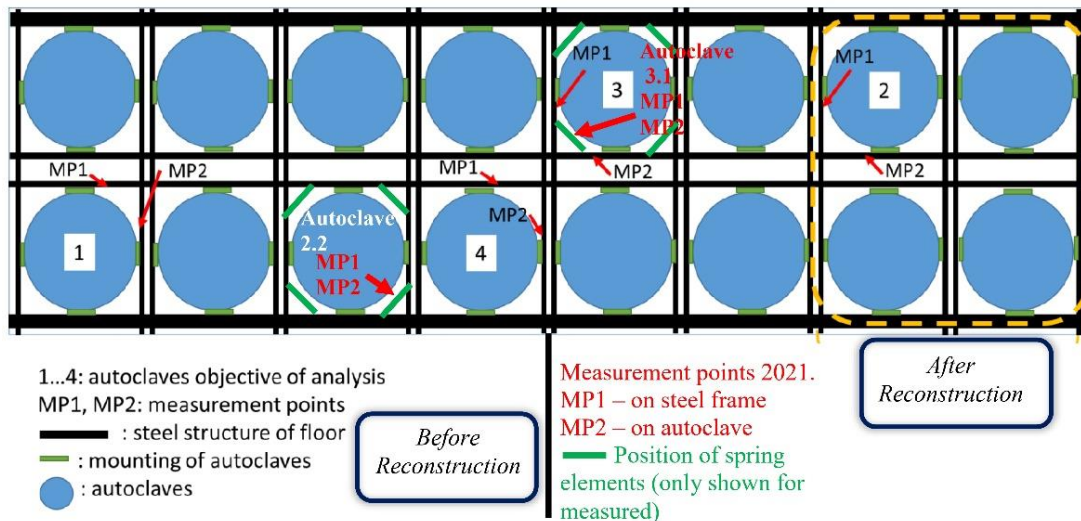

Figure 2. Layout of measurement elements (sensors)
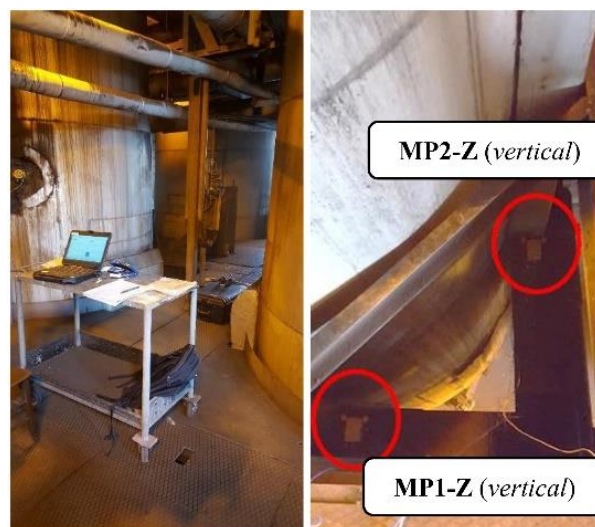
Figure 3. Location of installation of sensors on the original supports of the vessel

After autoclave reconstruction was completed, control measuring of new type supports was conducted, using measuring equipment by the same manufacturer as previously mentioned, along with post-processing of data using this software package. A sensor Piezoelectric accelerometer, S/N LW225020; LW225021 made by PCB model 356A16 was used to measure the dynamic load of new supports. Fig. 4 shows how sensors were installed and their locations for the new supports for two reconstructed autoclaves.
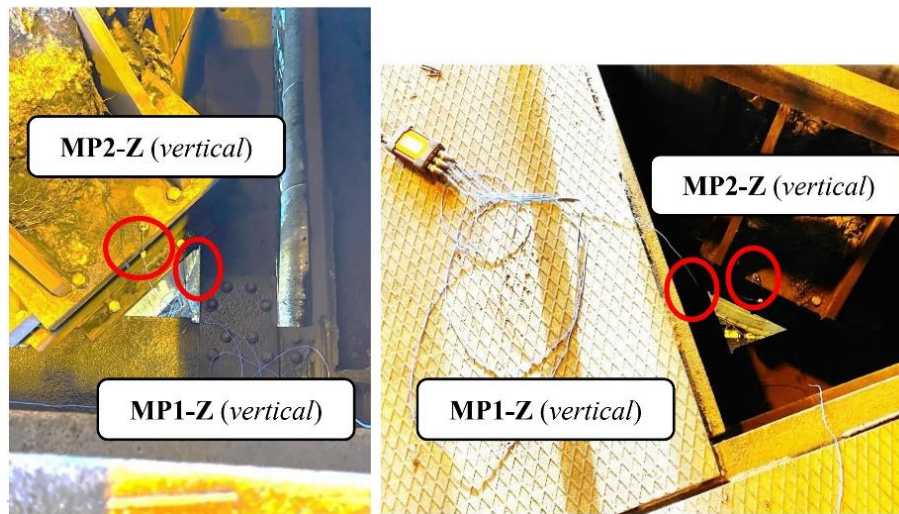
Figure 4. Locations of installation of sensors on the new type of vessel support

3. Analysis of results – vibration measurement

Firstly, vibration measurements were performed before the installation of spring elements on the supports. The results will be used to define spring elements for an improved mounting solution with optimised vibration characteristics during operation. The vibration level is analysed by calculating peak values and RMS values of the measured time series. Results are shown in Table 1.

Table 1 Analysis of operational vibrations

Measurement No.	Date	Time	Autoclave No.	Process	MP1-Z RMS [mm/s]	MP1-Z peak value [mm/s]	MP2-Z RMS [mm/s]	MP2-Z peak value [mm/s]
1	23. July	13:13	1	Loading	0.3	6.6	0.4	8.3
2	23. July	13:19	1	Drying	0.1	1.0	0.1	1.3
3	23. July	13:25	1	Drying	0.1	1.3	0.1	1.3
4	23. July	13:30	1	Drying	0.1	0.7	0.1	0.5
5	23. July	13:36	1	Drying	0.1	0.8	0.1	0.6
6	23. July	13:42	1	Drying	0.1	0.8	0.1	0.9
7	23. July	13:53	1	Drying	0.2	2.9	0.2	2.8
8	23. July	14:03	1	Drying	0.4	26.7	0.5	25.1
9	23. July	14:14	1	Drying	0.1	0.3	0.1	0.3
10	23. July	14:25	1	Drying	0.1	0.3	0.1	0.3
11	23. July	14:36	1	Drying	0.1	0.6	0.1	0.7
12	23. July	14:47	1	Drying	0.1	0.7	0.1	0.5
13	23. July	14:58	1	Drying	0.2	4.5	0.2	5.0
14	23. July	15:09	1	Drying	0.1	0.4	0.1	0.4
15	23. July	15:20	1	Drying	0.1	1.1	0.1	1.2
16	23. July	15:31	1	Unloading	1.3	30.9	1.1	25.7
17	23. July	15:42	1	Loading	0.4	5.0	0.4	8.5
1	24. July	09:26	2	Not in operation	0.5	1.1	0.1	0.6
2	24. July	09:39	2	Not in operation	0.6	1.1	0.1	0.5
3	24. July	10:23	3	Unloading	0.8	44.6	1.0	40.1
4	24. July	10:34	3	Loading	0.4	9.0	0.4	4.6
5	24. July	10:44	3	Drying	0.1	1.3	0.1	1.1
6	24. July	11:23	4	Drying	0.1	0.7	0.1	0.6
7	24. July	11:35	4	Drying	0.2	1	0.1	0.8
8	24. July	11:46	4	Drying	0.2	0.8	0.2	0.9
9	24. July	11:57	4	Unloading	2.0	44.5	1.8	56.9
10	24. July	12:07	4	Loading	6.3	0.3	0.4	8.9

The highest vibration amplitudes are observed during unloading. The loading process shows higher values, too, whereas the drying process shows very low values.

The time series of an unloading process is shown in Fig. 5. and 6. Unloading shows vibrations with a typical shape of impulse loads as excitation. A series of excitations with impulses every 4 seconds follows a sequence without excitation.
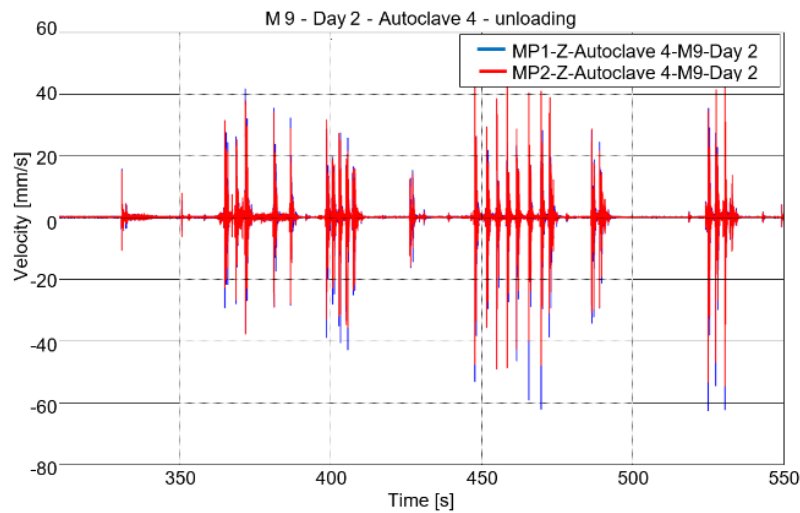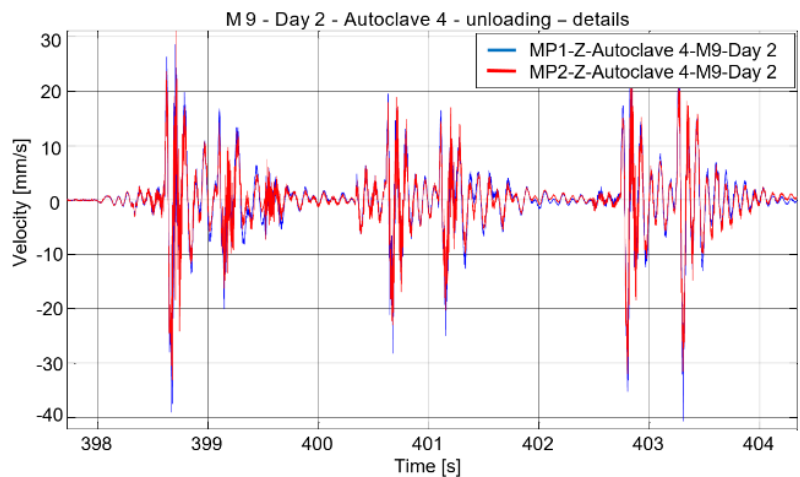

Figure 5. Time series of unloading

Figure 6. Time series of unloading – details

In order to analyse vibrations in the frequency domain, the measured time series have been transformed by Fast Fourier Transformation (FFT). The loading and unloading process results in impulse loads on the vessels and the connected floor. A structure which is excited by impulses responds in its natural frequencies. Therefore, the measured frequency peaks show the structure's natural frequency, which is the objective of this analysis. The results of an unloading process are shown in Fig. 7. Two natural frequencies are identified at around 5 Hz and 11 Hz.
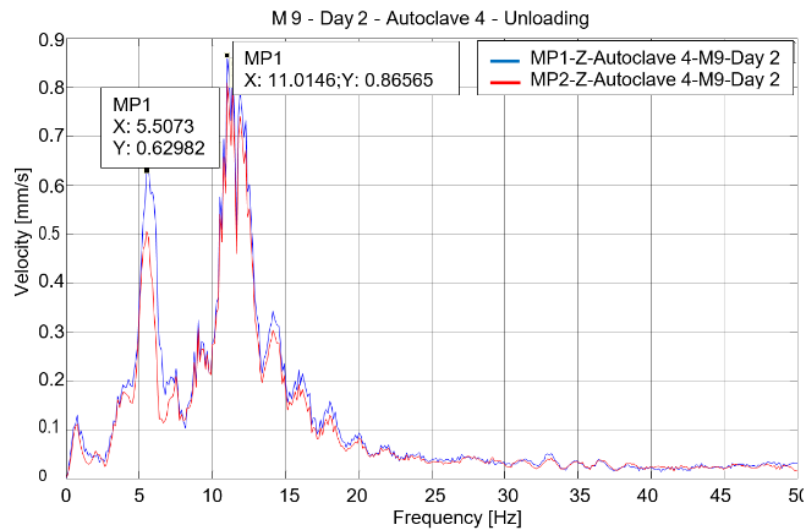
Figure 7. Dominant frequency during the unloading process

Then, vibration measurements were taken after the reconstruction, i.e. installation of the spring elements on the supports. The objective was to compare the results before and after installing spring elements and to show the optimised vibration characteristics during operation. The measured time of the aforementioned FFT has transformed the series to analyse vibrations in the frequency domain. The natural frequency of the autoclaves was calculated to be 4.6 Hz (empty Autoclave) and 3.4 Hz (fully loaded). Measured frequencies range from 4.0 to 4.6 Hz (full) and 4.9 to 5.3 Hz (empty). Whether the "full" load corresponds to the theoretical maximum values could not be detected. However, the deviations are within limits and do not produce any negative effects on the operation (Fig. 8):
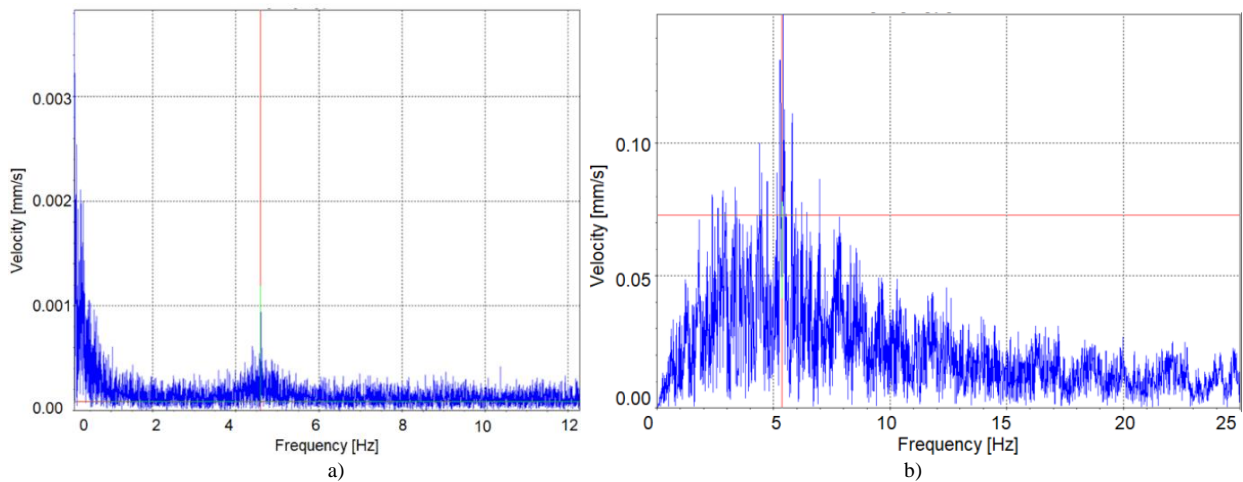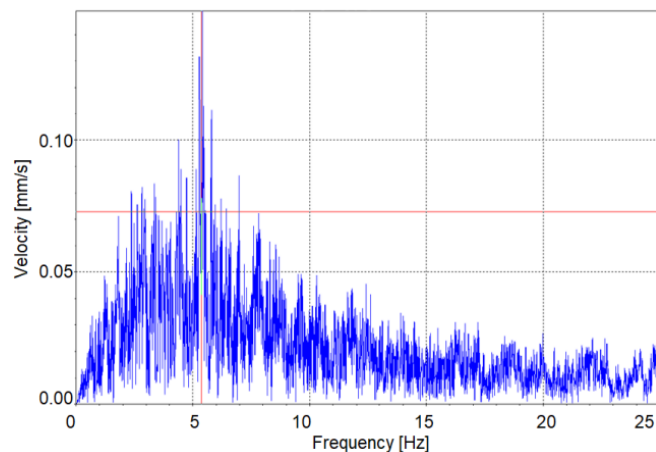
c)

Figure 8. a) Autoclave 3.1, full, dominant peak at 4.5 Hz; b) Autoclave 3.1, full, dominant frequency 4.6 Hz; c) Autoclave 3.1, empty, dominant frequency 5.3Hz

The structural response due to the dynamic behaviour of the autoclaves was significantly improved by the installation of the spring elements, which can be observed from the comparison diagram shown in Fig. 9. The vibration level within the steel beams is significantly lower than before. The peak values in the beams could be reduced from around 40 mm/s to 4 mm/s. As a result, the dynamic forces could be reduced as desired. The measured displacement amplitudes at the measured "worst" load cases, i.e. unloading, are below the predicted ones.
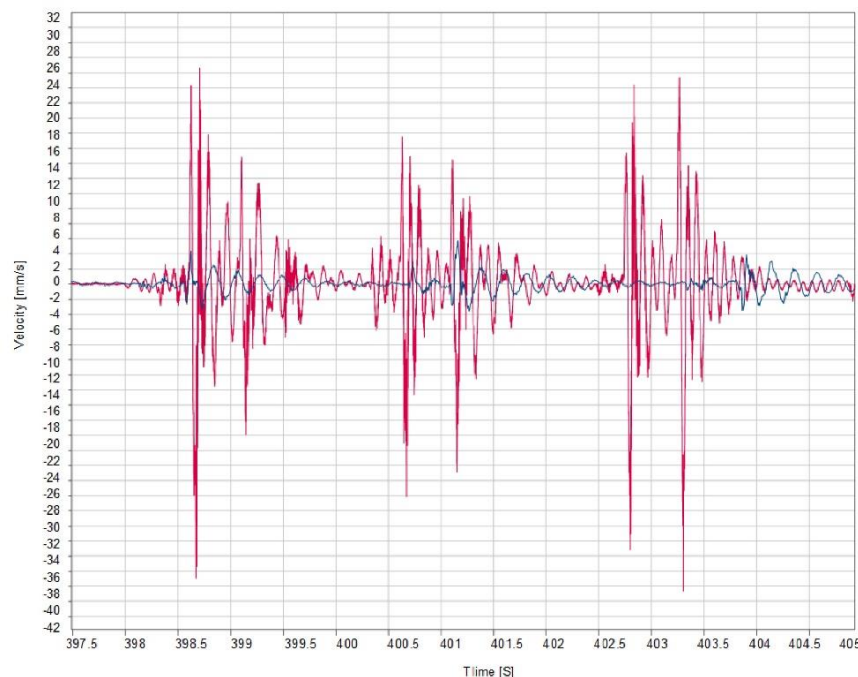
Figure 9. Red line – unloading autoclave MP1 (steelwork, without spring elements); blue line – unloading Autoclave 3.1 MP1 (steelwork with spring elements)

The obtained results of vibration measurement proved that the mounting of proposed spring element supports leads to a decrease in dynamic impacts on the supporting structure and relative displacement between the supporting structure and the Autoclave itself. Indirectly, this will decrease the likelihood of cracks appearing on the autoclave shell and, most importantly, on welded joints. Applying this type of spring-damping support will solve the problem related to high-impact forces and loads during loading/unloading of the Autoclave, which will compensate for radial dilatation as well.

5. Techno-economic analysis and sustainability feature of novel approach

From an engineering point of view, the advantages of the novel approach are obvious; however, economic aspects and compliance with them must also be checked. Economic features of both approaches for 16 autoclaves in the form of techno-economic analysis, with a thorough list of activities, along with a direct comparison of their costs, are presented in Table 2. As can be seen, the new approach demands introducing some new activities compared to the traditional repair process. Activates such as the development of technical documentation, material procurement, manufacturing and delivery of the autoclave bottom lid, flanged ring, and middle and bottom sections of the autoclave shell, procurement and delivery of spring supports for the Autoclave with reinforced load-bearing steel structure for pressure equipment represent the basis of the newly proposed solution for autoclave reconstruction speaking in terms of economy. However, the overall sustainability aspect shows the superiority of the new solution in the long run, primarily in the final factor – the downtime costs due to failure or maintenance. To repair 16 autoclaves in total, which has to be performed every second year (shown by engineering practice in this particular case), 30 days of downtime is required. Taking a daily working capacity of 153 t/per autoclave, severe financial losses are observed compared to losses caused by reconstruction using spring damping elements. From the sustainability perspective, the novel approach for supporting is the better solution, as it requires less additional maintenance work and reduces downtime over the Autoclave's design life.

Table 2. Techno-economic analysis of both approaches used for Autoclave restoring functionality

#	Activities	Autoclave reconstruction (by using the newly proposed spring supports)	Repairing of existing autoclaves (by repairing of existing supports)	Notes
		Cost (EUR)		
1	Development of technical documentation – design documentation and project supervision	137,000.00	0.00	*Not needed for repairs*
2	Development of the repair report and proposal of solution for repairs of damage that had occurred	0.00	40,000.00	*Necessary for any and all repairs, statistically speaking, failures like this occur once per year, per Autoclave.*
3	Material procurement, manufacturing and delivery of the autoclave bottom lid, flanged ring, and middle and bottom sections of the autoclave shell	928,000.00	0.00	*Procurement of new equipment not required for repairs*
4	Procurement and delivery of spring supports for the Autoclave with reinforced load-bearing steel structure for pressure equipment	160,000.00	0.00	*A new solution, as required by the reconstruction*
5	Procurement and delivery of remaining pipes, sheets and equipment, as per project	80,000.00	0.00	*During repairs, there is no need for these replacements*
6	Cost of a Notified Body for pressure equipment engagement regarding manufacturing, installation and final inspections, along with making a non-conformity evaluation report	96,000.00	0.00	*The scope of NDT engagement is smaller during repairs since reconstruction is much more complex regarding monitoring.*
7	Cost of a Notified Body for pressure equipment engagement regarding equipment repairs and issuing all of the necessary documentation	0.00	64,000.00	
8	Manufacturing of temporary support structure for the Autoclave	1,440,000.00	880,000.00	*These activities are identical for repair and reconstruction, although repairs involve significantly fewer work hours on locksmithing and welding activities during installation.*
9	Installation work, including non-destructive testing of welded joints			
10	Cold test			
11	Development of technical and certification documentation			
12	Insulation of the bottom part of the Autoclave			
13	Preparation for finishing works			
14	Costs of downtime due to failure	14,688,000.00	146,880,000.00	*Downtime costs for 40 years (design work life)* • *Reconstruction – 60 days downtime over 40 years* • *Repairs – 30 days downtime every second year* *Daily capacity of 153 t/per autoclave; coal price of 100 EUR/t*
	Total	**17,529,000.00**	**147,864,000.00**	

* Techno-economic analysis refers to 16 autoclaves in total, which represents the number in a facility for coal production in this particular case

4. Conclusion

The application of a novel approach for decreasing dynamic influence on autoclave supports showed improved results in terms of structural response. From this analysis, the following conclusions can be drawn:

- Installed spring elements on supports caused the vibration level within the steel beams to decrease. The final measurements showed that the loads were up to 10 times less than the original rigid connection. The displacement amplitudes at the measured "worst" load cases – unloading – are below the predicted ones. This suggests that replacing fixed (rigid) supports with new ones further improved the integrity of the Autoclave by ensuring support flexibility, providing a favourable stress state in the autoclave shell, and reducing the likelihood of crack formation.
- With this new method, the problem of the occurrence of cracks in the area of the supports on the autoclave casing was solved. In addition, the dynamic load transferred to the object's structure was also reduced.
- The novel approach for autoclave support proposed here offers a sustainable solution applicable to pressure vessel equipment, requiring less additional maintenance and reducing downtime. This results in a more favourable economic outcome than the traditional method involving classic repairs.

Still, some suggestions by the authors of this paper for further work related to autoclave monitoring and the use of risk assessment methods to quantify further the improvements in the reliability of the newly reconstructed Autoclave or assess failure probabilities, which would serve as another indicator of reconstruction quality.

Acknowledgement

References

Benac, D. J. (2002). Failure analysis and life assessment of structural components and equipment. *In ASM International eBooks*, 227–242. DOI: https://doi.org/nmw8

Benac, D. J., Cherolis, N., Wood, D. (2016). Managing cold temperature and brittle fracture hazards in pressure vessels. *Journal of Failure Analysis and Prevention*. 16(1), 55–66. DOI: https://doi.org/nmw7

Chavoshi, S. Z., Bradford, R., Booker, J. (2021). A validated approach for probabilistic structural integrity design code implementation. *Engineering Fracture Mechanics*. 257, 108028. DOI: https://doi.org/nmxc

Di Nicola, F., Lonardi, G., Fantuzzi, N., Luciano, R. (2024). Structural integrity assessment of an offshore platform using RB-FEA. *International Journal of Structural Integrity*. DOI: https://doi.org/nmxm

Filipović, N., Gerić, K., Sedmak, S. (2007). Loading Condition Effect on the Fracture of Welded Thin-walled Storage Tank. *Structural Integrity and Life*. 7(1), 21–28.

Horváth-Kálmán, E., Elek, B. (2023). Risks and the management of construction in the environment of nuclear facilities. *Acta Technica Jaurinensis*. 16(4), 143–151. DOI: https://doi.org/nmxd

Ilić, V., Radić, N. S. (2003). Redesign and damage repair experience related to manufacturing requirements for new "bidons". *Zavarivanje I Zavarene Konstrukcije*. 48(4), 211–214. URL: https://scindeks-clanci.ceon.rs/data/pdf/0354-7965/2003/0354-79650304211I.pdf

Jarić, M., Budimir, N., Petronić, S., Sedmak, S., Vitas. N. (2024a). Analysis of remediation of manifold line damaged by longitudinal crack in the piping elbow of oil and gas well collector. *Structural Integrity and Life*. 24(1), 111–115. DOI: https://doi.org/nmxg

Jarić, M., Petronić, S., Čolić, K., Opačić, M., Svetel, I. (2024b). Analysis of service problems of caustic tanks installed in oil and gas plants. *Structural Integrity and Life*. 24(1), 117–123. DOI: https://doi.org/nmxf

John, E., Boxall, J., Collins, R., Bowman, E., Susmel, L. (2024). Fatigue failure analysis of grey cast iron water pipes accounting for fatigue strength variation. *Engineering Failure Analysis*. 165, 108762. DOI: https://doi.org/nmxn

Jovanović, A., Đorđević, B., Jeremić, L., Milovanović, N.,Smoljanić, T. (2022). Integrity assessment of autoclaves after reconstruction. *Structural Integrity and Life*. 22(3), 347–352.

Jovanović, A., Bakić, G., Golubović, T., Kirin, S., Sedmak, A. (2023). Integrity and Risk Assessment of Reconstructed Steam Line. *Structural Integrity and Life*. 23(3), 367–371.

Kirin, S., Sedmak, A., Zaidi, R., Grbović, A., Šarkočević, Ž. (2020). Comparison of experimental, numerical and analytical risk assessment of oil drilling rig welded pipe based on fracture mechanics parameters. *Engineering Failure Analysis*. 114, 104600. DOI: https://doi.org/nmxb

Kurz, J. H., Jüngert, A., Dugan, S., Dobmann, G., Boller, C. (2013). Reliability considerations of NDT by probability of detection (POD) determination using ultrasound phased array. *Engineering Failure Analysis*. 35, 609–617. DOI: https://doi.org/f5mxkh

Lancaster, J. (2005). Engineering Catastrophes. In: Causes and Effects of Major Accidents. 3rd edition. Woodhead Publishing. ISBN 978-1-84569-016-8.

Leshchinskii, L., Ivanov, V., Lavrova, E., Il'yaschenko, D., Verkhoturova, E.V. (2024). Fracture resistance of the deposited metal under dynamic and cyclic loading. *Structural Integrity and Life*. 24(2), 187–192. DOI: 10.69644/ivk-2024-02-0187

Maneski, T., Milošević-Mitić, V., Anđelić, N., Milović, L. (2008). Overhaul and reconstruction of an autoclave. *Structural Integrity and Life*. 8(3), 171-180.

Mastilovic, S., Djordjevic, B., Sedmak, A., Kirin, S. (2024). Data-driven prediction of fracture toughness size effect in ductile-to-brittle transition using Two-Step-Scaling procedure. *Engineering Fracture Mechanics*, 307, 110339. DOI: https://doi.org/nmw9

Németh, A., Major, Z., Fischer, S. (2020). FEM modelling Possibilities of glued Insulated rail joints for CWR tracks. *Acta Technica Jaurinensis*. 13(1), 42–84. DOI: https://doi.org/nmxh

Popović, I., Đorđević, M., Skerlić, J., Čamagić, I., Kirin, S. (2024). Determining the Reliability Function of the Thermal Power System in Power Plant' Nikola Tesla, Block B1' Using The Weibull Distribution. *Structural Integrity and Life*. 24(2), 145–149. DOI: 10.69644/ivk-2024-02-0145

Ruggieri, C. (2024). A probabilistic model to predict specimen geometry effects on fracture toughness in ferritic-pearlitic steels. *Engineering Fracture Mechanics*, 110493. DOI: https://doi.org/nmts

Sedmak A., Grbović A., Zaidi R., Kirin S., Vitas N., Golubović T., Vučetić I. (2023). Numerical, Analytical and Experimental Determination of Remaining Life of A Pipe With an Axial Crack. *Structural Integrity and Life*. 23(3), 239–244. URL: http://divk.inovacionicentar.rs/ivk/ivk23/239-IVK3-2023-AS-AG-RZ-SK-NV-TG-IV.pdf

Sedmak, S., Grabulov, V., Momčilović, D. (2009). Chronology of Lost Structural Integrity Initiated from Manufacturing Defects in Welded Structures. *Structural Integrity and Life*. 9(1), 39–50. URL: http://divk.inovacionicentar.rs/ivk/ivk09/039-IVK1-2009-SS-VG-DM.pdf

Sedmak, S., Burzić, Z., Perković, S., Jovičić, R., Aranđelović, M., Radović, L., Ilić, N. (2019). Influence of welded joint microstructures on fatigue behaviour of specimens with a notch in the heat affected zone. *Engineering Failure Analysis*. 106, 104162. DOI: https://doi.org/nmxk

Stosiak, M., Karpenko, M., Deptuła, A. (2022). Coincidence of pressure pulsations with excitation of mechanical vibrations of hydraulic system components: An experimental study. *Cognitive Sustainability*. 1(2). DOI: https://doi.org/gr2bdn

Towoju, O., Enochoghene, S., Adeyemi, J. (2023). Structural Integrity of Turbine Stator Blades Using Different Super Alloys with Internal Cooling at Fluid Temperature Range of 600 K – 700 K. *Acta Technica Jaurinensis*. 16(4), 152–157. DOI: https://doi.org/nmxj

Zoldy, M., Szalmane Csete, M., Kolozsi, P. P., Bordas, P., & Torok, A. (2022). Cognitive Sustainability. Cognitive Sustainability. 1(1). DOI: https://doi.org/10.55343/cogsust.7

A Federated Multi-Task Meta-Learning Framework for Collaborative Perception and Adaptation in Connected and Automated Vehicles

Chandra Priya J[1*],

https://orcid.org/0000-0003-3891-0950

Department of Computer Science and Engineering, Department of Mechanical Engineering,
Mepco Schenk Engineering College
Sivakasi, India
jchandrapriya@mepcoeng.ac.in

Dhinesh Balasubramanian[2]

https://orcid.org/0000-0003-2687-9095,

Department of Computer Science and Engineering, Department of Mechanical Engineering,
Mepco Schenk Engineering College
Sivakasi, India
dhineshbala91@mepcoeng.ac.in

Abstract

Connected and Automated Vehicles (CAVs) operate in dynamic environments influenced by traffic patterns and pedestrian behaviour, which complicates the development of real-time navigation algorithms with voluminous data communicated by CAVs, raising privacy concerns. To address these challenges, we propose Federated Learning (FL) for concurrent and collaborative learning across fleets to generate privacy-preserving personalised models that adapt to diverse environments. Combining graph neural networks (GNNs) enables the real-time modelling of vehicle interactions and captures spatial and temporal dependencies. Utilising a message-passing paradigm, GNNs facilitate dynamic communication among vehicles. By aggregating information from neighbouring nodes, GNNs learn meaningful feature representations that enhance perception in CAVs, improving their responsiveness and enabling route optimisation and traffic flow enhancement. In this work, Model Predictive Control (MPC) influences GNNs to improve vehicle state prediction. It optimises control actions that minimise a cost function, such as travel time, fuel consumption, or collision risk, while adhering to constraints. GNNs enable the system to adapt its predictive model based on evolving vehicle relationships. At the same time, MPCs re-optimise control actions in response to these changes, allowing the CAVs to manage trajectories and make informed decisions adaptively in dynamic environments. The Federated Multi-Task Meta-Learning Framework for Collaborative Perception and Adaptation in Connected and Automated Vehicles (FedCAV) model is deployed across Edge, Fog, and Cloud layers to optimise performance, with a total estimated latency of 210 ms for 10 vehicles, influenced by local model training. Its low first-byte latency of 25 to 34 ms enhances communication efficiency, facilitating real-time decision-making and adaptive interactions.

1. Introduction

Connected and Automated Vehicles (CAVs) are equipped with technology that allows them to communicate with each other and their environment, enhancing road safety and operational efficiency. CAVs utilise many technologies, including sensors, cameras, and machine learning algorithms, to perceive their environment and make informed decisions (Gregurić et al., 2023). Applications of CAVs span autonomous driving, intelligent traffic management, and vehicle-to-everything (V2X) communication, all of which contribute to improved traffic flow and reduced vehicular accidents (Chellapandi et al., 2023). Despite their potential, CAVs face challenges like data privacy concerns, high communication overhead, and the need for robust machine learning models that can learn from diverse driving environments.

Federated Learning (FL) is increasingly recognised as an essential technology for enhancing the capabilities of CAVs within the Internet of Vehicles (IoV). It enables vehicles to collaboratively learn from data while preserving privacy, addressing significant concerns related to data sharing in cooperative perception and decision-making processes (Drissi, 2023).

Integrating FL with IoT facilitates improved traffic management and routing optimisation, contributing to sustainable urban development (Zhang et al., 2023). However, data heterogeneity and the need for efficient client selection remain critical, as they can affect model accuracy and increase communication overhead (Liu et al., 2024). Additionally, the introduction of blockchain in FL frameworks can mitigate data silos and enhance privacy protection by ensuring high-quality data source selection (Acar and Sterling, 2023). Furthermore, robust defence mechanisms are essential to counteract emerging cyber threats in mobile environments, ensuring the integrity of federated learning systems (Pang et al., 2024).

Collaborative perception and adaptation in CAVs enhance situational awareness and operational efficiency. Research indicates that integrating vehicle-road systems, such as self-powered vehicle-road integrated electronics (SVRIE), significantly improves collaborative sensing capabilities, allowing vehicles to accurately monitor road conditions and tyre health (Qu et al., 2024). Additionally, unicast-based cooperative perception strategies enable CAVs to share information dynamically, optimising resource allocation and enhancing decision-making in mixed traffic scenarios (Shao et al., 2024). The evolution from single-agent to collaborative detection models, facilitated by Vehicle-to-Everything (V2X) communication, further underscores the importance of real-time data sharing to address occlusion and sensor failures (Jahn et al., 2024; Yang and Liu, 2023). Moreover, unified frameworks that integrate perception and mapping tasks can enhance the accuracy and consistency of situational awareness, demonstrating the potential for collaborative mapping among vehicles (Khoshkangini et al., 2022).

Research Query: How can federated learning enable privacy-preserving, real-time collaborative perception and adaptive decision-making in CAVs operating in dynamic environments?

The proposed FedCAV framework combines three core methodologies: (1) federated multi-task meta-learning to train shared models across CAV fleets, (2) GNNs with Model Predictive Control (MPC) to model spatial-temporal vehicle interactions and optimise real-time trajectory planning, and (3) a multi-layered edge-fog-cloud architecture that balances latency and computational efficiency.

The rest of the article is organised as follows. Section 2 elaborates on previous research relevant to our problem statement, while Section 3 provides the Federated Multi-Task Meta-Learning Framework for Collaborative Perception and Adaptation in Connected and Automated Vehicles (FedCAV) system overview. A novel architecture is pictographically illustrated in Section 4 with the key elements such as FedCAV: system architecture with federated learning-enabled DSRC algorithm for V2V communication, cooperative decision-making in CAVs with GNN and MPC, state-space representation of CAV dynamics, and model personalisation with cloud analytics. Section 5 is concerned with the observed effects of the performance analysis. Finally, the conclusion gives a summary and critique of the findings, paving the way for identifying areas for further research.

2. Literature review

Recent studies (Avianto et al., 2022; Priya et al., 2024) have highlighted the importance of federated multi-task learning (MTL) frameworks that accommodate diverse data distributions across vehicles. The work on applying FL in CAVs with MTL enhances model performance with the challenges associated with training models on non-IID (Independent and Identically Distributed) data, which is common in vehicular environments. The algorithms based on Expectation-Maximization (EM) can be computationally intensive, which holds back their practical implementation. This is especially true in resource-constrained environments typical of CAVs, where computational power and communication bandwidth are limited. Although the framework addresses non-IID data distributions, the inherent variability in data across different vehicles can still pose challenges. If the local data distributions are too diverse, the model may fail to generalise well across different tasks, leading to suboptimal performance for certain clients.

The need for rapid adaptation in CAVs has led to the exploration of federated meta-learning techniques focused on enhancing the efficiency of federated meta-learning (Chai et al., 2021). Their research demonstrates how meta-learning can facilitate quick adaptation to new driving conditions, thereby improving the overall performance of CAVs. This is particularly crucial in real-time scenarios, where vehicles must respond promptly to changing environments and traffic conditions (You et al., 2024). Validation on larger-scale and diverse datasets that capture the complexity of real-world traffic conditions is necessary to ensure the scalability and generalizability of the approach. The paper does not address potential security and privacy concerns associated with federated learning, such as model inversion or membership inference attacks.

The state-of-the-art studies present a model-agnostic approach to federated learning that supports multi-task optimisation with the significance of maintaining data privacy while enabling vehicles to learn collaboratively from diverse datasets. This approach is particularly relevant for CAVs, where sensitive data must be protected (Basnet and Ali, 2021). By

employing clustered federated learning techniques, the authors demonstrate how vehicles can optimise their learning processes without compromising individual data security, thus addressing a critical challenge in the deployment of FL in CAVs (Bas et al., 2021). Although the framework focuses on fast convergence, the actual speed of adaptation to rapidly changing environments may still be limited. Factors such as network latency, communication delays, and the computational constraints of edge devices can hinder the responsiveness of CAVs in critical situations.

The adaptability of federated learning is further demonstrated through research that examines its applications for Lidar super-resolution in automotive contexts (Zheng et al., 2020). This work highlights the necessity of tailoring learning algorithms to meet the unique requirements of CAVs, particularly in enhancing their perception capabilities within intricate environments. Vehicles can improve their situational awareness by utilising federated learning while preserving privacy and adopting safer and more efficient navigation systems (Okegbile et al., 2023; Barrachina et al., 2019). However, the study by Zheng et al. (2020) does not specifically tackle the temporal aspects of vehicle movements or how federated learning might be employed to recognise and adjust to these dynamics over time.

The cross-silo heterogeneous model federated multi-task learning strategy enables vehicles from different silos to collaborate, promoting the exchange of knowledge and experiences across various driving environments (Han et al., 2022; Cao and Zoldy, 2021). This collaboration contributes to creating resilient and flexible CAV systems that perform effectively in diverse conditions. It can be concluded that cross-silo federated learning can greatly improve the adaptability and efficiency of CAVs, thus advancing the development of smarter transportation systems (Qu et al., 2020; Tollner et al., 2024). However, the effectiveness of this cross-silo federated learning approach is heavily dependent on a strong infrastructure, which includes high-speed internet and dependable communication networks. In areas where infrastructure is lacking, the effectiveness of this method may be considerably compromised.

3. FedCAV: Generic Overview

Figure 2 depicts a multi-layered architecture for CAVs, enabling collaborative perception and adaptation through the seamless integration of edge, fog, and cloud computing. The automotive layer encompasses individual CAVs engaging in Vehicle-to-Vehicle (V2V) communication using decentralised networking resources, while the edge layer facilitates local decision-making through real-time interaction modelling and processing complex vehicle interactions. The fog layer aggregates data from multiple CAVs, coordinates GNN-based vehicle interactions, performs predictive analytics, and manages traffic through Vehicle-to-Network (V2N) communication. Meanwhile, the cloud layer provides centralised data processing, extensive analytics on aggregated data, and model training and updates, ensuring dynamic communication and adaptation across all layers for optimised performance and decision-making in CAV systems.
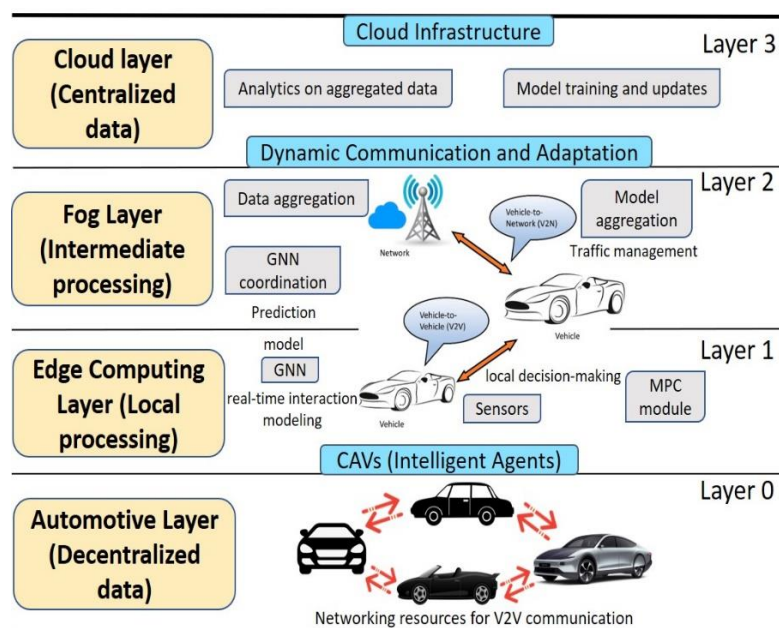

Fig.2. FedCAV: Multi-layered federated learning framework

3.1. Layer 0: Automotive Layer (Decentralised Data)

The Automotive Layer, comprising intelligent agents, serves as the foundational tier of the architecture, featuring individual CAVs that actively engage in direct communication with one another. These vehicles utilise advanced V2V communication protocols to facilitate seamless data exchange in a decentralised manner, thereby enhancing situational awareness and collaborative decision-making while eliminating reliance on centralised infrastructure. This decentralised approach provides a more resilient network and empowers vehicles to operate autonomously and responsively in dynamic environments.

3.2. Layer 1: Edge Computing Layer (Local Processing)

The Edge Layer involves local decision-making by utilising onboard sensors and computational resources to process real-time data, allowing vehicles to respond immediately to their environment. Integrated within this layer is a Model Predictive Control (MPC) module, which empowers the vehicle to make informed decisions based on predictive models, optimising its actions for efficiency. Additionally, the layer facilitates real-time interaction modelling, enabling vehicles to dynamically assess and adapt to interactions with their surroundings and other vehicles, thereby enhancing overall adaptive behaviour. GNNs are used to analyse and interpret the complex web of vehicle interactions, significantly improving the decision-making processes and promoting a more intelligent and responsive autonomous driving experience. This layer is responsible for real-time data processing and decision-making by utilising GNNs to analyse data from the interface layer, capturing spatial and temporal dependencies essential for CAV operations. This layer focuses on real-time analysis and decision-making, where analysis enables immediate processing of data collected from CAVs, traffic signals, and pedestrian movements. Decision-making implements control actions based on the processed data, ensuring timely responses to dynamic traffic conditions.

3.3. Layer 2: Fog Layer (Intermediate Processing)

The Fog Layer serves as an intermediate processing hub, where data from multiple CAVs is aggregated to form a comprehensive dataset, enabling GNNs to coordinate vehicle interactions and optimise performance based on the aggregated information. This layer also conducts predictive analytics to predict traffic conditions while combining data from various vehicles to support extensive traffic management strategies, enhance overall decision-making capabilities, and facilitate cohesive operational frameworks through Vehicle-to-Network (V2N) communication between CAVs and centralised infrastructure. An intermediary between the edge and cloud layer facilitates intermediate processing to reduce latency by processing data closer to the source before sending it to the cloud—moreover, storage for temporarily holding data or model updates, optimising bandwidth and response times.

3.4. Layer 3: Cloud Layer (Centralized Data)

The Cloud Layer is dedicated to centralised data processing and storage, facilitating comprehensive analysis and decision-making. This layer exploits advanced analytics on aggregated data collected from diverse sources, yielding valuable insights that enhance operational efficiency. It enables model training and updates, managing the development of complex models, including those utilising GNNs from the lower layers, and ensuring that these models are continually refined and disseminated throughout the architecture to maintain optimal performance and adaptability. The cloud layer provides extensive computational resources for model training and updates. Its primary functions include model training that involves aggregating data from multiple edge devices to train a global model. This process ensures the model learns from diverse driving environments, enhancing its robustness. Model updates distribute updated models back to edge devices, allowing them to refine their local models based on the latest global insights.

4. FedCAV: System Architecture

The FedCAV architecture consists of multiple layers, such as Edge, Cloud, and a Fog layer, each serving distinct functions in data processing and model training. Layer 0 focuses on the V2V communication using a Federated Learning-Enabled Dedicated Short-Range Communications Algorithm. Layer 1 handles cooperative decision-making in CAVs with GNN and MPC. Layer 2 manages dynamic communication and adaptation with the state-space representation of CAV dynamics, while Layer 3 is dedicated to model personalisation, as depicted in Figure 3.

4.1 Federated Learning-Enabled DSRC (FL-DSRC) for V2V Communication

Step 1: Network Initialization and Model Distribution

Each vehicle V_i initialises its communication and model training system by initialising the parameters,

- Max_Range ← Range of DSRC communication (e.g., 300 meters)
- Max_Slots ← Number of time slots available per frame (e.g., 100 slots)
- $Model_i^0$ ← Global model distributed to the vehicle V_i by a central server
- Current_Channel ← Default DSRC channel

Step 2: Local Model Training

Each vehicle trains its local model using its data $Model_i^{t+1} \leftarrow Model_i^t - \eta \nabla L_i (Model_i^t)$ where η is the learning rate and ∇L_i is the gradient of the loss function L_i concerning the model parameters.

Step 3: Channel Sensing and Access for Model Update Sharing

To share model updates, each V_i senses the communication channel before transmitting,

$RSSI_i$ ← Received Signal Strength Indicator for each nearby V_i

$$SINR_i = \frac{P_i \cdot G_{i,j}}{\sum_{k \neq 1} P_k \cdot G_{k,j} + N_j}$$

If $SINR_i$ is below a threshold, V_i waits before transmitting its model update. V_i, with a sufficiently high $SINR_i$ transmits their model updates.

Step 4: Time Slot Assignment Using TDMA

To prevent collisions during model update sharing, a Time Division Multiple Access (TDMA) scheme is used where slot selection is based on $Slot_i \leftarrow \min (Slot_{avail} (t))$, with which V_i chooses the earliest available slot for transmission. If a collision is detected, a backoff mechanism is applied, Backoff $Time_i$ = random (0, Max_Backoff_Time), where random(a,b) generates a random number between a and b. Messages are prioritised based on their importance (e.g., emergency messages) with $P_{emergency} > P_{control} > P_{informational}$ where P represents priority with queue management Q_i ← Sort messages in descending order of priority and transmit messages in order from the queue.

Step 5: Model Aggregation and Update

Once vehicles have transmitted their local model updates, they aggregate the models,

$$Global\ Model_j^{t+1} = \frac{1}{n} \sum_{i=1}^{n} wi \cdot Model_i^{t+1}$$

where n is the number of vehicles participating in the update, and w_i is the weight assigned to each V_i update, which is proportional to the size of the local dataset or based on the quality of the update.

Step 6: Data Transmission and Update Sharing

Vehicles transmit their aggregated models during their assigned time slot

$TX_{model,j} \leftarrow Global\ Model_j^{t+1}$

Step 7: Adaptive Communication and Learning

After transmission, the communication channel is re-evaluated, and vehicles adapt their transmission strategies.

$$SINR_i(t+1) \leftarrow \frac{P_i \cdot G_{i,j}}{\sum_{k \neq 1} P_k \cdot G_{k,j} + N_j}$$

If SINR drops, vehicles adapt by selecting a better communication channel or adjusting transmission power. Vehicles adjust their learning rate or other training parameters based on the quality of communication, $\eta(t+1) = \eta(t) \cdot$ Adaptation Factor, where the Adaptation Factor depends on factors like latency and SINR.

Step 8: Periodic Global Model Update and Synchronisation

Periodically, vehicles synchronise with the central server or other vehicles to update the global model. The central server aggregates models from all vehicles and distributes the updated global model.

$$Global\ Model_{server}^{t+2} \leftarrow \frac{1}{m} \sum_{j=1}^{m} wi \cdot Model_j^{t+1}$$

4.2 Cooperative Decision-Making in CAVs with GNN and MPC

CAVs are represented as a graph $G = (V, E)$, where V is the set of vertices representing the vehicles in the fleet, and E is the edges representing the communication links between vehicles. Each vehicle $V_i \in V$ is associated with a feature vector $x_i \in R^d$, where d is the dimension of the feature space that encodes information such as position p_i, speed s_i direction d_i, and status $stat_i$ as idle or active. Edges have features representing the nature of vehicle interactions, such as distance or communication quality $E = [e_{ij}$ for $(V_i, V_j) \in E]$. The message m_{ij} sent from node V_j to node V_i is defined as $m_{ij} = Msg(x_j, x_i, e_{ij})$. The updated state of node V_i is computed by aggregating messages from its neighbours

$x_i^{(t+1)} = $ Aggregate $(\{m_{ij} \mid j \in N(i)\}) + x_i^{(t)}$

where $N(i)$ is the set of neighbours of node V_i, and t denotes the iteration step in the message-passing process. The vehicle updates its state based on the aggregated messages

$x_i^{(t+1)} = $ Update$(x_i^{(t)}, m_i)$

This iterative process allows vehicles to adapt their states based on the collective information from the fleet, leading to improved decision-making. The information sharing and effective action coordination among vehicles can be mathematically formulated as an optimisation problem aimed at minimising a collective loss function across all vehicles in a fleet. The primary goal of cooperative decision-making among CAVs is to optimise their collective behaviour while considering individual vehicle objectives. This optimisation can be framed mathematically as min u $\sum_{i=1}^{n} Li(xi, u)$ where u represents the control inputs for the vehicles (e.g., acceleration, steering angle), L_i (x_i, u) is the loss function for vehicle V_i, which quantifies its performance based on its state x_i and the shared control inputs u and n is the total number of vehicles in the fleet.

4.1 State-Space Representation of CAV Dynamics

The dynamics of a CAV can be represented using a state-space model. Let the state of the vehicle at the time t be represented as $X(t) = [x(t), y(t), \phi(t), v(t)]^T$ where $x(t)$ and $y(t)$ are the V_i position coordinates, $\phi(t)$ is the heading angle, and $v(t)$ is the velocity. The control inputs are defined as $u(t) = [a(t), \delta(t)]^T$ where $a(t)$ is the acceleration and $\delta(t)$ is the steering angle. The V_i dynamics can be described by the following kinematic equations $\dot{x}(t) = v(t) \cos(\phi(t))$, $\dot{y}(t) = v(t) \sin(\phi(t))$, $\dot{\phi}(t) = v(t)/L \tan(\delta(t))$ and $\dot{v}(t) = a(t)$ where L is the distance between the front and rear axles. MPC optimises the control inputs over a finite prediction horizon N to minimise a cost function J,

$J = \sum_{k=0}^{N-1}(\alpha. $ cost $_{travel}(t+k) + \beta.$ cost $_{collision}(t+k))$

where cost$_{travel}(t) = $ travel time(t)+fuel consumption(t) and collision cost$_{collision}(t) = \sum_{j=N} collision\ risk(t, j)$ where N represents neighbouring vehicles and pedestrians. The GNN predicts the future trajectories of surrounding vehicles based on historical data and is represented as $X_{pred}(t+k) = f(h_i^{(t)}, u(t), k)$ where f is a function learned by the GNN that outputs the predicted state. The predicted trajectories from the GNN are incorporated into the MPC optimisation problem. The MPC then updates its cost function to include collision avoidance constraints based on these predictions

$J = J + \lambda . \sum_{k=1}^{N} collision\ risk\ (X_{pred}(t+k))$

where λ is a weighting factor that adjusts the importance of collision avoidance. The MPC continuously re-optimises control actions based on the updated state predictions from the GNN, enabling adaptive trajectory management in dynamic environments.
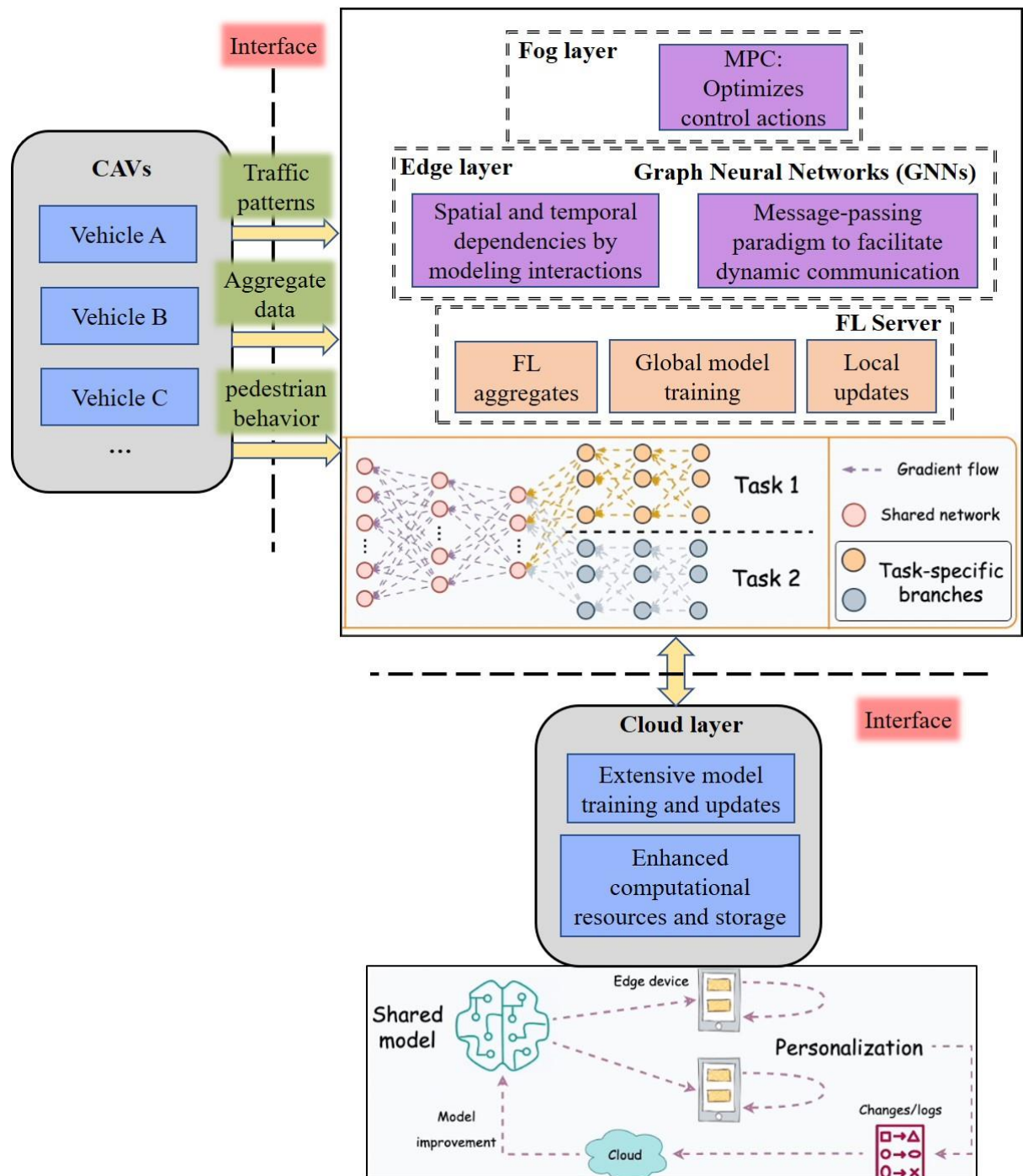
Fig.3: FedCAV for collaborative perception, dynamic communication, and model adaptation in CAVs

4.2 Model Personalisation with Cloud Analytics

The Cloud Layer functionality aggregates local models, performs extensive training with regularisation, personalises models for individual vehicles, and manages storage and retrieval of model data. After updating the global model, the Cloud Layer supports model personalisation by tailoring the global model to specific vehicles based on their unique environments or preferences. Each V_i receives a personalised model $Model_i^{personal}$ from the Cloud $Model_i^{personal} = Global\ Model^{t+2} + \Delta_i$ where Δ_i is the personalisation term that accounts for Vi's specific conditions or preferences. The personalisation term can be derived from V_i unique data or feedback and is typically small compared to the global model. The cloud receives periodic updates or feedback from edge and fog layers to continually improve the shared model, with each V_i sending feedback on the model performance, $feedback_i^{t+3}$, which can be used to refine the global model further

$$\text{Model}_{\text{improved}}{}^{\text{t+4}} = \text{Global Model}^{\text{t+2}} + \frac{1}{N} \sum_{i=1}^{N} Feedback_i{}^{\text{t+3}}$$

The feedback may include error rates, performance metrics, or other indicators that help improve the model in future iterations. This setup ensures that the federated learning process is scalable, efficient, and adaptable to the dynamic needs of CAVs.

5. Performance Analysis

The inference from the key latency components in the V2V communication using an FL-DSRC algorithm highlights several critical aspects of the communication process and their impact on overall latency. Local model training introduces variability in latency, primarily influenced by the dataset size and model complexity. In a hypothetical scenario with 10 vehicles, the estimated latency is approximately 210 ms, with local model training contributing the most at 80 ms, followed by data transmission at 40 ms, and channel sensing and access at 10 ms. This sample (Table 1) demonstrates how various stages of optimisation contribute to the overall reduced latency in FedCAV:

Table 1. Estimated Latency of Federated Learning Components in a Vehicular Network

Component	Estimated Latency (ms)
Network Initialization	20
Local Model Training	80
Channel Sensing and Access	10
Time Slot Assignment	5
Model Aggregation	10
Data Transmission	40
Adaptive Communication	5
Periodic Global Model Update	30
Total Estimated Latency	**210 ms**
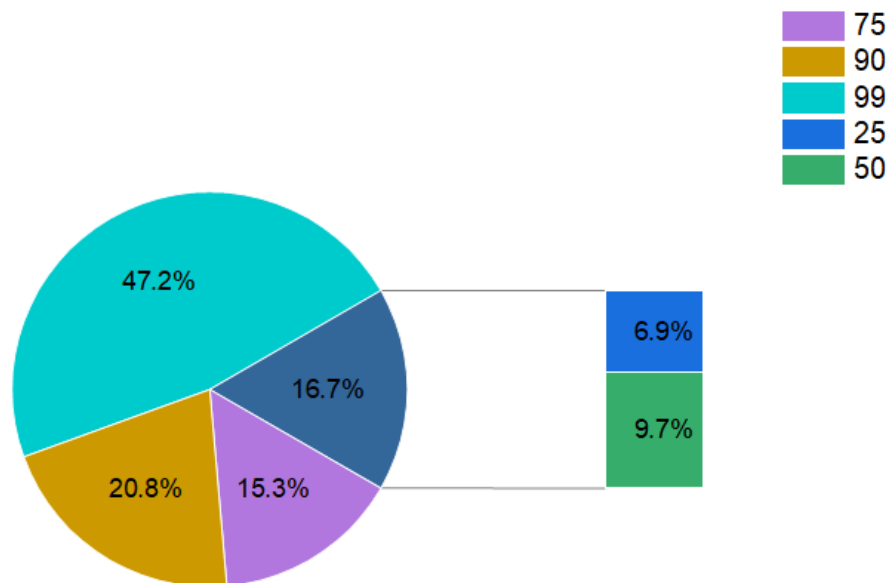
Fig.4: FedCAV latency measure

The relatively low first-byte latency observed in the FedCAV system significantly enhances communication efficiency. With initial latency values starting at 25 ms and only rising to 34 ms at the highest observed level, the system demonstrates a robust capability to maintain swift communication among vehicles. This efficiency is important for real-time decision-making and data sharing, enabling vehicles to respond promptly to dynamic road conditions and traffic scenarios. The gradual increase in communication time relative to latency indicates that the system can effectively manage higher loads without a drastic decline in performance, thereby supporting seamless interactions among connected vehicles. As a result, the FedCAV framework optimises operational efficiency and enforces a safer driving environment by ensuring that vehicles

can communicate effectively and adaptively in real time. This positive relationship between low latency and enhanced communication efficiency underscores the potential of FedCAV systems to revolutionise the landscape of CAVs.

Table 2 First-byte latency and time

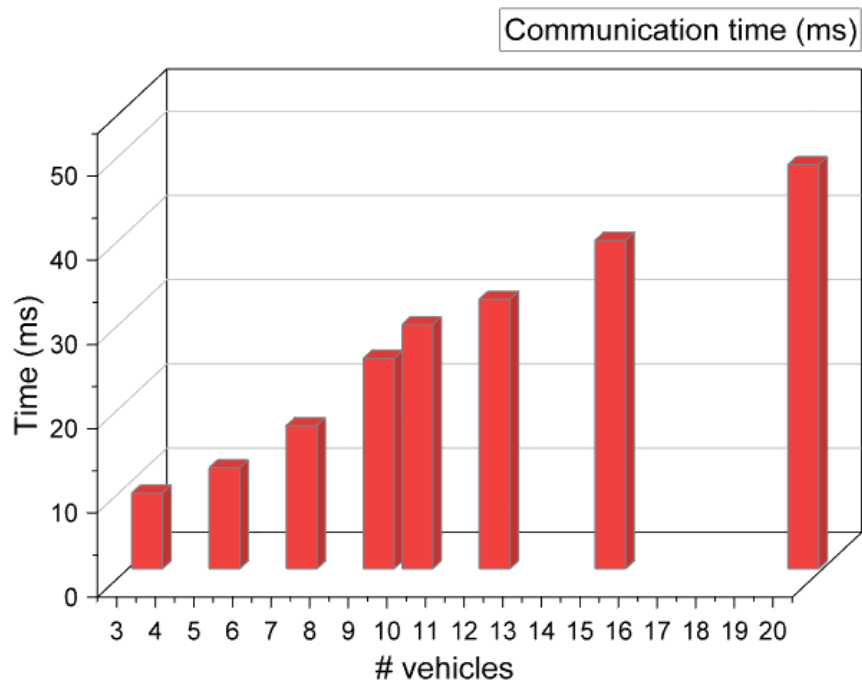| First-byte Latency	Time (ms) Proposed FedCAV
25	5
50	7
75	11
90	15
99	34

Fig.5: Communication times versus number of vehicles

The plot in Figure 5 shows a clear trend where communication time increases with the number of vehicles. There is a positive correlation between the two variables. The increase in communication time is not linear, with more evident escalation as the number of vehicles grows. For instance, the communication time increases by 3 ms from 3 to 5 vehicles (9 ms to 12 ms) and by 4 ms from 9 to 10 vehicles (25 ms to 29 ms). As the number of vehicles rises, the communication time escalates due to increased data-sharing demands among vehicles, greater complexity in managing communication, and possible interference and delays in data transmission.

6. Practical implications in real-world scenarios

- ✓ By utilising V2V communication, CAVs share real-time data about their ambiences, improving situational awareness and reducing the likelihood of accidents through collaborative decision-making.
- ✓ The integration of edge, fog, and cloud computing allows predictive analytics to predict traffic conditions, enabling better traffic flow management and reducing congestion through coordinated vehicle interactions.
- ✓ The multi-layered architecture supports local decision-making through onboard sensors, allowing vehicles to respond immediately to dynamic environments, thus enhancing responsiveness in driving behaviour.
- ✓ The decentralised approach prevents failures and enables vehicles to operate autonomously, even in challenging conditions.
- ✓ The Cloud analytics for model personalisation enables custom-configured driving models to individual vehicle conditions and preferences, enhancing user experience and operational efficiency.

7. Conclusion

In this work, the FedCAV framework is presented as a robust multi-layered architecture that effectively integrates edge, fog, and cloud computing to enhance the performance of CAVs. The system optimises communication efficiency and reduces latency using federated learning, graph neural networks, and model predictive control. It also facilitates real-time decision-making and adaptive vehicle interactions, ultimately contributing to a safer and more responsive driving environment. The performance analysis indicates that while local model training significantly contributes to overall latency, the system maintains low first-byte latency and efficiently manages higher communication loads, promoting real-time responsiveness and safety in dynamic driving environments. Future research directions should prioritise enhancing the scalability of federated learning algorithms to support larger vehicle fleets while ensuring effective low latency. Advanced optimisation techniques can be explored for real-time decision-making and adaptive communication strategies in highly dynamic environments to maximise system performance and resilience in diverse traffic scenarios.

References

Acar, B., Sterling, M. (2023). Ensuring Federated Learning Reliability for Infrastructure-Enhanced Autonomous Driving. *Journal of Intelligent and Connected Vehicles*. 6(3), 125–135. DOI: http://doi.org/10.26599/JICV.2023.9210009

Avianto, D., Harjoko, A., Afiahayati (2022). CNN-Based Classification for Highly Similar Vehicle Model Using Multi-Task Learning. *Journal of Imaging*. 8(11), 293. DOI: http://doi.org/10.3390/jimaging8110293

Barrachina, D. G., Boldizsár, A., Zoldy, M., Torok, A. (2019). Can Neural Network Solve Everything? Case Study of Contradiction in Logistic Processes with Neural Network Optimisation. *2019 Modern Safety Technologies in Transportation (MOSATT)*. Kosice, Slovakia. 21–24, DOI: http://doi.org/10.1109/MOSATT48908.2019.8944120

Bas, J., Zou, Z., Cirillo, C. (2021). An interpretable machine learning approach to understanding the impacts of attitudinal and ridesourcing factors on electric vehicle adoption. *Transportation Letters*. 15(1), 30–41. DOI: http://doi.org/10.1080/19427867.2021.2009098

Basnet, M., Ali, M. H. (2021). A Deep Learning Perspective on Connected Automated Vehicle (CAV) Cybersecurity and Threat Intelligence. *ArXiv*. abs/2109.10763. DOI: http://doi.org/10.48550/arXiv.2109.10763

Cao, H., Zoldy, M. (2021). MPC Tracking Controller Parameters Impacts in Roundabouts. *Mathematics*. 9(12), 1394. DOI: http://doi.org/10.3390/math9121394

Chai, H., Leng, S., Chen, Y., Zhang, K. (2021). A Hierarchical Blockchain-Enabled Federated Learning Algorithm for Knowledge Sharing in Internet of Vehicles. *IEEE Transactions on Intelligent Transportation Systems*. 22(7), 3975–3986. DOI: http://doi.org/10.1109/TITS.2020.3002712

Chellapandi, V. P., Yuan, L., Brinton, C. G., Żak, S. H., Wang, Z. (2023). Federated Learning for Connected and Automated Vehicles: A Survey of Existing Approaches and Challenges. *IEEE Transactions on Intelligent Vehicles*. 9(1), 119–137. DOI: http://doi.org/10.1109/TIV.2023.3332675

Drissi, M. (2023). A state-of-the-art on federated learning for vehicular communications. *Vehicular Communications*. 45(3), 100709. DOI: http://doi.org/10.1016/j.vehcom.2023.100709

Gregurić, M., Vrbanić, F., Ivanjko, E. (2023). Impact of federated deep learning on vehicle-based speed control in mixed traffic flows. *Journal of Parallel and Distributed Computing*.186(2), 104812. DOI: http://doi.org/10.1016/j.jpdc.2023.104812

Han, M., Xu, K., Ma, S., Li, A., Jiang, H. (2022). Federated learning-based trajectory prediction model with privacy preserving for intelligent vehicle. *International Journal of Intelligent Systems*. 37(1), 10861–10879. DOI: http://doi.org/10.1002/int.22987

Jahn, L. L., Park, S., Lim, Y., An, J., Choi, G. (2024). Enhancing lane detection with a lightweight collaborative late fusion model. *Robotics and Autonomous Systems*. 175(1),104680. DOI: http://doi.org/10.1016/j.robot.2024.104680

Khoshkangini, R., Mashhadi, P., Tegnered, D., Lundström, J., Rögnvaldsson, T. S. (2022). Predicting Vehicle Behavior Using Multi-task Ensemble Learning. *Expert Systems with Applications*. 212(6), 118716. DOI: http://doi.org/10.1016/j.eswa.2022.118716

Liu, S., Yu, G., Yin, R., Yuan, J., Qu, F. (2024). Communication and Computation Efficient Federated Learning for Internet of Vehicles with a Constrained Latency. *IEEE Transactions on Vehicular Technology*. 73(1), 1038–1052. DOI: http://doi.org/10.1109/TVT.2023.3309088

Okegbile, S. D., Cai, J., Zheng, H., Chen, J., Yi, C. (2023). Differentially Private Federated Multi-Task Learning Framework for Enhancing Human-to-Virtual Connectivity in Human Digital Twin. *IEEE Journal on Selected Areas in Communications*. 41(11), 3533–3547. DOI: http://doi.org/10.1109/JSAC.2023.3310106

Pang, Y., Zhu, X., He, T., Liu, S., Zhang, Z., Lv, Q., Yi, P., Lee, C. (2024). AI-Assisted Self-Powered Vehicle-Road Integrated Electronics for Intelligent Transportation Collaborative Perception. *Advanced Materials*. 36(36), e2404763. DOI: http://doi.org/10.1002/adma.202404763

Priya, J.C., Nanthakumar, G., Choudhury, T., Karthika, K. (2024). 6G-DeFLI: enhanced quality-of-services using distributed hash table and blockchain-enabled federated learning approach in 6G IoT networks. *Wireless Networks*. 31(1), 361–375. DOI: http://doi.org/10.1007/s11276-024-03759-5

Qu, Y., Gao, L., Luan, T. H., Xiang, Y., Yu, S., Li, B., Zheng, G. (2020). Decentralised Privacy Using Blockchain-Enabled Federated Learning in Fog Computing. *IEEE Internet of Things Journal*. 7(6), 5171–5183. DOI: DOI: http://doi.org/10.1109/JIOT.2020.2977383

Qu, K., Zhuang, W., Ye, Q., Wu, W., Shen, X. (2024). Model-Assisted Learning for Adaptive Cooperative Perception of Connected Autonomous Vehicles. *IEEE Transactions on Wireless Communications*. 23(8), 8820–8835. DOI: http://doi.org/10.1109/TWC.2024.3354507

Shao, Z., Yang, K., Sun, P., Hu, Y., Boukerche, A.F. (2024). The evolution of detection systems and their application for intelligent transportation systems: From solo to symphony. *Computer Communications*. 225(6), 96–119. DOI: http://doi.org/10.1016/j.comcom.2024.06.015

Tollner, D., Ziyu, W., Zöldy, M., Török, Á. (2024). Demonstrating a new evaluation method on ReLU based Neural Networks for classification problems. *Expert Systems with Applications*. 250(6), 123905. DOI: http://doi.org/10.1016/j.eswa.2024.123905

Yang, Z., Liu, C. (2023). Unified Perception and Collaborative Mapping for Connected and Autonomous Vehicles. *IEEE Network*. 37(4), 273–281. DOI: http://doi.org/10.1109/mnet.017.2300121

You, L., Zhu, R., Kwan, M., Chen, M., Zhang, F., Yang, B., Wong, M. S., Qin, Z. (2024). Unraveling adaptive changes in electric vehicle charging behavior toward the postpandemic era by federated meta-learning. *The Innovation*. 5(2):100587. DOI: http://doi.org/10.1016/j.xinn.2024.100587

Zhang, X., Liu, J., Hu, T., Chang, Z., Zhang, Y., Min, G. (2023). Federated Learning-Assisted Vehicular Edge Computing: Architecture and Research Directions. *IEEE Vehicular Technology Magazine*. 18(4), 75–84. DOI: http://doi.org/10.1109/MVT.2023.3297793

Zheng, Z., Ruan, T., Wei, Y., Yang, Y., Mei, T. (2020). VehicleNet: Learning Robust Visual Representation for Vehicle Re-Identification. *IEEE Transactions on Multimedia*. 23, 2683–2693. DOI: http://doi.org/10.1109/TMM.2020.3014488

Mathematical Model Derivation of Protean In-Wheel-Motor Used in EV Applications

Mahmoud Said Jneid

https://orcid.org/0000-0001-5407-285X
Department of Automotive Technologies, Budapest University of Technology and Economics, Budapest, Hungary
mah.jneid@edu.bme.hu

Peter Harth

https://orcid.org/0000-0003-4400-3986
Department of Automotive Technologies, Budapest University of Technology and Economics, Budapest, Hungary
harth.peter@kjk.bme.hu

Abstract

A Protean in-wheel-motor (IWM) is a special type of permanent magnet synchronous motor developed by Protean Electric for direct drive electric vehicle applications. The Protean IWM features a high fault-tolerance substantial for EV applications by dividing the stator into eight independent sub-motors. Each sub-motor features a balanced three-phase system with a spanning of 45º/360º mechanical/electrical on the stator periphery. In total, there are $8 \times 3 = 24$ phases on the stator distributed with a displacement between any two subsequent phases of 15º/120º mechanical/electrical. In this paper, the mathematical model of a Protean motor in a synchronous rotor frame *(d-q)* is derived based on a set of Park transforms corresponding to each sub-motor spatial and electrical distribution. The set of Park transforms is then adapted into one generalised Park transform that can be applied to any sub-motor by introducing an angle representing the beginning of each sub-motor.

Keywords
Protean, in-wheel-motor, sub-motor, fault-tolerance, mathematical model

1. Introduction

The rapid evolution of electric vehicles (EVs) has driven the demand for advanced motor technologies that offer high efficiency, reliability, and integration simplicity. In-wheel motors (IWMs) have become a groundbreaking technology for vehicle electrification, providing improved efficiency, reduced size, and greater design versatility compared to conventional onboard motors (Said Jneid et al., 2020). In addition, EVs that use IWMs as propulsion systems transport the traditional centralised vehicle motion control into allocated control through independent wheel torque control (Said Jneid, 2024). This does not only simplify the vehicle structure, but also takes the vehicle dynamic control integration to new levels where main elements (sensors, actuators) in the vehicle can be shared among different systems allowing for a holistic control with a reduced number of elements, smaller space, and lower costs (Said Jneid, 2024). The integration can happen not only on the hardware level but also on the vehicle system control level. For instance, IWMs actuators can be integrated with brake system actuators, namely electronic wedge brakes (EWBs) producing a pure brake-by-wire (BBW) system (Said Jneid and Joukhadar, 2019; Said Jneid, Zöldy and Harth, 2023). Brake actuator integration allows the blending of frictional and regenerative braking torques enabling functionalities of anti-lock braking system (ABS) based on an electronic version, namely regenerative anti-lock braking system (RABS) (Said Jneid and Harth, 2023a). On the vehicle control system level, IWMs allow the integration between different advanced chassis active-safety systems (ACAS) such as ABS and traction control system (TCS) (Said Jneid and Harth, 2023c), ABS, traction control systems (TCS), and torque vectoring (TV) (Said Jneid and Harth, 2023c, 2023b, 2023d). Several leading automotive and tyre manufacturers have introduced the conceptual designs of IWMs. Inspired by early conceptual IWMs, several companies have introduced advanced IWMs today, each distinguished by unique design, specifications, and target applications (Said Jneid, 2024). Permanent Magnet Synchronous

Motors (PMSMs) are the ideal option for IWMs due to their high torque density, attributed to utilising Neodymium permanent magnets(Deepak et al., 2023; Feng et al., 2023). In terms of magnetic design, essential IWMs utilise radial flux configuration where the magnetic lines are aligned radially between the stator and the rotor across the air gap (Said Jneid, 2024). Recently, several companies have adopted axial flux topology for IWMs as they boast impressive power and torque densities strongly required for EV applications.

As a radial flux IWM, the Protean drive stands out as a cutting-edge solution designed to meet the unique challenges of EV applications(Hilton, 2016). Developed by Protean Electric, this innovative motor integrates the drive system directly into the wheels, eliminating the need for traditional drivetrains and significantly enhancing the overall vehicle design (Perovic, 2012; Fraser, 2018). The Protean IWM is a specialised permanent magnet synchronous motor (PMSM) engineered for direct-drive applications. Its design is notable for its high fault tolerance, a critical feature for ensuring reliability in EVs (Whitehead and Hilton, 2018). This is achieved by dividing the stator into eight independent sub-motors, each with a balanced three-phase system. These sub-motors are distributed around the stator periphery, with each one covering a 45° mechanical span or 360° electrical span (Perovic, 2012). This modular approach enhances fault tolerance, simplifies maintenance, and improves overall performance. A significant aspect of the Protean IWM's design is its ability to maintain performance even in the event of a failure in one or more sub-motors. This is crucial for the operational reliability of EVs, where motor failure can lead to significant downtime and safety concerns (Ifedi et al., 2012). The distributed nature of the sub-motors ensures that the motor can continue to operate, even with reduced performance, thereby providing a level of redundancy that is highly valued in automotive applications (Ifedi et al., 2011). In this paper, we delve into the mathematical modelling of the Protean IWM given in a synchronous rotor frame *(d-q)*.

To obtain the mathematical model for the Protean sub-motors, it is essential to first understand the motor winding configuration. In total, there are 24 phases distributed across eight sub-motors (8-sub-motor × 3-phase = 24). Each sub-motor occupies of 45º mechanical angle (mech.) on the stator periphery. The angle between two phases belonging to the same sub-motor is 15º mech. Phase A_1 of the sub-motor 1 starts at angle 0º mech., follows phase B_1 at 15º, and phase C_1 at angle 45º. Following, the sub-motor 2 A_2 phase begins at 45º, B_2 at 60º, and phase C_2 at 75º. This pattern repeats for the remaining six sub-motors. Figure 1 illustrates a schematic for the mechanical span and phase distributions of each Protean sub-motor along with the dedicated number of poles. Each sub-motor's phases are denoted by the letters A_n, B_n, and C_n, with '*n*' indicating the sub-motor number (*n*=1 to 8). The complete motor is designed with a 72/64 slots/poles configuration. Each phase of any sub-motor is distributed for three coils, resulting in a total of nine coils occupying nine slots on the stator. The number of poles corresponding to each sub-motor is eight, resulting in a mechanical angle reserved by each sub-motor of 45º as depicted in Figure 1 corresponding to an electrical angle of 360º. The electrical angle between the two phases is 15º × 8-Poles = 120º. Figure 2 presents a schematic diagram for sub-motor phase angle distributions in electrical degrees. Table 1 provides the mechanical and electrical span on the machine periphery with three-phase spatial and electrical angle distributions of each sub-motor.
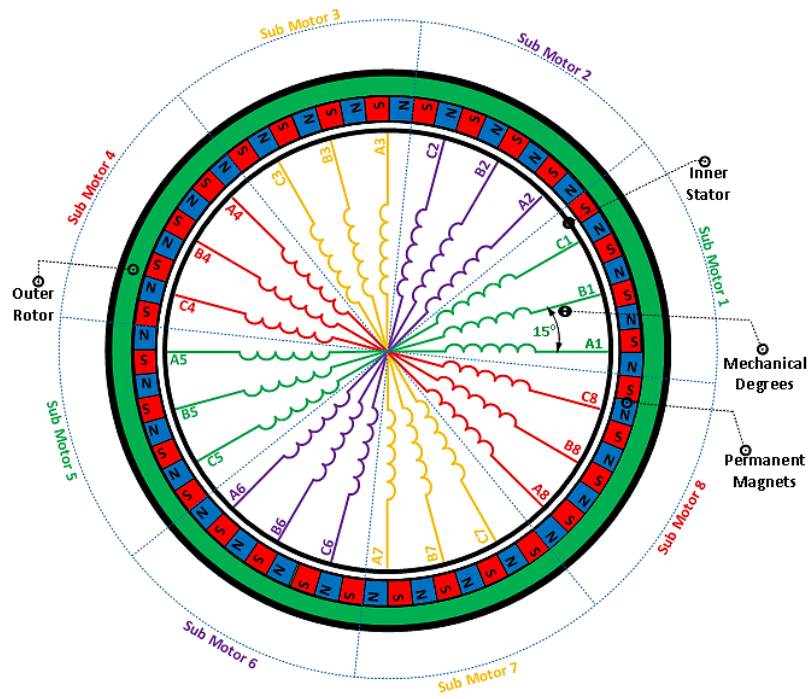
Figure 1. The mechanical span and phase angle distributions of each Protean sub-motor.
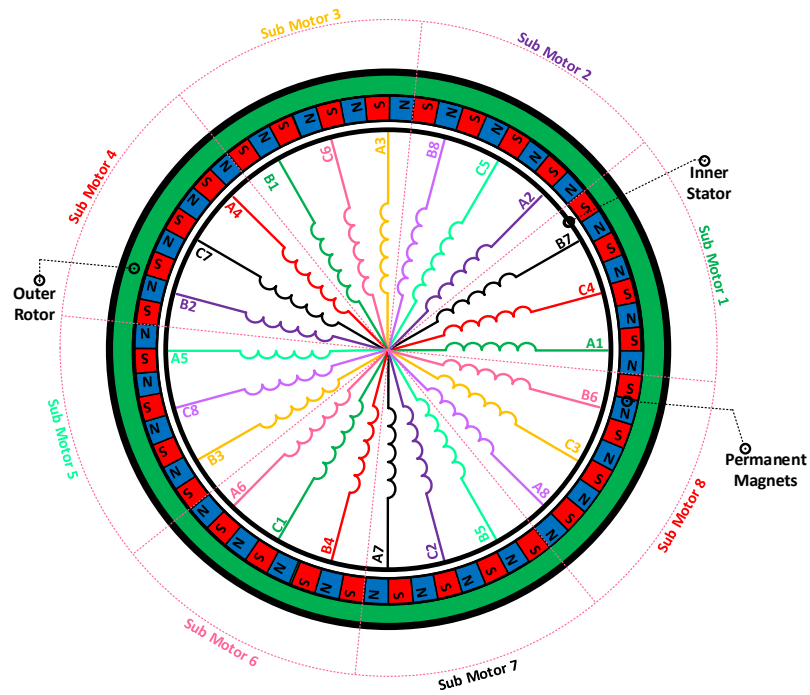

Figure 2. The electrical span and phase angle distributions of each of the Protean sub-motors.

Table 1. The mechanical and electrical span on the machine periphery with a spatial and electrical three-phase distribution of each sub-motor.

Sub-motor No. (n)	Span Angle [Mech]	Span Angle [Elec]	Phase A Angle [Mech/ Elec]	Phase B Angle [Mech/ Elec]	Phase C Angle [Mech/ Elec]
1	0°–45°	360°	0° / 0°	15° / 120°	30° / 240°
2	45°–90°	360°	45° / 45°	60° / 165°	75° / 285°
3	90°–135°	360°	90° / 90°	105° / 210°	120° / 330°
4	135°–180°	360°	135° / 135°	150° / 255°	165° / 15°
5	180°–225°	360°	180° / 180°	195° / 300°	210° / 60°
6	225°–270°	360°	225° / 225°	240° / 345°	255° / 105°
7	270°–315°	360°	270° / 270°	285° / 30°	300° / 150°
8	315°–360°	360°	315° / 315°	330° / 75°	345° / 195°

2. Protean IWM Mathematical Model Given In The Stationary Reference Frame (A, B, C)

To obtain a simplified mathematical model for the Protean motor, the following considerations were imposed:

- Uniform air gap with constant width;
- Negligible magnetic leakage, as well as iron losses;
- Gaussian distribution of the magnetic field along the air gap;
- Perfect symmetry for the stator windings, i.e., equal resistances and inductances;
- Star point for each sub-motor is not connected;
- The mutual flux between the phase C_n of any sub-motor (n) and the phase A_{n+1} of the following sub-motor is neglected.

The voltage and flux for any balanced three-phase Protean sub-motor are given through the following equations:

$$u_{a_n} = R_s i_{a_n} + \frac{d\varphi_{a_n}}{dt} \tag{1}$$

$$u_{b_n} = R_s i_{b_n} + \frac{d\varphi_{b_n}}{dt} \tag{2}$$

$$u_{c_n} = R_s i_{c_n} + \frac{d\varphi_{c_n}}{dt} \tag{3}$$

$$\varphi_{a_n} = l_s i_{a_n} + M_s i_{b_n} + M_s i_{c_n} + \varphi_{fa_n} \tag{4}$$

$$\varphi_{b_n} = M_s i_{a_n} + l_s i_{b_n} + M_s i_{c_n} + \varphi_{fb_n} \tag{5}$$

$$\varphi_{c_n} = M_s i_{a_n} + M_s i_{b_n} + l_s i_{c_n} + \varphi_{fc_n} \tag{6}$$

where:

$u_{a_n}, u_{b_n}, u_{c_n}$: three-phase voltages of sub-motor *(n)*.

$i_{a_n}, i_{b_n}, i_{c_n}$: three-phase currents of sub-motor *(n)*.

$\varphi_{a_n}, \varphi_{b_n}, \varphi_{c_n}$: three-phase fluxes of sub-motor *(n)*.

$\varphi_{fa_n}, \varphi_{fb_n}, \varphi_{fc_n}$: three-phase flux linkages of each sub-motor *(n)*.

R_s, l_s, M_s: stator phase resistance, self-inductance, and mutual inductance of any sub-motor *(n)*, respectively.

The three-phase induced voltages are given as follows:

$$e_{a_n} = \varphi_{fa_n}\omega_r \cos(\theta_e - (n-1)\theta_{sm}) \tag{7}$$

$$e_{b_n} = \varphi_{fb_n}\omega_r \cos\left(\theta_e - \frac{2\pi}{3} - (n-1)\theta_{sm}\right) \tag{8}$$

$$e_{a_n} = \varphi_{fa_n}\omega_r \cos(\theta_e - \frac{4\pi}{3} - (n-1)\theta_{sm}) \tag{9}$$

Since all sub-motors' start points are not connected, the sum of the three-phase currents equals zero. Consequently, the equations for the voltages of the previous sub-motors can be rewritten as follows:

$$L_s \frac{di_{a_n}}{dt} = u_{a_n} - R_s i_{a_n} + e_{a_n} \qquad (10)$$

$$L_s \frac{di_{b_n}}{dt} = u_{b_n} - R_s i_{b_n} + e_{b_n} \qquad (11)$$

$$L_s \frac{di_{c_n}}{dt} = u_{c_n} - R_s i_{c_n} + e_{c_n} \qquad (12)$$

where:

$e_{a_n}, e_{b_n}, e_{c_n}$: the three-phase induced voltages of sub-motor *(n)*.

L_s: the stator phase transient inductance of any sub-motor *(n)*.

ω_r: mechanical rotor speed of Protean motor.

θ_e: rotor position in electrical degrees, equal $d\theta_e/dt = \omega_{re}$.

ω_{re}: electrical rotor speed of Protean motor, equal $\omega_{re}\ P\omega_r$.

P: rotor pole pairs of any sub-motor *(n)*.

θ_{sm}: angle between two same phases of subsequent sub-motors (e.g., A_1, A_2) equals 45°.

n: sub-motor number in the Protean motor, takes the range $n = 1\ to\ 8$.

The electromagnetic torque equation for any sub-motor *(n)* in the Protean motor is expressed in terms of the three-phase currents and electromagnetic forces according to the following:

$$T_{em_n} = \frac{1}{\omega_r}\left(e_{a_n} i_{a_n} + e_{b_n} i_{b_n} + e_{c_n} i_{c_n}\right) \qquad (13)$$

The total torque of the Protean motor is the sum of all sub-motor torques, according to the following:

$$T_{em_n} = \frac{1}{\omega_r}\left(e_{a_n} i_{a_n} + e_{b_n} i_{b_n} + e_{c_n} i_{c_n}\right) \qquad (14)$$

$$T_{em_{Eq}} = \sum_{n=1}^{8} T_{em_n} R \qquad (15)$$

The rotor mechanical speed is given as follows:

$$J_r \frac{d\omega_r}{dt} = T_{em_{Eq}} - T_L \qquad (16)$$

With

$$T_L = (F_r + F_w + F_x)\omega_r \qquad (17)$$

where:

J_r: the rotor moment of inertia, T_L: the motor's total load.

$T_{em_{Eq}}$: equivalent electromagnetic torque of Protean motor (all sub-motors),

F_r, F_w: friction coefficient of rotor and wheel, respectively.

F_x: wheel's longitudinal force.

Figure 3 illustrates the complete block diagram of Protean sub-motors in a stationary reference frame *(ABC)*.
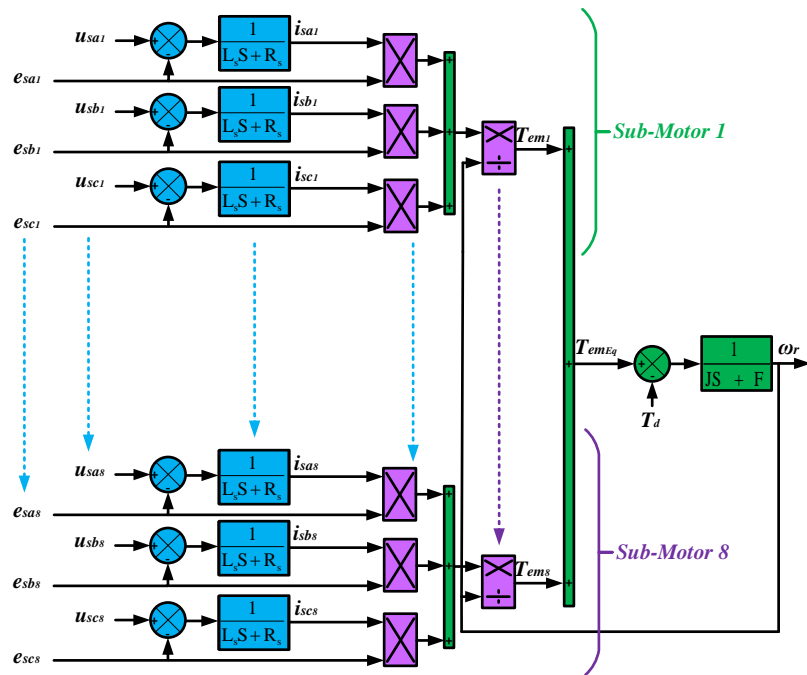
Figure 3. Block diagram of Protean sub-motors in a stationary reference frame *(ABC)*.

3. Protean In-Wheel-Motor Model Given in the Synchronous Reference Frame *(d-q)*

The mathematical model that describes the Protean IWM in the synchronous rotor frame *(d-q)* can be obtained by performing a Park transform from stationary three-axis frame *ABC* into synchronous two-axis frame *d-q* for each sub-motor equation set. First, the three-axis stationary frame *ABC* quantities are projected onto the two-axis stationary frame α-β (Clarke transform), which are rotated at the synchronous speed, resulting in orthogonal rotating components *d-q*. Equation (18) presents the Park transform for sub-motor 1.

$$\begin{bmatrix} f_{d_1} \\ f_{q_1} \end{bmatrix} = n_P \begin{bmatrix} \cos(\theta) & \cos(\theta - \frac{2\pi}{3}) & \cos(\theta - \frac{4\pi}{3}) \\ -\sin(\theta) & -\sin(\theta - \frac{2\pi}{3}) & -\sin(\theta - \frac{4\pi}{3}) \end{bmatrix} \begin{bmatrix} f_{A_1} \\ f_{B_1} \\ f_{C_1} \end{bmatrix}, n = 1 \tag{18}$$

The previous matrix can transform the first sub-motor's electrical quantities (voltage, current, and flux) from the three-axis system into the two-axis system. Figure 4 illustrates the Protean sub-motors' phase displacement in stationary α-β and synchronous *d-q* reference frames. The Park transform for sub-motor two can be obtained by subtracting the displacement angle of 45° from (18), as follows:

$$\begin{bmatrix} f_{d_2} \\ f_{q_2} \end{bmatrix} = n_P \begin{bmatrix} \cos(\theta - \frac{\pi}{4}) & \cos(\theta - \frac{2\pi}{3} - \frac{\pi}{4}) & \cos(\theta - \frac{4\pi}{3} - \frac{\pi}{4}) \\ -\sin(\theta - \frac{\pi}{4}) & -\sin(\theta - \frac{2\pi}{3} - \frac{\pi}{4}) & -\sin(\theta - \frac{4\pi}{3} - \frac{\pi}{4}) \end{bmatrix} \begin{bmatrix} f_{A_2} \\ f_{B_2} \\ f_{C_2} \end{bmatrix} \tag{19}$$

Similarly, the Park transform for the third sub-motor is obtained by subtracting an angle of 90° according to (20):

$$\begin{bmatrix} f_{d_3} \\ f_{q_3} \end{bmatrix} = n_P \begin{bmatrix} \cos(\theta - \frac{\pi}{2}) & \cos(\theta - \frac{2\pi}{3} - \frac{\pi}{2}) & \cos(\theta - \frac{4\pi}{3} - \frac{\pi}{2}) \\ -\sin(\theta - \frac{\pi}{2}) & -\sin(\theta - \frac{2\pi}{3} - \frac{\pi}{2}) & -\sin(\theta - \frac{4\pi}{3} - \frac{\pi}{2}) \end{bmatrix} \begin{bmatrix} f_{A_3} \\ f_{B_3} \\ f_{C_3} \end{bmatrix} \tag{20}$$

Based on the previous calculations, a general form of the Park transform can be derived for any sub-motor according to (21):

$$\begin{bmatrix} f_{d_n} \\ f_{q_n} \end{bmatrix} = n_P \begin{bmatrix} \cos(\theta - (n-1)\theta_{sm}) & \cos\left(\theta - \frac{2\pi}{3} - (n-1)\theta_{sm}\right) & \cos\left(\theta - \frac{4\pi}{3} - (n-1)\theta_{sm}\right) \\ -\sin(\theta - (n-1)\theta_{sm}) & -\sin\left(\theta - \frac{2\pi}{3} - (n-1)\theta_{sm}\right) & -\sin\left(\theta - \frac{4\pi}{3} - (n-1)\theta_{sm}\right) \end{bmatrix} \begin{bmatrix} f_{A_n} \\ f_{B_n} \\ f_{C_n} \end{bmatrix} \tag{21}$$
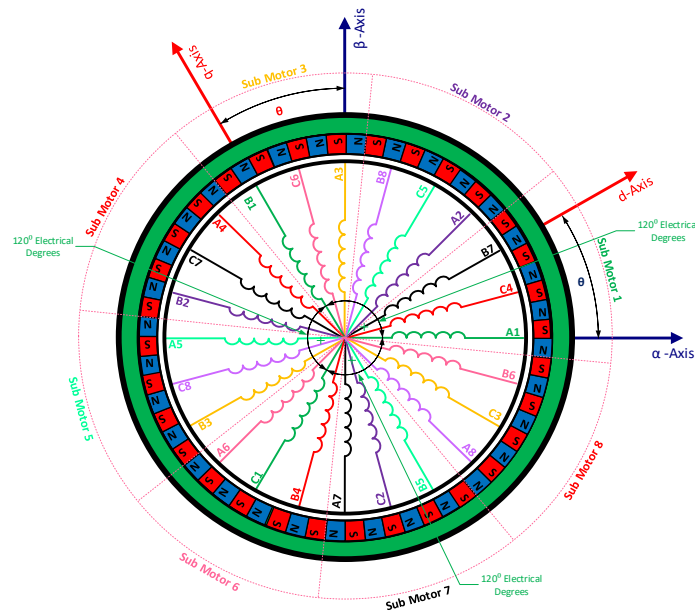
Figure 4. A Protean sub-motors' phase displacement in stationary *α-β* and synchronous *d-q* reference frames, respectively.

where:

f_{d_n}, f_{q_n}: direct and quadrature magnetic and electrical quantities for any sub-motor *(n)* in synchronous reference frame *d-q*.

$f_{A_n}, f_{B_n}, f_{C_n}$: three-phase magnetic and electrical quantities for any sub-motor *(n)* in stationary reference frame *ABC*.

n_P: the Park transform constant, which has two values: $n_P = \frac{2}{3}$ for transforming while maintaining fixed magnitudes (to be adopted in this research) and $n_P = \sqrt{\frac{2}{3}}$ for transforming while maintaining fixed powers.

Each sub-motor in the Protean motor can be considered an independent permanent magnet motor, considering that in the surface-mounted permanent magnets (SPM) motor, the *d-q* inductances are equal *(L_d = L_q)*. Thus, stator voltages and fluxes of any sub-motor *(n)* are given in the *d-q* synchronous reference frame as follows:

$$L_d \frac{di_{d_n}}{dt} = -R_s i_{d_n} + P\omega_r L_q i_{q_n} + u_{d_n} \tag{22}$$

$$L_q \frac{di_{q_n}}{dt} = -R_s i_{q_n} - P\omega_r L_d i_{d_n} - P\omega_r \varphi_f + u_{q_n} \tag{23}$$

$$\varphi_{d_n} = l_d i_{a_n} + \varphi_f \tag{24}$$

$$\varphi_{q_n} = l_q i_{q_n} \tag{25}$$

The electromagnetic torque resulting from each sub-motor in the Protean motor is expressed in terms of the orthogonal interaction of the flux and current components according to the following equation:

$$T_{em_n} = \frac{3}{2} P(\varphi_{d_n} i_{q_n} - \varphi_{q_n} i_{d_n}) \tag{26}$$

Considering that each sub-motor will be controlled to provide the maximum torque per ampere (MTPA) with $i_{q_n} = I_{s_n}$ and $i_{d_n} = 0$, the electromagnetic torque equation for any sub-motor *(n)* can be rewritten as follows:

$$T_{em_n} = \frac{3}{2} P(\varphi_f i_{q_n}) \tag{27}$$

The previous equation is also applicable for controlling the motor to achieve speeds beyond base speed through field weakening (FW), where the inductance torque component is negligible due to the inductance equality: $(L_{sd} - L_{sq}) i_{d_n} i_{q_n} = 0$ in the SPM motor. As for the total torque of a Protean motor, it is the sum of all sub-motors torques according to:

$$T_{em_{Eq}} = \sum_{n=1}^{8} T_{em_n} \tag{28}$$

Equivalently, torque can be expressed in terms of the orthogonal interaction current and flux of all sub-motors as follows:

$$T_{em_{Eq}} = \frac{3}{2} P \left(\varphi_{d_{Eq}} i_{q_{Eq}} - \varphi_{q_{Eq}} i_{d_{Eq}} \right) \qquad (29)$$

where:

$$i_{d_{Eq}} = \sum_{n=1}^{8} i_{d_n} \qquad (30)$$

$$i_{q_{Eq}} = \sum_{n=1}^{8} i_{q_n} \qquad (31)$$

$$\varphi_{d_{Eq}} = \sum_{n=1}^{8} \varphi_{d_n} \qquad (32)$$

$$\varphi_{q_{Eq}} = \sum_{n=1}^{8} \varphi_{q_n} \qquad (33)$$

As for the speed of the common rotor is given in the equation (34):

$$J_r \frac{d\omega_r}{dt} = T_{em_{Eq}} - T_L \qquad (34)$$

The rotor position can be obtained by integrating the mechanical speed according to (35):

$$\theta_r = \int \omega_r \, dt \qquad (35)$$

where:

u_{d_n}, u_{q_n}: direct and quadrature voltage components of sub-motor (n) in the synchronous reference frame d-q.

i_{d_n}, i_{q_n}: direct and quadrature current components of sub-motor *(n)* in the synchronous reference frame d-q.

I_{s_n}: current vector of sub-motor *(n)*.

L_d, L_q: direct and quadrature inductance components for sub-motor *(n)* in the synchronous reference frame d-q.

$\varphi_{d_n}, \varphi_{q_n}$: direct and quadrature flux components for sub-motor *(n)* in the synchronous reference frame d-q.

$i_{d_{Eq}}, i_{q_{Eq}}$: equivalent direct and quadrature current components for all sub-motors in the synchronous reference frame d-q.

$\varphi_{d_{Eq}}, \varphi_{q_{Eq}}$: equivalent direct and quadrature flux components for all sub-motors in the synchronous reference frame d-q.

$T_{em_n}, T_{em_{Eq}}$: torque and equivalent torque for one sub-motor *(n)* and all sub-motors, respectively.

φ_f: permanent magnet's flux.

Figure 5 illustrates the complete block diagram of the Protean motor represented in the synchronous reference frame *d-q*. This is presented by displaying the first and last sub-motors (where the other sub-motors have the same model). The upper section illustrates the current model. As for the flux and electromagnetic torque model, it is shown in the lower section. The total torque for the Protean motor is the torque sum of all sub-motors, where the torque balance of the total torque and the load torque is the input to the common rotor of the Protean motor.
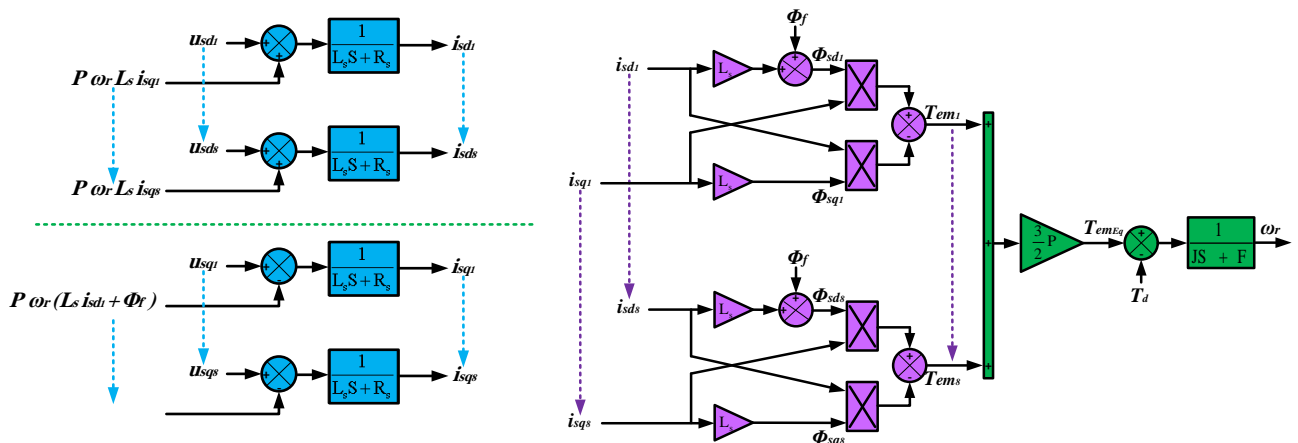

Figure 5. A block diagram of the Protean sub-motors is represented in the synchronous reference frame *d-q*.

4. Simulation Results

To validate the Protean IWM mathematical model, simulation models for the motor and its vector control were built in MATLAB/Simulink. The control is designed to run the motor primarily in the MTPA mode at speeds below the base speed (1000 rpm). Upon exceeding this speed, it automatically switches to FW mode using the state flow logic in MATLAB. To

validate the independent control of sub-motors, MTPA mode is activated first, followed by FW mode running when a higher speed is requested.

Figure 6 illustrates the motor speed response to a gradual speed request. Initially, a reference speed corresponding to the base speed of 1000 rpm is requested, representing an operation in the constant torque region (CTR). The time to reach the desired speed is 0.7 seconds, and at second 1, the motor is loaded with the nominal load, causing a slight decrease in speed, as shown in the magnified portion. The controller quickly compensates for this decrease, restoring the motor speed. Working under MTPA mode continues until second 2 when the system switches to the constant power region (CPR) through the FW. The required speed in this case corresponds to maximum speed at 1400 rpm, where this condition lasts until the end of the simulation at second 3.5.
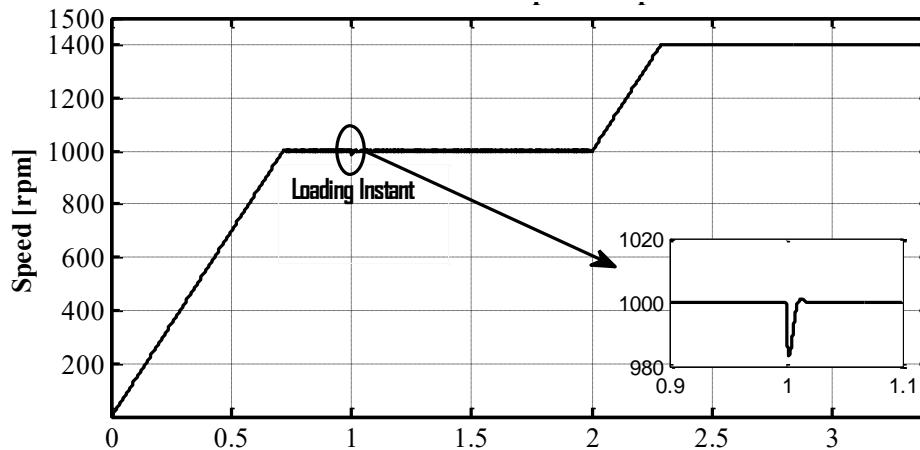
Figure 6. Protean IWM speed response under CTR-MTPA and CPR-FW control modes.

Figure 7 shows the Protean motor response to a working point with nominal torque at a speed of 1000 rpm. It is noted that the motor was able to develop the full torque of 500 Nm, which is the continuous operating torque indicating the validation of the motor model. When operating in the CPR region, we observe a decrease in the developed torque to approximately 370 Nm due to the position change of the current vector of each sub-motor I_{s_n} in response to field weakening.
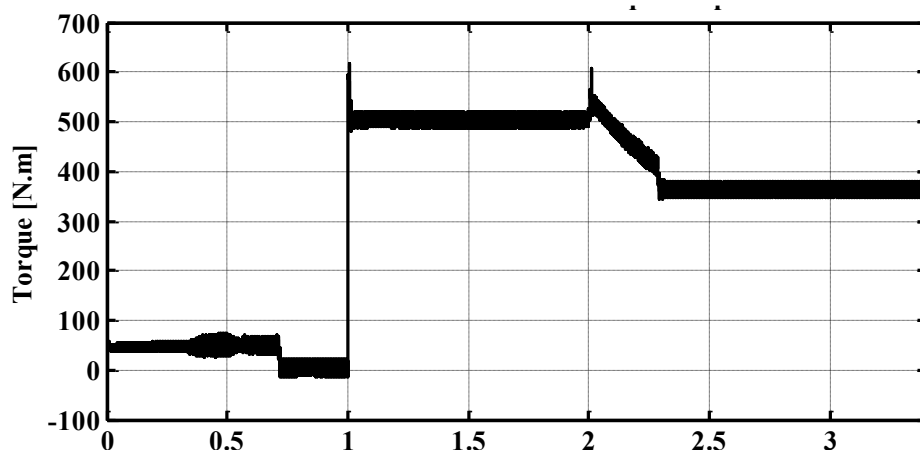
Figure 7. Protean IWM torque response under CTR-MTPA and CPR-FW control modes.

5. Conclusion

This paper presents and studies a new type of advanced IWM system designed by Protean Electric. The Protean IWM system is considered a highly integrated system with high torque density and high fault tolerance. Fault tolerance is ensured by dividing the stator into eight independent sub-motors with a common rotor. Each of the eight sub-motors constitutes a completely independent unit with its drive system and integrated micro-inverter. This motor has a high continuous torque of

up to 500 Nm and a maximum torque of up to 1000 Nm. The mathematical model of this motor is derived based on a set of Park transforms corresponding to each sub-motor's spatial and electrical distribution.

A Protean motor system was developed in the MATLAB/Simulink environment to validate the mathematical model derivation, allowing independent control of each sub-motor. The simulation results show the correctness of mathematical model derivation by applying vector control independently to each sub-motor.

Abbreviations

ABS	Anti-lock braking System
ACAS	Advanced Chassis Active-Safety Systems
BBW	Brake-by-Wire
EV	Electric Vehicle
EWB	Electronic Wedge Brake
FW	Flux Weakening
IWM	In-Wheel-Motor
MTPA	Maximum Torque per Ampere
PMSM	Permanent Magnet Synchronous Motor
RABS	Regenerative Anti-lock braking System
SPM	Surface-Mounted Permanent Magnet
TCS	Traction Control System
TV	Torque Vectoring

References

Deepak, K., Frikha, M. A., Benômar, Y., El Baghdadi, M., Hegazy, O. (2023). In-Wheel Motor Drive Systems for Electric Vehicles: State of the Art, Challenges, and Future Trends. *Energies*. 16(7), 1–31. DOI: 10.3390/en16073121

Feng, Z., Zhao, S., Gao, W., Zhang, Y., Fei, L. (2023). Study on a Novel In-Wheel Motor Driving System Driven by Two Permanent Magnet Synchronous Disc Motors. *IEEE Transactions on Vehicular Technology*. 72(5), 5922–5933. DOI: 10.1109/TVT.2023.3233997

Fraser, A. (2018). *In-Wheel Electric Motors – The Packaging and Integration Challenges*. Protean Electric. URL: https://www.proteanelectric.com/f/2018/04/In_Wheel_Electric_Motors_AFraser_ProteanV4.pdf.

Hilton, C. (2016) *Wheel Torque and Speed in a Vehicle with In-Wheel Motors*. Protean Electric. URL: https://www.proteanelectric.com/f/2018/04/Wheel_Torque_and_Speed_in_a_Vehicle_with_In-Wheel_Motors.pdf

Ifedi, C. J., Mecrow, B. C., Brockway, S. T. M., Boast, G. S., Atkinson, G. J., Kostic-Perovic, D. (2011). Fault tolerant in-wheel motor topologies for high performance electric vehicles. *2011 IEEE International Electric Machines and Drives Conference, IEMDC 2011*. 1310–1315. DOI: 10.1109/IEMDC.2011.5994794

Ifedi, C. J., Mecrow, B. C., Widmer, J. D., Atkinson, G. J., Brockway, S. T. M., Kostic-Perovic, D (2012). A high torque density, direct drive in-wheel motor for electric vehicles. *IET Conference Publications*, 2012(592 CP). DOI: 10.1049/cp.2012.0254

Perovic, D. K. (2012). Making the impossible, possible-overcoming the design challenges of in wheel motors. *World Electric Vehicle Journal*. 5(2), 514–519. DOI: 10.3390/wevj5020514

Said Jneid, M. (2024). Radial Flux In-Wheel-Motors for Vehicle Electrification. *Cognitive Sustainability*. 3(3). DOI: 10.55343/cogsust.105

Said Jneid, M., Harth, P. (2023a). Blended Regenerative Anti-Lock Braking System and Electronic Wedge Brake Coordinate Control Ensuring Maximal Energy Recovery and Stability of All-Wheel-Motor-Drive Electric Vehicles. *Journal of Transportation Technologies*. 13(03), 465–495. DOI: 10.4236/jtts.2023.133022

Said Jneid, M., Harth, P. (2023b). Coordinate Torque Vectoring Control For Enhancing Handling and Stability of All-Wheel-Drive Electric Vehicles Through Wheel Slip Control Integration. *2023 IEEE Cognitive Mobility Conference (CogMob)*. 177–186. Budapest, Hungary: IEEE.

Said Jneid, M., Harth, P. (2023c). Integrated Braking and Traction Torque Vectoring Control Based on Vehicle Yaw Rate for Stability Improvement of All-Wheel-Drive Electric Vehicles. *2023 IEEE International Conference on Electrical Systems for Aircraft, Railway, Ship Propulsion and Road Vehicles & International Transportation Electrification Conference (ESARS-ITEC)*. 1–6. Venice, Italy: IEEE. DOI: 10.1109/ESARS-ITEC57127.2023.10114899

Said Jneid, M., Harth, P. (2023d). Integrated Torque Vectoring Control Using Vehicle Yaw Rate and Sideslip Angle for Improving Steering and Stability of All Off-Wheel-Motor Drive Electric Vehicles, *Acta Polytechnica Hungarica*. 21(7), 87–106. DOI: 10.12700/APH.21.7.2024.7.6

Said Jneid, M., Joukhadar, A. (2019). LQR-Based Control of a Single Motor Electronic Wedge Brake EWB for Automotive Brake-By-Wire System. *Soft Computing and Electrical Engineering*. 1(1), 12–35. URL: https://paper.ieti.net/scee/2019Volume1Issue1/paper02.pdf

Said Jneid, M., Harth, P., Ficzere, P. (2020). In-Wheel-Motor Electric Vehicles And Their Associated Drivetrains. *International Journal For Traffic And Transport Engineering*. 10(4). DOI: 10.7708/ijtte.2020.10(4).01

Said Jneid, M., Zöldy, M., Harth, P. (2023). Sensorless optimal control of electronic wedge brake based on dynamic model and Kalman filter state multiple-estimation. *Proceedings of the Institution of Mechanical Engineers, Part D: Journal of Automobile Engineering*. 238(1): 095440702311681. DOI: 10.1177/09544070231168168

Whitehead, A., Hilton, C. (2018). Protean Electrics In-Wheel Motors Could Make EVs More Efficient. *IEEE Spectrum*. 1–10.

Design and Construction of a Handling Station to Interlace PCBs

Miroslav Blatnický

0000-0003-3936-7507

Department of Transport and Handling Machines, University of Žilina
Žilina, Slovak Republic
miroslav.blatnicky@fstroj.uniza.sk

Ján Dižo

0000-0001-9433-392X

Department of Transport and Handling Machines, University of Žilina
Žilina, Slovak Republic
jan.dizo@fstroj.uniza.sk

Alyona Lovska

0000-0002-8604-1764

Department of Transport and Handling Machines, University of Žilina
Žilina, Slovak Republic
alyona.lovska@fstroj.uniza.sk

Abstract

This study discusses the design and construction of an automatic handling station to interlace two-part printed circuit boards (PCBs), with special attention to the methodology of constructing its handling nodes. The valuable result of this work is a presentation of the acquired cognitive experience with centric grippers and a new approach to gripping fingers. At the same time, the work describes an overview of the current state of the mechanisms of single-purpose machines. The task is to design a structure of a horizontal manipulator, a stopper for the PCB bed plates, a two-axis manipulator and a gripping head focusing on a sustainable production process. The concept of individual parts' arrangement, interactions, and resulting parameters have been developed following the stated requirements. The design meets all requirements in terms of simplicity of construction, adjustment, reliability of grasping, non-damage of the manipulated part, and sustainability of the whole manufacturing process.

1. Introduction

New technologies constantly emerge, posing new requirements for production and development daily. For that reason, industrial manipulators have become an essential part of most production lines (Blatnický et al., 2020a; 2020b). A significant advantage of manipulators is their possible continuous operation and high accuracy, power, and speed, in contrast with significant physical limitations for humans. This way of operating companies allows manufacturers to reduce the production costs of their products, which significantly increases competitiveness. In the production of devices intended for work in the automatic production process, great emphasis is placed on the reliability and fault-freeness of the device (Blatnická et al., 2018; Blatnický et al., 2018a).

The presented research is focused on the design of the main structural units of an automatic handling station. This station will interlace two-piece printed circuit boards (PCB). PCBs are essential modules incorporated in a wide range of industrial equipment to control or signal manipulation applications. These boards are subjected to various loads, such as vibrations, shocks and static loads (Homza et al., 2024; Zhang et al., 2024). PCBs are applied to connect components to form a working

circuit; thus, they play a crucial role in modern electronics. Integrating more components onto PCBs is becoming increasingly common, which presents significant challenges for quality control processes (Kahn et al., 2024). One of the main challenges in factories that use robotic manipulators for "pick and place" tasks is object orientation because the robotic manipulator can misread the object's orientation and thereby grasp it incorrectly. Object segmentation solves this problem (Glucina et al., 2023). The assembly of PCBs is one of the standard processes in chip production, directly contributing to the quality and performance of the chips. In the automated PCB assembly process, machine vision and coordinate localization methods are commonly employed to guide the positioning of assembly units (Peng et al., 2025). Regarding recycling, Naito et al. (2021) present the development of a system for recycling PCB boards through classification, recovery and management of electronic parts. The considered new technologies are applied in many engineering fields and are used to improve the processes in manufacturing and production (Szalai et al., 2023a; 2023b).

The design is based on the authors' long-term acquisition of knowledge and skills. All needed functionalities, demands and limits were understood and taken into consideration. At the same time, the engineering design also focuses on the requirements of a sustainable process of production and operation. The effectiveness of operation and sustainability of the design were among the most important factors considered during the design procedure.

Different types of drives are used in single-purpose machines. Manual, pneumatic, electric and hydraulic drives are known. Logically, their choice depends on the individual requirements of the machine. Table 1 summarizes drives' analyzed advantages and disadvantages for designing an automatic handling line (Chen et al., 2021; D'Souza Costa, Pires, 2020).

An analysis of its components is necessary to design a single-purpose machine successfully. These are mainly manipulators, conveyors, sensors, pneumatic cylinders and effectors. Manipulators in single-purpose machines are applied in any product manipulation (Blatnický et al., 2020c). Manipulators can be manual, electric, pneumatic or pneumatic. Electric manipulators use servomotors or stepper motors for manipulation. Their significant advantage is the achieved transmission speeds (Festo, 2024). Pneumatic manipulators are structurally simple because they use combinations of pneumatic cylinders, and their main advantage is the low purchase price (Venkatesan and Capelleri, 2017; Zhang et al., 2022).

Table 1 Advantages and disadvantages of individual drive types

Style name	Manual drive	Electric drive	Pneumatic drive	Hydraulic drive
Advantages	High reliability	Precise positioning	High movement speed	High lifting and clamping forces
	Simple design	Good positioning speeds	Simple construction	
	Low procurement costs	Simple assembly	Low price	High accuracy and reliability
	Low failure rate			
Disadvantages	Low lifting and clamping forces		Poor positioning	Low movement speed
	Low positioning speeds	Cost	Low lifting and clamping forces	Ecologically objectionable (possibility of leakage of working fluid)
	Short-term operation		Sensitivity to loss of pressure	

Conveyors are used in single-purpose machines to transport products over longer distances. Widely used conveyors in single-purpose machines are belt conveyors, which stand out for their simple installation and regulation. In addition, less standard types of conveyors are also used. An example is a vibrating conveyor that is driven by a vibrating drive. Its disadvantages include that it is only available for horizontal transport and the demanding initial optimization for the moved material (Callegari et al., 2020; Ciubucciu et al., 2017; Han et al., 2022).

Sensors serve as feedback for the controlled element. They are used, e.g., for location, temperature, humidity and motion sensing. In machines, they are used on drives, where they sense individual positions, and for any operations where it is necessary to detect the presence of a part. Both touch and non-touch sensors are used in practice. Examples of sensors are inductive, ultrasonic, capacitive, optoelectronic and magnetic. The leading manufacturers are Balluff, Turck and SICK (Euchner.cz, 2024a; Euchner.cz, 2024b; Linear drives, 2024).

Compressed air as an energy carrier is considered the oldest form of increasing physical performance in pneumatic cylinders. In the past decades, pneumatic systems have come to the fore, mainly thanks to the automation of production processes. A pneumatic cylinder is a mechanical device used to convert the force of compressed air into mechanical motion. It is a system of energy transmission between two or more places in space. Usually, the system's pressure is 2 to 16 bar. At a pressure lower than 2 bar, it is impossible to ensure stable movement of the piston due to the frictional resistance of the

piston in a cylinder. For pressures higher than 16 bar, using air as a medium for energy transfer is not economically advantageous compared to hydraulic cylinders (Linear drives, 2024).

An effector is a functional part of a manipulation unit. It allows the machine to grasp or otherwise work with manipulated objects. The effector is in direct contact with a manipulated object. A unique effector is proposed for each application. The design can be implemented directly by the manufacturer of the robot/single-purpose machine or the user of the manipulator. When designing the effector, it is crucial to consider that it can perform manipulative and technological tasks. The manipulation task mainly means executing operations to ensure the change of position and orientation of the manipulated object, secure its position, and clamp it. In the technological task, the effector performs welding and assembly operations (Blatnická et al., 2018).

Operational practice led to a request to design a handling station to interlace two-part PCB boards. The main requirement in the station's design and its gripper is that the gripping of the two-part board is stable, repeatable and does not damage the board. Automatic adaptability to dimensional inaccuracies in PCB board production was also required. The presented research aims to design suitable solutions for handling NX Siemens 12 program nodes that will meet all requirements.

2. Requirements for the proposed device

The proposed OPR30 station (Figure 1) is to be integrated into an automatic line whose task is the fully automatic assembly of a servo motor. In addition to manually loading parts and removing the finished product, the process is fully automatic. At the other stations, various activities are performed, such as bending electrical wires, applying the heat-conductive paste, dispaneling and loading the two-part PCB board onto the pallet, screwing the PCB board, pressing contacts, resistance welding, turning the electronics part onto the motor part, applying glue, loading and then pressing the cover Multiple cameras are also installed for controlling the process. All requirements for the proposed manipulator are listed in Table 2.

Table 2 Requirements for the proposed manipulator

No.	Feature Requirements	Importance	Explanation
1.	Speed of handling	Required	The clock of the device is up to 36 seconds
2.	Rounded/chamfered edges	Required	All edges of manufactured parts are rounded at least R2 – for sheets thinner than 2.5 mm, edging/edge protection is preferred.
3.	Surface treatment of sliding parts	Required	Nitriding or coating the surfaces of contact surfaces of moving parts
4.	Damping movements	Required	Ensuring damping of end positions during movements
5.	Use of commonly available springs	Required	Guaranteed availability of spare parts
6.	Maximum weight of the product	Required	It must not exceed 15 kg
7.	Easily replaceable preparation	Required	Replacement of the preparation without the use of tools
8.	Simple construction of the preparation	Optional	
9.	Pneumatic elements	Required	All pneumatic elements from Festo or Schunk
10.	Pneumatic cylinders	Required	The cylinders must contain end position sensors and damping
11.	ESD ionizers	Required	Air ionizers will be placed in the part of the equipment for loading and unloading components.
12.	PCB loading position sensing	Required	In the basic position of the horizontal manipulator, ensure the correctness of the loading of the PCB.
13.	Repeatability of PCB sampling	Required	The design of the effector prevents the risk of PCB slipping
14.	Preventing dirt build-up	Required	The frame construction is made up of closed profiles of the NVS type
15.	Spring-loaded fingers of the gripping head	Required	The fingers of the gripper placed in a linear guide are pressed by a compression spring.

As it emerged from the requirements, the supporting structure was designed from aluminium profiles closed from the outside by Bosch Rexroth (Bosch Rexroth, 2024). Lightweight profiles with dimensions of 90 × 90 mm, 45 × 90 mm and 45 × 45 mm were used. Since the entire device is placed on the support structure of the lower frame (Figure 1), the structure should have sufficient load-bearing capacity and rigidity.
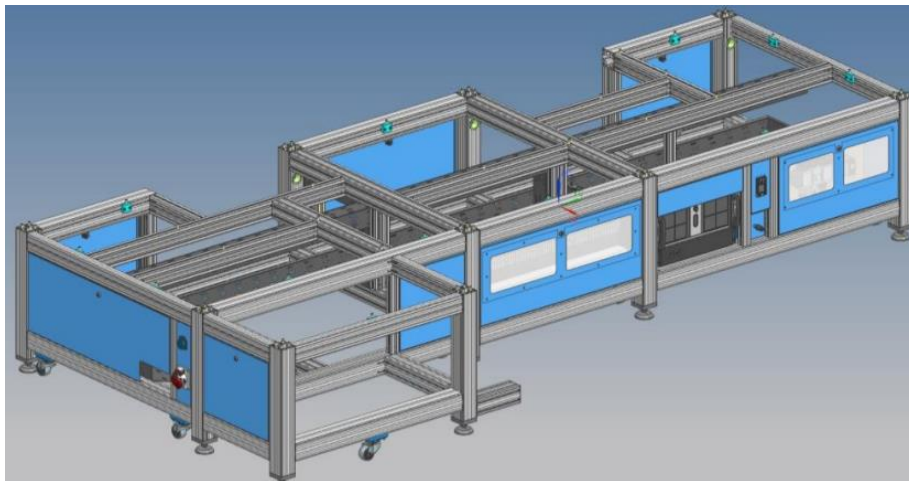
Figure 1. 3D CAD model of the lower frame of the proposed manipulator

The choice of profile geometry resulted from experience constructing similar devices with similar loads (Blatnický et al., 2018a; Blatnicky et al., 2018b). The used aluminium profiles are very advantageous in price and weight, while they have relatively high strength (Bosch Rexroth, 2024). A significant advantage is the grooves along the entire length of the profiles, on which any accessories can be placed with the help of special rotating nuts. Pin connectors connect the profiles themselves. In addition to the adjustable legs, the lower part has swivel wheels for transportation. The lower frame also includes a pneumatic component that controls the pneumatic part of the station. A sheet metal box for milled panels is also included in the lower part of the frame. See the red part in Figure 2a. The panels fall out of the dispaneling device near the station via a conveyor and fall through the base plate into the box by a gravity slide.

(a)   (b)

Figure 2. Scrap box placed on the linear guide (a) and 3D CAD model of the upper frame of the proposed manipulator (b)

The upper frame is fixed to the base plate of the station. There are three doors to access the OPR30 station, as shown in Figure 2b. All doors are blocked by an electronic security lock that prevents unauthorized entry into the station during operation. Safety locks on station doors are essential parts of every automatic station to ensure the safety of operating personnel. The inner part of the door is filled with 5 mm thick transparent antistatic polycarbonate. The upper part of the frame is covered with a 2 mm thick anodized aluminium sheet.

3. Structural design of a horizontal manipulator

The operation of relocating the PCB board from the dispanelisation device to the pallet proceeds as follows. After dispanelisation, the PCB board is inserted into the bed fixed by a linear pneumatic drive. With the help of this drive, the bed moves between three positions: PCB loading position, dirt extraction and PCB board unloading. The assembly of the horizontal manipulator in the PCB board unloading position is shown in Figure 3.
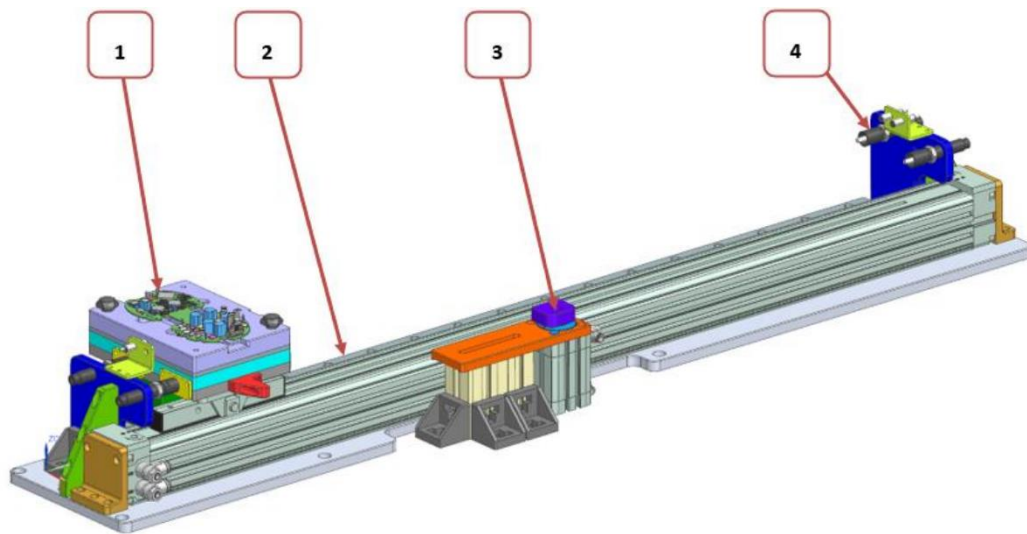
Figure 3 An assembly of the horizontal manipulator: 1 – a bed with the PCB board, 2 – a linear drive, 3 – a stopper, 4 – a damper

The role of the bed is to hold and centre the PCB board. It consists of a shaped bed that corresponds to the board's dimensions. The shaped bed is made of POM ESD material because it conducts an electric discharge. If an electric charge occurs during the folding of the PCB board, the bed will safely dissipate it. In this way, protection against electrostatic damage to sensitive electronics is ensured. This shaped bed contains two nitrided steel centring pins that ensure the repeatability of the part's placement. It also contains two centring bushings for centring the gripping head of the two-axis manipulator. The manufactured parts used to ensure the accuracy and repeatability of the interlacing are stored in precise holes of H7 tolerance and screwed with an M4 screw. This bed is screwed onto a duralumin plate with a thickness of 5 mm because the POM ESD material deforms over time. This bed is replaceable if part modifications occur or a new version is added. Figure 4 shows a picture of the bed and a pair of optical sensors.
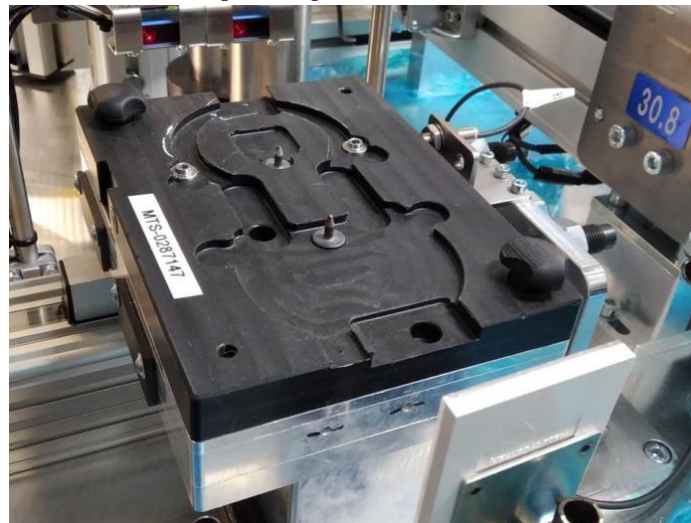
Figure 4. A detail of the PCB board bed

The sensor located on the left side of the sensor holder is used to detect the presence of a piece. The sensor located on the right side is used to detect the correct loading of the piece. If the plate is loaded incorrectly, this sensor will send a signal to the station's control unit and prohibit the removal of the piece.

The research team has used the POM ESD material several times in previous designs. Therefore, the experiences with this material and its properties, such as excellent machinability, abrasion resistance and, in this particular case, the conduction of electric current, have predetermined it for its further direct application presented in the work. The entire plate serving as a bed for the product (PCB board) can be dismantled and, if necessary, replaced with another piece or a different material design.

The replaceable fixture is placed on a duralumin plate with a thickness of 16 mm, on which a washer is screwed together with a rail carriage of size 25 BR from Bosch Rexroth. On the other hand, this bed is attached to the movable carrier of the pneumatic pistonless cylinder Festo DGC-K40-900-PPV-A-GK-FK. It has a lift of 900 mm, a low-moving dead weight and a symmetrical construction. The driver is equipped with a pin to compensate for alignment errors when using an external guide. The linear drive is fixed with the help of a pair of identical duralumin holders on a duralumin plate firmly mounted on the base plate of the station. Its position is secured by a pair of purchased pins with a diameter of 8 mm and a tolerance of H7.

In Figure 5, shown in yellow, stop plates serve for direct contact with the motion damper and the stop nut. They are made by cutting with a laser beam from material STN 12 050 with a thickness of 3 mm, and then they are nitrided. Each time the bed is moved, they transfer the impact force to the bed. Both the surface treatment and the choice of material were chosen to maximize the service life of the functional parts of the station. Also, the stop pin, depicted in Figure 5 and shown in red, is nitrided. Two screws are inserted in the upper part of the model, which allows the replacement of the fixture without the need for tools.
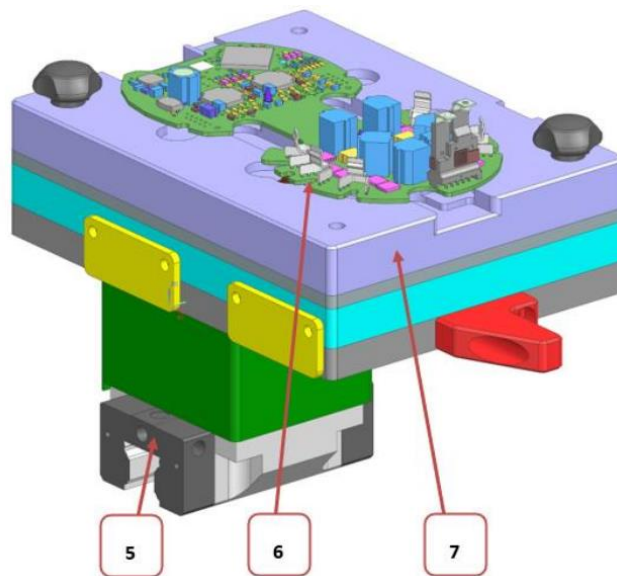
Figure 5. A horizontal manipulator bed: 5 – a carriage, 6 – a PCB board, 7 – a plate

Damping the end positions of the device was one of the essential requirements. A pair of ACE MC150MH dampers serve to dampen the kinetic energy of bed movements in extreme positions. On their outer thread, which also serves as a mounting element of the damper, a stop nut is screwed, which can be seen in Figure 6. Its task is to touch the stop plate.
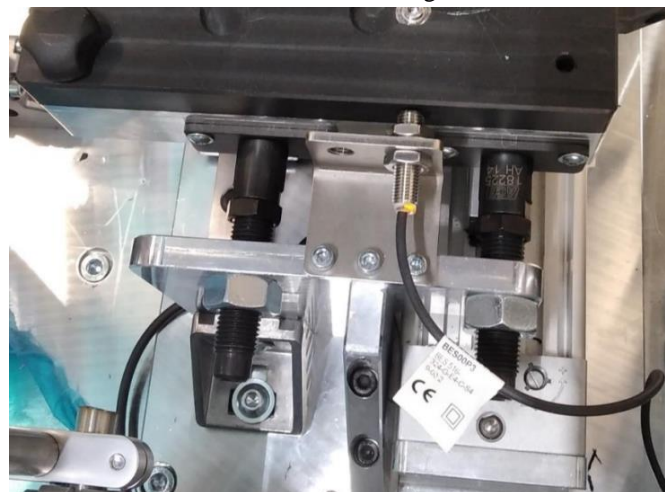

Figure 6. External damping with the end position stop

The pneumatic drive has its end damping and stop, but for use in this application, its repeatability is insufficient, and therefore, it was necessary to make external damping with a stop. Fixing the threaded body of the shock damper in a duralumin plate allows the operator to set the end positions in the longitudinal direction. The damping path can be adjusted by tightening or loosening the stop nut. A Balluff BES00P3 inductive sensor with a range of 2 mm is placed on the upper part of a 10 mm thick duralumin plate. It is fixed with the help of a 3 mm thick sheet metal holder and AISI 304 material. The task of the induction sensor is to detect whether the bed has reached the end position and is in the secured position, which is ensured by the constantly pressurized chamber of the pistonless cylinder.

In general, its application must be justified if a high-speed manipulator is equipped with an external damping mechanism. If the reason is increasing the stabilization (or arresting) of the final position of the product, then there is a certain difference in the specifics of individual cases. In our specific case, the life of the integrated solution (consulted with Festo as the manufacturer of the specific implemented drive for the needs of a single-purpose machine, OPR 30, with the required frequency of work cycles) plays a decisive role. Therefore, integrating an external damping mechanism will ensure a longer and more reliable operation for the user of the proposed line.

Another component proposed here is the so-called stopper. The task of the stopper is to stop the moving bed. The Festo DFSP-Q40-15-DF-PA stop cylinder plays the main role in this assembly, as shown in Figure 7. It is a double-acting pneumatic cylinder in the design with a pin with an internal thread with protection against overturning.

Figure 7. A bed stopper in a basic position

This is a primarily custom-made version with a stroke of only 15 mm. Such a small lift was necessary due to the mounting dimensions of the entire assembly between the base plate of the station and the stop pin. Stop cylinders work like classic pneumatic cylinders but are designed to stress the piston rod in the radial direction. This means in the direction perpendicular to the direction of the cylinder's extension. Therefore, such cylinders have a reinforced and adapted piston rod to guide the cylinder in withstanding this type of stress. The stop cylinder is working (extended) when the bed returns to the dispaneling station. The bed hits the stopper and is acted upon by the force of the pistonless cylinder. This centre position is necessary to stop the bed to allow blowing and suction of debris from the bed after milling the PCB board from the panel.

On the piston rod of the cylinder, a shaped member is screwed, which has a recess in the lower part that copies the shape of the groove of the piston rod, with an M8 screw, which is in direct contact with the stop pin after the cylinder is extended. Since it was a requirement that the movements be damped even at this intermediate position, no damping occurred apart from guiding the stop cylinder piston rod; throttle valves were fitted to the pistonless cylinder. With the help of throttle valves, the filling speed of the air chamber in the cylinder can be continuously regulated. This way, we can achieve smooth truck operation at a low speed. At the manufacturing station, the practical bed speed was less than 0.3 m/s. The plate on which the piston is screwed has a groove in the longitudinal direction of the bed displacement. This enables fine-tuning of the stop point of the bed. To reduce production costs and simplify the device's design, the stopwatch assembly is designed to produce only three manufactured parts, as seen in Figure 8. These are the stop cylinder holder, the shaped member and the stop mandrel.
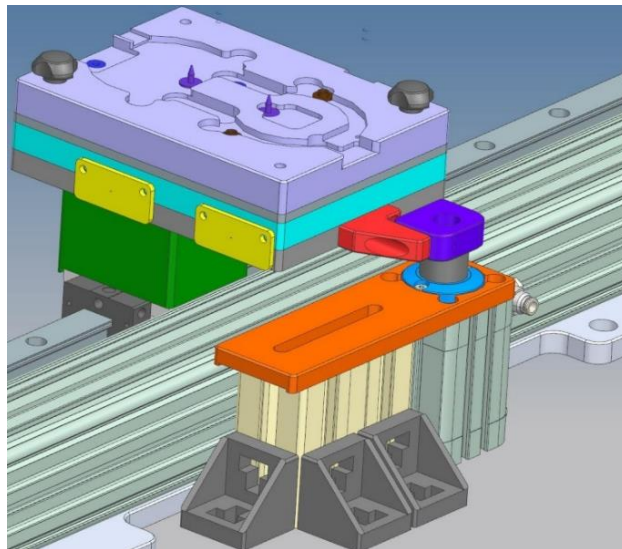
Figure 8. A stopper with a bed in a suction position

Cleaning the empty bed of the PCB board is an essential part of the handling process, as dust particles are created by milling the printed circuit board. The bed cover, i.e., the suction head, is shown in Figure 9.
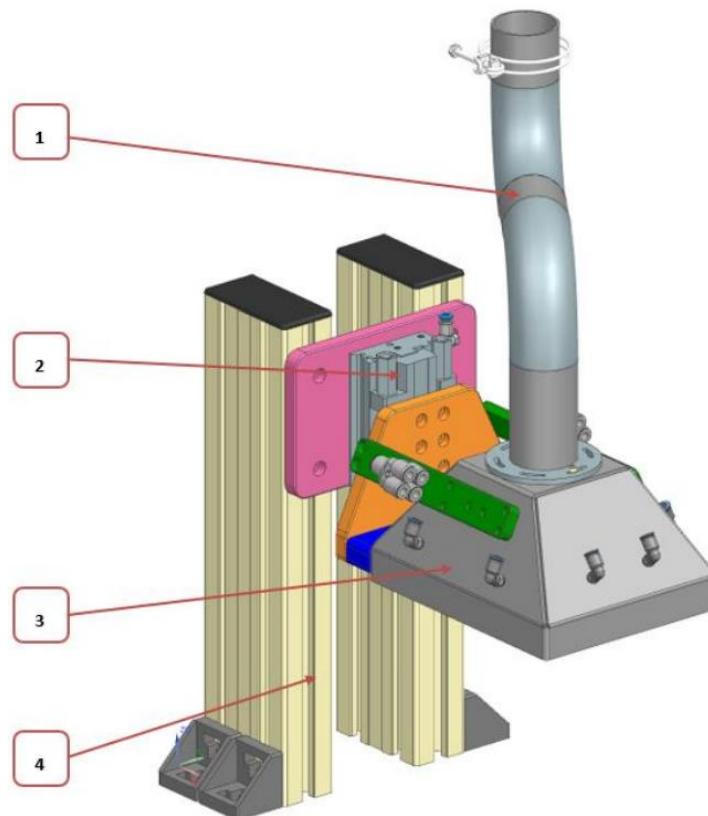

Figure 9. An extraction head with an integrated blower: 1 – an exhaust tube, 2 – a cylinder with guidance, 3 – a cover, 4 – a stand

The dirt extraction stand comprises two aluminium profiles measuring 45 × 90 mm. It is attached to the base plate with the help of 45 × 45 mm angles. The manufacturer designs the mounting holes in a very shape that allows fine-tuning of the position of the stand relative to the base plate in the two axes, X and Y. In the Z axis, the position adjustment is ensured by profile grooves. Fine-tuning of the Z-axis is possible using the integrated adjustment screws in the cylinder body. The stand is loaded for bending because the suction head is placed eccentrically on the assembly's base. For this reason, the orientation of the profiles was chosen, which is more advantageous for the bending load.

The plate on which the pneumatic cylinder with the guide is located is mounted in the groove of the profile using four M6 screws. The cylinder is also fixed with three M6 screws. The cylinder contains precise recesses of H7 tolerance on its mounting part for centring rings. The mounting plates also contain such recesses with an accuracy of ±0.02mm relative to each other. The centring rings are used for the assembly to be repeatable. In the case of replacing the pneumatic cylinder, it must be placed on the original mounting holes, and the position of the nozzle relative to the stand will be identical. The centring rings are made of ordinary quality steel, and their surface is ground. They are stressed only in the radial direction. In the axial direction, there is always at least 0.1 mm clearance in the mounting plate to ensure maximum contact between the cylinder mounting plate and the holder. Centring rings are also produced in a thin-wall version, with a maximum of 0.2 mm wall thickness. Such undemanding space has a favourable effect on the dimensions of the pneumatic cylinder.

The suction head serves to cover the empty bed of the PCB board. It consists of a 3 mm thick AISI 304 sheet welded cover, which has pneumatic push-in couplings screwed into it, which act as nozzles. They bring clean, compressed air under the cover. The nozzles help swirl the air under the head to remove all debris from the bed. The nozzles are connected in series to compressed air with a pressure of 6 bar. Their connection, the suction head and the pneumatic mechanical valve, can be seen in Figure 10.

Figure 10. The top view of the suction head

Dirt is removed by a vacuum cleaner located outside the station. The transmission of the vacuum is ensured by an air hose VULCANO PUH 09 with an inner diameter of 51 mm, designed for vacuuming up to -0.5 bar. Between the suction head and the pneumatic hose is a welded pipe made of AISI 304 material. A sheet flange with grooves for six pieces of M4 screws is used for mounting this pipe. Their location and length allow smooth rotation of the exhaust pipe to set the most suitable position. The sheet thickness of 3 mm provides a sufficient length of the cut thread for the screws used. A pneumatically controlled valve is used to close the pipe at the end of the exhaust. The role of the valve is to close the pipe and increase the suction power at other suction points because one vacuum cleaner is intended for three suction points. The valve is controlled by a pneumatic double-acting cylinder DSNU-8-50-P-A. The entire production line is located in a clean zone; therefore, the extracted dust is removed outside the premises of this zone.

The last assembly member addressed in this work is the gravity slide of milled panels (Figure 11). It is a simple passive assembly with the possibility of adjusting the position with the help of grooves in the X, Y and Z axes ±5mm.
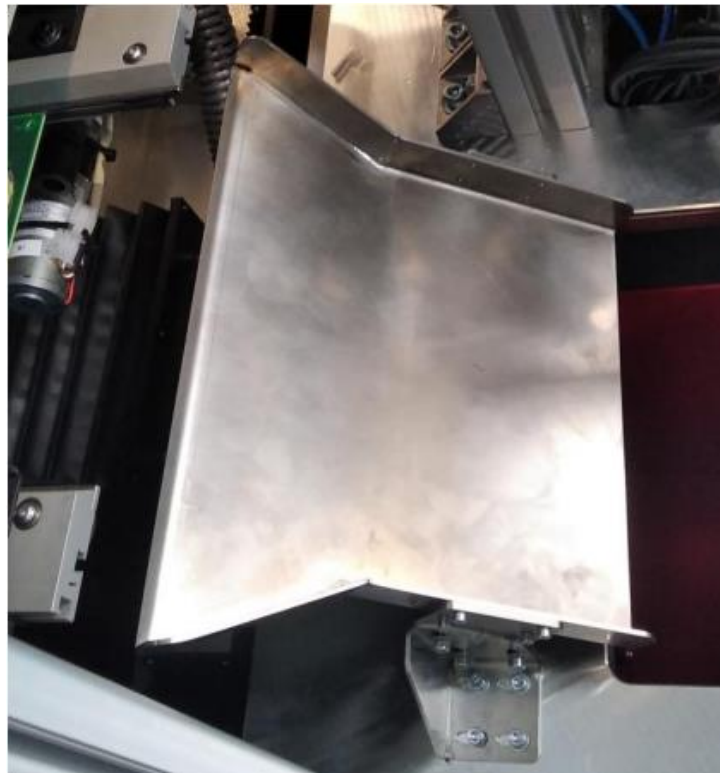

Figure 11. A sheet metal gravity chute

The sheet metal punch bent into a funnel primarily transports empty PCB board panels between the conveyor of the depanelization station and the scrap box. If the camera inspection of the depanelization device evaluates any of the PCB boards as NOK (not OK), it falls into the scrap box along with the panel by gravity.

The entire device is designed as a single-purpose machine for a specific product type. If the shape or dimensions of the PCB board are changed, the shape of the POM bed can also be changed very easily and quickly to the currently required geometry. When only the diameter of the (circular) part of the PCB board, which is gripped by a three-finger gripper (6 fingers in total because the board is two-part and connected only by a flex cable), will be changed, the current design could adapt to this. Changing the shape of the PCB board from a rotating part to a planar part could be considered a challenge. This requirement has not yet been encountered in applied research for practical use. However, this does not exclude the possibility of a solution being needed.

4. Conclusion

The paper aimed to describe the structural design and the development of handling nodes of a single-purpose machine, i.e., an automatic station called OPR30 used for handling two-part printed circuit boards utilized in electric vehicles of various categories by a real engineering company. The work briefly described and provided an overview of the current state of the mechanisms used to construct single-purpose machines. Tasks, i.e., the design of the horizontal manipulator and PCB bed stopwatch, can be considered fulfilled, as evidenced by the documentary images illustrating the arrangement of individual parts and their parameters. These results stem from adhering to the stated requirements. The design meets all requirements in terms of simplicity of construction, adjustment, and reliability of grasping, as well as non-damage of the manipulated part. In further research, the authors will focus on the structural design of the two-axis manipulator and the gripping head to complete the basis of the structural design of this device.

References

Blatnická, M., Sága, M., Blatnický, M., Dižo, J. (2018). Analysis of adaptive gripper effector. *Proceedings of the 22nd International Scientific on Conference Transport Means 2018*. 522–526.

Blatnický, M., Dižo, J., Blatnická, M. (2018a). Structural design of soldering station chain conveyor working positions. *Proceedings of the 22nd Slovak-Polish Scientific Conference on Machine Modelling and Simulations, MMS 2017*. 01002. DOI: 10.1051/matecconf/201815701002

Blatnický, M., Dižo, J., Blatnická, M. (2018b). Transport machine design for adaptive gripping of automotive industry products. *Proceedings of the 22nd International Scientific on Conference Transport Means 2018, Part III*. 1199–1203. URL: https://transportmeans.ktu.edu/wp-content/uploads/sites/307/2018/02/Transport-means-A4-III-2018-09-25-persp.pdf

Blatnický, M., Dižo, J., Barta, D., Rybicka, I. (2020a). Engineering design of a manipulator for mounting an air suspension compressor to a car chassis. *Scientific Journal of Silesian University of Technology. Series Transport*. 109, 05–16. DOI: 10.20858/sjsutst.2020.109.1

Blatnický, M., Dižo, J., Sága, M., Gerlici, J., Kuba, E. (2020b). Design of a mechanical part of an automated platform for oblique manipulation. *Applied Sciences*. 10(23), 8467. DOI: 10.3390/app10238467

Blatnický, M., Dižo, J., Gerlici, J., Sága, M., Lack, T., Kuba, E. (2020c). Design of a robotic manipulator for handling products of automotive industry. *International Journal of Advanced Robotic Systems*. 17(1), 1–11. DOI: 10.1177/1729881420906290

Bosch Rexroth (2024). Rfid System Sales Catalog Available on: https://m.boschrexroth.com/en/xc/products/product-groups/assemblytechnology/topics/rfid-systems/index (Downloaded 12 September 2024 09:49)

Callegari, M., Carbonari, L., Palmieri, G., Palpacelli, M.-C. (2020). Functional design of a manipulator for the automation of laboratory precision tasks. *International Journal of Mechanics and Control*. 21(2), 29–37.

Chen, Q., Qi, Y., Chen, G., Liu, J., Wang, Yu., Gao, Z. (2021). Design of positioning and mapping system for space station mobile robot based on ROS. *Proceeding - 2021 China Automation Congress, CAC 2021*. 3008–3012. DOI: 10.1109/CAC53003.2021.9727739

Ciubucciu, G., Solea, R., Filipescu, A., Filipescu, A. (2017). Visual servoing and obstacle avoidance method based control autonomous robotic systems servicing a mechatronics manufacturing line. *Proceedings of the 2017 IEEE 9th International Conference on Intelligent Data Acquisition and Advanced Computing Systems: Technology and Applications, IDAACS 2017*. 874–879. DOI: 10.1109/IDAACS.2017.8095212

D'Souza, F., Costa, J., Pires, J. N. (2020). Development of a solution for adding a collaborative robot to an industrial AGV. *Industrial Robot*. 47(5), 723–735. DOI: 10.1108/IR-01-2020-0004

Euchner.cz (2024a). Clampless Metal Case Available on: http://www.euchner.cz/data/pdf/Download/Katalogy/safety/Euchner_elmech_bezp_spinace_kovove_pouzdro.pdf (Downloaded: 8 August 2024 08:58)

Euchner.cz (2024b). Security Clips Available on: http://www.euchner.cz/produkty/bezpecnost/bezpecnostnispinace/ (Downloaded: 9 September 2024 15:40)

Festo (2024), Electrical Automation Available on: http://www.elektroprumysl.cz/automatizace/vsechno-elektricky (Downloaded: 10 September 2024 08:48)

Glucina, M., Andelic, N, Lorencin, I., Car, Z. (2023). Detection and Classification of Printed Circuit Boards Using YOLO Algorithm. *Electronics*. 12(3), 667. DOI: 10.3390/electronics12030667

Han, S., Li, M., Luo, O., Duan, M., Ma, X. (2022). Design alternative for automobile door trim strip production line. *Proceedings of the 37th International Conference of the Polymer Processing Society, PPS 2022*. 193724. DOI: 10.1063/5.0168903

Homza, G., Barkallah, M., Louati, J., Haddar, M. (2024). Preliminary Design for the Vibration Analysis of a PCB Model: An Analytical Approach. *Proceedings of the 4th International Conference on Advanced Materials Mechanics and Manufacturing (A3M2023)*. 320–326. DOI: 10.1007/978-3-031-57324-8_34

Kahn, R.U., Shah, F., Kahn, A.A., Tahir, H. (2024). Advancing PCB Quality Control: Harnessing YOLOv8 Deep Learning for Real-Time Fault Detection. *Computers, Materials and Continua*. 81(1), 345–367. DOI: 10.32604/cmc.2024.054439

Linear drives (2024). Linear Actuators Available on: https://www.festo.com/cat/en-gb_gb/data/doc_SK/PDF/SK/DGC-K_SK.PDF (Downloaded: 1 August 2024 12:03)

Naito, K., Shirai, A., Kaneko, S., Capi, G. (2021). Recycling of printed circuit boards by robot manipulator: A Deep Learning Approach. *Proceedings of the IEEE International Symposium on Robotic and Sensors Environments, ROSE 2021*. DOI: 10.1109/ROSE52750.2021.9611773

Peng, J., Wang, D., Zhai, J., Teng, Y., Kimmig, A., Tao, X., Ovtcharova, J. (2025). Meta-learning enhanced adaptive robot control strategy for automated PCB assembly. *Journal of Manufacturing Systems*. 78, 46–57. DOI: 10.1016/j.jmsy.2024.11.009

Szalai, S., Herold, B., Kurhan, D., Németh, A., Sysyn, M., Fischer, S. (2023a). Optimization of 3D Printed Rapid Prototype Deep Drawing Tools for Automotive and Railway Sheet Material Testing. *Infrastructure*. 8(3), 43. DOI: 10.3390/infrastructures8030043

Szalai, S., Szívós, B. F., Kurhan, D., Németh, A., Sysyn, M., Fischer, S. (2023b). Optimization of Surface Preparation and Painting Processes for Railway and Automotive Steel Sheets. *Infrastructure*. 8(2), 28. DOI: 10.3390/infrastructures8020028

Venkatesan, V., Cappelleri, D. J. (2017). Development of an automated flexible micro-soldering station. *Proceedings of the ASME Design Engineering Technical Conference*. 131761. DOI: 10.1115/DETC2017-68107

Zhang, A., Kandubai, R. V. P. P., Hammarberg, S. (2022). A Functional Retro-Fitting Robotic Smart Lock Manipulator. *International Journal of Mechanical Engineering and Robotics Research*. 11(3), 123–128. DOI: 10.18178/ijmerr.11.3.123-128

Zhang, J. T., Shi, X. Y., Qu, D., Xu, H. D., Chang, Z. F. (2024). PCB Defect Recognition by Image Analysis using Deep Convolutional Neural Network. *Journal of Electronic Testing-Theory and Applications*. 40, 657–667. DOI: 10.1007/s10836-024-06145-3

Polymerization of purified residual glycerol from biodiesel production

António André Chivanga Barros[*]

https://orcid.org/0000-0001-5922-5368

Center for Research and Development (CpD) of Sonangol, Rua Rainha Ginga Nº29/31
Luanda, Angola

Curso de Mestrado em Engenharia Química, Departamento de Engenharia e Tecnologias, Instituto Superior
Politécnico de Tecnologias e Ciências (ISPTEC),
Avenida Luanda Sul, Rua Lateral, S10, Talatona
Luanda, Angola
*Corresponding author: chivanga@gmail.com

Feliciano José Ricardo Cangue

https://orcid.org/0000-0003-0560-3815

Curso de Mestrado em Engenharia Química, Departamento de Engenharia e Tecnologias, Instituto Superior
Politécnico de Tecnologias e Ciências (ISPTEC),
Avenida Luanda Sul, Rua Lateral, S10, Talatona
Luanda, Angola.

Vinicyus Rodolfo Wiggers

https://orcid.org/0000-0003-2273-8025

Departamento de Engenharia Química, Universidade Regional de Blumenau, Rua São Paulo, 3250,
Itoupava Seca, CEP: 89030-000,
Blumenau, Santa Catarina, Brazil

Fernando Darci Pitt

https://orcid.org/0000-0003-2106-3222

Serviço Nacional de Aprendizagem Industrial (SENAI), Rod. Admar Gonzaga, 2765,
Florianópolis, Santa Catarina, Brazil

Abstract: In the face of climate change and the increasing frequency of climate-related disasters, there is a growing emphasis on renewable fuel sources to mitigate greenhouse gas emissions. Biodiesel, produced from crude or residual vegetable oils and animal fats, represents a significant biofuel option. Its production process involves transesterifying triglycerides with short-chain alcohols, resulting in biodiesel and low-purity glycerol as byproducts. This study explores the polymerization of residual glycerol as a sustainable strategy to enhance its value, particularly in light of the rising biodiesel production rates, which generate approximately 10% residual glycerol. The research focuses on synthesizing polymers from glycerol and highlights its potential as a method to repurpose a byproduct of biodiesel production. Experimental tests were conducted in a batch reactor, utilizing glycerol and adipic acid polycondensation in ratios of 1:0.75, 1:1, 1:1.5, and 1:2 to produce adipic polyglycerol. The reactions were carried out at 160 ºC with stirring at 60 RPM, using dibutyl phthalate as a catalyst, and monitored for water accumulation. Both partially purified and commercially bi-distilled glycerol were employed in the experiments. Infrared spectrophotometry analysis revealed significant molecular transformations in the polymers synthesized under varying reaction conditions. These findings provide promising prospects for utilizing this material in the production of polymers with the potential to serve as robust alternatives to petroleum-based plastics.

This study concludes that residual glycerol from biodiesel production can be effectively utilized as a raw material for polymer synthesis, offering considerable potential to replace fossil-based polymers and significantly reduce environmental impact.

Keywords: Biodiesel, Glycerol, Polycondensation, Polyglycerol, Transesterification

1. Introduction

The glycerol residue generated during the biodiesel production process via transesterification exhibits low purity, with its quality varying based on the conversion methods, type of alcohol, and catalyst employed. This residue typically contains excess alcohol, residual catalysts, and soaps formed as byproducts of parallel chemical reactions occurring during transesterification. These impurities significantly reduce the commercial value of residual glycerol and limit its potential applications. As a result, such residues are often discarded in biodiesel production processes due to the aforementioned limitations (Domingos et al., 2019; Attarbachi et al., 2023; Aziz et al., 2018; Kalvelage et al., 2017; Kumar et al., 2019; Nasir et al., 2017; Barros et al., 2008; Cai et al., 2013; Chol et al., 2018; Colombo et al., 2017; Colombo et al., 2019; Silva et al., 2021; Rahman et al., 2022; Oliveira et al., 2020; Gupta et al., 2023; Santos et al., 2021).

In biodiesel production processes, glycerol has been produced in significant volumes, primarily because biodiesel is used as an additive to fossil fuels. Therefore, in recent decades, with the advent of biodiesel production, residual glycerol with a low degree of purity has been generated in the ratio of 1 mole of glycerol for every 3 moles of methyl or ethyl esters (biodiesel) produced, corresponding to approximately 10% by weight of the total mass of the products of the transesterification reaction (Kumar et al., 2019; Nasir et al., 2017; Barros et al., 2008; Colombo et al., 2017; Colombo et al., 2019; Zeleme and Barros, 2022; Barros, 2022, Silva et al., 2021; Rahman et al., 2022; Oliveira et al., 2020; Gupta et al., 2023; Santos et al., 2021, Calderon et al., 2023).

In this context, Domingos et al. (2019) and Al-Haimi et al (2024) conducted studies on glycerol purification and optimization of crude glycerol purification, respectively, to enhance the commercial value of this product. The methodologies developed aimed to define a route for the purification of crude glycerol to yield a higher purity product, involving the following steps: a) neutralization of residual glycerol with phosphoric acid; b) vacuum filtration; and c) adsorption onto activated carbon heated to 60 °C to reduce its viscosity. The combination of these steps aimed to produce glycerol of higher purity, which would be more suitable for commercial applications. This purification route could potentially increase the economic value of crude glycerol, a by-product of biodiesel production, by making it usable in more demanding industries such as pharmaceuticals, cosmetics, and food.

A study conducted by Aziz et al. (2018) showed that the glycerol generated as a byproduct in biodiesel production from waste cooking oil has low purity. The crude glycerol sample contained impurities such as methanol, catalyst, soap, and water, with analysis revealing 67.7% water, 16.7% ash, and a density of 1.1217 g/mL. The impurities were adsorbed onto bentonite that had been activated in 1.5 M sulfuric acid and characterized by SEM-EDX. After treatment with bentonite at 60 °C for 75 minutes, the purified glycerol sample contained 89.5% glycerol, 4.3% water, and 3.6% ash, with a density of 1.2212 g/mL. The cited authors concluded that activated bentonite could be used for the adsorption and removal of impurities from waste cooking oil.

Raman et al. (2019) utilized crude glycerol from biodiesel production to produce high-purity glycerol

through neutralization, ultrafiltration, ion exchange resins, and vacuum distillation operations. The results verified that high-purity glycerol could be produced by combining these techniques.

Aziz et al. (2018) and Nanda et al. (2014) purified crude glycerol obtained from biodiesel production through acidification using sulfuric, hydrochloric, or phosphoric acids, and the results were compared. The effects of pH on the purification efficiency were also investigated, and both the crude glycerol and the purified products were characterized. The authors concluded that phosphoric acid was a better purifying agent than the other acids.

Statistics from the European Biodiesel Board (EBB, 2023a) indicate that the European Union (EU) continues to be a major producer of biodiesel, with an annual production exceeding 13.7 million tons in 2022. This large-scale production generates a significant amount of crude glycerol as a by-product, estimated at approximately 1,37 million tons per year (assuming a 10% glycerol yield from biodiesel production). The oversupply of glycerol has further intensified market challenges, driving down prices and creating economic and environmental pressures.

Statistics show that the European market produces more than 13.7 million tons of biodiesel per year EBB (2023a), and the residual glycerol from this process drives down the price of industrial glycerol in the international market and contributes to observed environmental impacts (Tomatis, Zilli, & Pavan, 2024).

However, the advancement in biodiesel production rates has had worldwide repercussions. In 2023, Brazil's biodiesel production reached approximately 7.5 million cubic meters (7.5 billion liters), marking a significant increase from the previous year, while in the same year, the European Union produced approximately 19.02 million metric tons of biodiesel, marking a decrease from the previous year. In Asia, Indonesia led biodiesel production with an estimated 13.57 billion liters in 2023, a 25% increase from 2022. Malaysia and Thailand's specific biodiesel production figures for 2023 are not readily available in the provided sources. Collectively, these countries significantly contribute to global biodiesel production, with Indonesia alone accounting for a substantial portion (Rahmanulloh and Osinski, 2023).

Therefore, statistics indicate that in 2023, the leading countries in biodiesel production and usage produced, approximately, 35 million tons of biodiesel, which, in relation to the glycerol fraction described in this work, represents approximately 3.5 million tons of glycerol (EBB, 2023b; OECD/FAO, 2023a; IEA, 2023a).

Glycerol is a colorless, odorless, viscous chemical component used in pharmaceutical formulations, the food industry, and explosives. It is an alcohol designated by IUPAC as 1,2,3-propanetriol, known for its high-water solubility and hygroscopic nature, comprising three hydroxyl groups. Commercial production of glycerol can also be achieved through microbial fermentation or chemical synthesis from petrochemical products. Alternatively, it can be obtained from soap production or as a byproduct of fat hydrolysis (da Silva et al., 2009; Dhabhai et al., 2016; Gabriel et al., 2019; Gabriel et al., 2015; Habaki et al., 2019).

Therefore, new applications for glycerol have emerged in the international market, particularly in the food industry, where it is utilized as a humectant, solvent, softener, sweetener, and lubricant in industrial equipment. In the medical and pharmaceutical industries, glycerol is used in ointments, syrups, cosmetics, toothpaste, and as a drug delivery agent (Gerpen, 2005; Wolfson et

al., 2009; Ciriminna et al., 2014; OECD/FAO, 2023b).

In the chemical industry, glycerol serves as a fiber softener and is incorporated into the composition of special papers, providing greater flexibility and tenacity. Additionally, it is applied as an antifreeze agent, in paint formulations, and as a precursor for bio-based polymers (Gerpen, 2005; Wolfson et al., 2009; Yang et al., 2012; Mota et al., 2017).

Glycerol is also widely used in chemical syntheses, particularly in the production of dendrimers, polyethers, and hyperbranched polyesters, which possess a large surface area and significant amounts of functional groups. It can be catalytically hydrogenated to produce propylene glycol, especially 1,3-propanediol, a high-value component for polyester synthesis. These processes require high-purity glycerol (Wolfson et al., 2009; Quispe et al., 2013; Ciriminna et al., 2014).

Wolfson et al. (2009) conducted alternative studies on using crude residual glycerol as a reaction medium for chemical synthesis. Similarly, Mota et al. (2009) researched the production of ethers, acetals, and esters from crude glycerol derived from biodiesel production. Recent studies have expanded these applications, exploring the use of glycerol in bio-based plastics, lubricants, and renewable fuels (Mota et al., 2017; OECD/FAO, 2023b; IEA, 2023b).

In this context, the prospect of depleting oil reserves and the ecological pressures resulting from the use of petroleum derivatives, combined with the geopolitical instabilities of oil-producing countries, have driven industrial and governmental efforts to develop scientific and technological research. These efforts aim to propose new renewable inputs for the chemical industry, replacing petrochemical feedstocks with sustainable alternatives like glycerol (Gerpen, 2005; Ciriminna et al., 2014; OECD/FAO, 2023a).

Recent research indicates that alcohol chemistry has developed over the last decade as a precursor to the petrochemical industry. Jewur (1984) highlighted the catalytic reactions of ethanol to produce ethylene, propylene, and acetylene, among other products. More recent studies, such as those by Zhang et al. (2020), have expanded on these findings, exploring advanced catalytic processes and the use of renewable alcohols like ethanol and butanol in the production of bio-based chemicals, further bridging the gap between renewable feedstocks and the petrochemical industry.

Additionally, the text notes that Dutch chemists had already produced gas from ethanol catalyzed by alumina, with the ethanol dehydration reaction being conducted on a mixed oxide of silica and alumina. Recent advancements, such as those by Shinde et al. (2021), have explored enhanced catalysts for ethanol dehydration, increasing efficiency and selectivity in producing biofuels and olefins, demonstrating the continued evolution of alcohol chemistry in industrial applications.

Biopolymerization processes, commonly used in scientific literature, refer to natural polymers obtained and used in their natural state, sometimes modified by unique processes or biosynthesized. Examples include animal skins, vegetable fibers, plant resins, and latex, commonly known as biopolymers. Synthetic polymers derived from natural sources, however, rely on chemical synthesis to achieve the desired physicochemical properties (Andrade et al., 2001; Pitt et al., 2011). Recent studies, such as those by Wu et al. (2022), have explored the functionalization of biopolymers with synthetic modifications to enhance properties like biodegradability, mechanical strength, and processability, making them more competitive with traditional synthetic polymers.

This research investigates the potential of producing polymers from industrial process residues, specifically glycerol residues generated during the transesterification of oils and fats in biodiesel production. This residue, after purification, can be polymerized to yield polyglycerol, a product that can compete with synthetic polyglycerol derived from petrochemicals. Polyglycerol, as the first hyperbranched polymer produced through controlled synthesis, exhibits a unique combination of stability, biocompatibility, high functionality of terminal groups, and compactness, referred to as dendrimer architecture (Frey and Haag, 2002). Wu et al. (2020) have also explored polyglycerol derivatives for drug delivery systems, showcasing their versatility beyond traditional polymer applications.

Garti et al. (1981) explored the possibility of producing polyglycerol by polymerizing PA glycerol through a chemical reaction within a temperature range of 260–280 °C under an inert atmosphere, using 2.5 mol% of NaOH as a catalyst. The author investigated the influence of temperature, catalyst type, and catalyst mass. The glycerol used had a purity level of 99%, and the reaction progress was monitored by measuring the volume of water produced. More recent studies, such as those by Zhang et al. (2023), have optimized glycerol polymerization under green chemistry conditions, using alternative, more sustainable catalysts and solvents, thereby improving yield and reducing environmental impact.

Brioude et al. (2007) conducted the esterification reaction of glycerol with adipic acid using molar ratios of 1:1, 1:1.5, and 1:2 of glycerol to adipic acid, employing 10% by weight of dibutyltin dilaurate as a catalyst in hexane. The reaction was performed under stirring conditions, maintaining a temperature of 100 °C for sufficient time to ensure complete homogenization. Subsequently, the temperature was increased to 150 °C to facilitate the glycerol and adipic acid reaction. The reaction progress was monitored by measuring the amount of condensed water recovered. In this context, this study enabled the evaluation of appropriate conditions for utilizing the potential of residual glycerol to produce polymers capable of replacing petroleum-derived polymers. These polymers offer reduced environmental impact and high biodegradation rates. Liu et al. (2023) has further refined esterification processes for glycerol-based polyesters, enhancing their mechanical properties and biodegradability, thereby increasing their competitiveness with traditional petrochemical plastics.

For other hand, the environmental impact assessment focuses on key sustainability categories, particularly the use of residual glycerol as a renewable raw material, which results in a significantly lower carbon footprint compared to petroleum-derived polymers. The potential CO_2 emissions associated with energy consumption during the polymerization process can be further minimized by utilizing renewable energy sources, such as solar or wind energy. Additionally, the substitution of fossil-based raw materials with residual glycerol reduces the overall carbon footprint of the final product, aligning with sustainable development goals (Zoldy et al., 2022; Virt and Arnold, 2022; Zöldy and Baranyai, 2023; Silva et al., 2025).

Residual glycerol is derived from biomass, a renewable source, which reduces reliance on non-renewable resources such as oil and natural gas. This shift contributes to the mitigation of non-renewable resource depletion. Furthermore, the adoption of greener technologies and the use of less harmful catalysts in the polymerization process help minimize environmental impacts. However, emissions of compounds such as NOx and SOx, generated from the combustion of fossil fuels for energy production, can contribute to the eutrophication of water bodies and the acidification of soil

and water. Therefore, reducing fossil fuel consumption in the polymer production process is critical to mitigating these adverse environmental effects (Zoldy et al., 2022; Virt and Arnold, 2022; Zöldy and Baranyai, 2023; Goldbach et al., 2022).

Thus, the goal of this paper is to explore the polymerization of residual glycerol as a sustainable strategy to enhance its value, particularly in light of the rising biodiesel production rates, which generate approximately 10% residual glycerol as a by-product. The study focuses on synthesizing polymers from glycerol, emphasizing its potential as a method to repurpose this by-product of biodiesel production. By transforming residual glycerol into high-value polymers, this research aims to address the economic and environmental challenges associated with glycerol oversupply, reduce reliance on fossil-based raw materials, and contribute to the development of sustainable materials with a lower carbon footprint.

2. Material and Methods

The characterization of glycerol and the produced polymer involved the use of a Shimadzu TCC240A spectrophotometer with the UVprobe 2.21 program for data collection, a gas chromatograph with a flame ionization detector Varian, model GC-450, and a Nicolet 4700 FT-IR infrared spectrometer.

The materials utilized included purified glycerol and bi-distilled glycerin from Quimidrol Com. Ind. Imp. Ltda with a molecular mass of 92.09 g/mol and highly pure adipic acid 1,4-Butanedioic Acid ($C_6H_{10}O_4$), from Vetec Química Fina Ltda. Additionally, dibutyl phthalate from Vetec Química Fina Ltda was used.

The glycerol used in the process was purified following the method by Domingos (2019), which involved neutralizing residual glycerol with phosphoric acid, vacuum filtration, and adsorption onto activated carbon heated to 60 °C to reduce its viscosity.

The polymerization reactions were carried out in a 0.750-liter stainless steel batch chemical reactor (Figure 1), heated by a 1,000 W electric resistance, controlled with a PID controller that receives temperature information from inside the reactor through a PT-100 sensor and a solid-state relay.

Figure 1: The polymerization reactor used in this study

The reactor was coupled with an agitation system with rotation control and a torque meter, and it was also insulated using a thermal insulation blanket. Purified glycerol and adipic acid were added to the reactor in the molar ratio given in Table 1. The reactor was sealed with screws, fixed to the support of the mechanical stirrer, and thermally insulated. The mechanical stirrer was set to a low rotation speed, and heating was initiated. When the reactor's internal temperature reached 100 °C, the agitation was increased to 60 rpm for 30 minutes to ensure complete homogenization of the reagents. Upon completing this stage, the catalyst (dibutyl phthalate) was added to the glycerol/adipic acid mixture, and the condenser assembly was attached to the reactor. These apparatuses were used to recover the water resulting from the polycondensation reaction conducted in the reactor. At this stage, the temperature was increased to 160 °C and maintained constant until the end of the reaction.

In all tests, a catalyst loading of 2% dibutyl phthalate (relative to the mass of glycerol) was used. The reaction was conducted at a constant temperature of 160 °C and an agitation rate of 60 rpm. The progress of the polycondensation reaction was monitored by tracking the accumulation of water produced, with time zero defined as the collection of the first drop of liquid. The reaction was considered complete when water condensation ceased, indicated by stability or a plateau in the accumulated water volume, which was monitored using PID controller.

Table 1. Polymerization test with different glycerols and varied molar ratio.

Glycerol	Glycerol/Acid Ratio	Agitation (rpm)	Temperature (ºC)
Adsorbed	1:0.76	60	160
	1:1.0		
	1:1.5		
	1:2.		
Standard	1:0.76		
	1:2		
Adsorbed	1:2		
Distilled	1:2		
Filtered	1:2		

The produced polymer was characterized using a Thermo Fischer Scientific Nicolet 4700 FT-IR infrared spectrometer, with a scanning range of 400–4000 cm^{-1}, a resolution of 4, and 32 scans in ATR mode with a germanium crystal.

3. Results and Discussion

The progress of the reaction was monitored by tracking the volume of water condensed (Figure 2), with time zero defined as the moment the first drop of liquid was collected. The polymerization tests followed the experimental plan outlined in Table 1, making it possible to assess the influence of glycerol quality on the polymerization process.
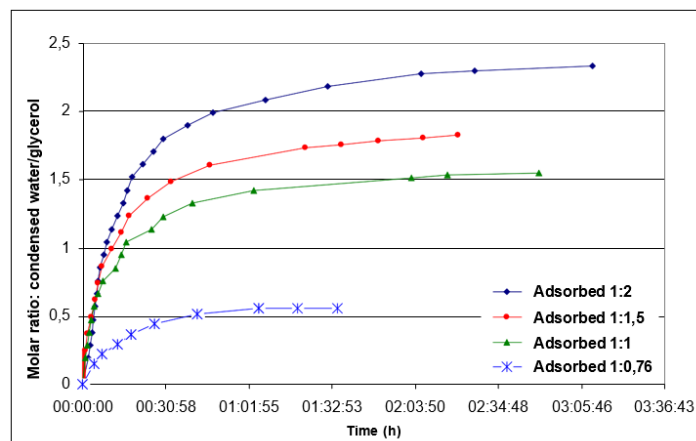

Figure 2. Reaction evolution as a function of the molar ratio of condensed water relative to the glycerol added to the reactor (Adsorbed Glycerol)

3.1. Evolution of Polymerization

The data collected during the polymerization tests revealed the relationship between glycerol volume and recovered water volume, as depicted in Figures 2, 3 and 4. These figures highlight the influence of the adsorbed glycerol to adipic acid ratio on the polymerization process. Figure 2 demonstrates the impact of this ratio, showing the importance of adipic acid in water recovery and, consequently, in improving polymerization performance.
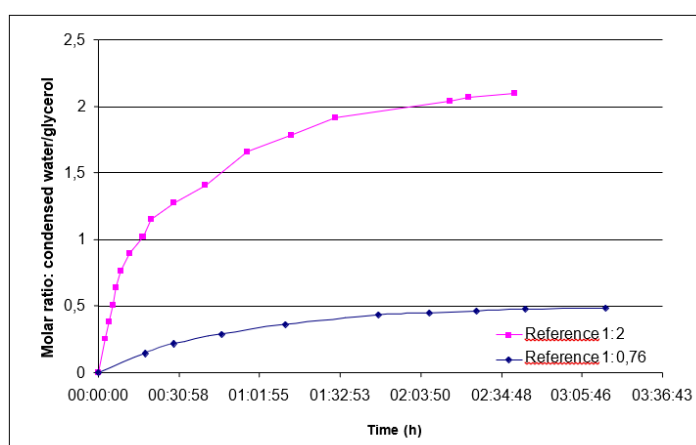

Figure 3. Reaction evolution as a function of the molar ratio of condensed water relative to the glycerol added to the reactor

The results indicate that a lower mass of adipic acid leads to a smaller volume of accumulated water and, consequently, lower process performance. The 1:2 ratio exhibited a more pronounced increase in polymerization water volume during the first hour of the reaction, after which the process stabilized and continued until the third hour. Lower ratios of adipic acid to glycerol resulted in decreased performances, directly proportional to the increase in adipic acid mass in the reaction mixture.

To confirm the influence of the glycerol-to-adipic-acid ratio, experimental tests were conducted using reference glycerol, observing the same behavior described in Figure 2. This indicates that increasing the mass of adipic acid in glycerol during the polymerization reaction increases the volume of polymerization water recovered by condensation (Figure 3).

Given the optimal performance based on the glycerol-to-adipic-acid ratio, the polymerization performance for different types of glycerol was evaluated based on the purification stages involved. Figure 4 shows three curves of polymerization progression involving the reactions of adsorbed, reference, and distilled glycerol with adipic acid in a molar ratio of 1:2. While all three types of glycerol exhibited similar polymerization performance, adsorbed glycerol consistently outperformed both distilled and reference glycerol.
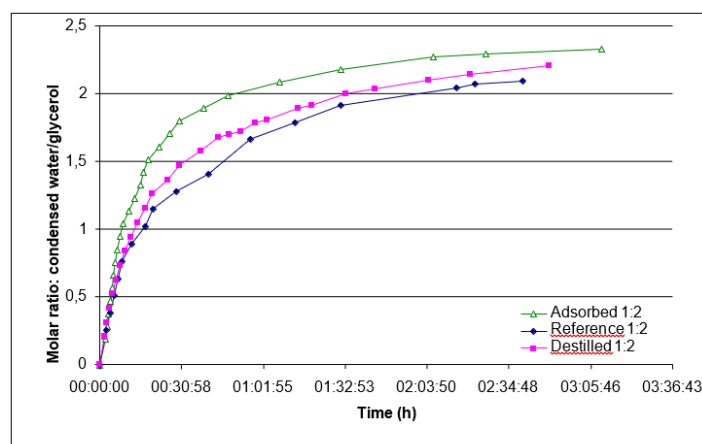

Figure 4. Reaction evolution as a function of the molar ratio of condensed water relative to the glycerol added to the reactor (Glycerol/Adipic Acid molar ratio of 1:2)

Domingos et al. (2019) conducted absorbance tests to assess the quality of the glycerol used, based on the attenuation of a light beam passing through a quartz filter. The glycerol samples were diluted in anhydrous ethanol and analyzed using a spectrophotometer. The measurements demonstrated that each stage of purification significantly influences the quality of the purified glycerol. The absorbance curves obtained from the analysis of the purified glycerol samples (adsorbed, neutralized, and crude glycerol) exhibited qualitative behavior similar to the reference glycerol curve (Figure 5). However, a marked deviation was observed, attributable to the presence of a high content of impurities. This distinction underscores the impact of residual contaminants on the optical properties of the glycerol samples.
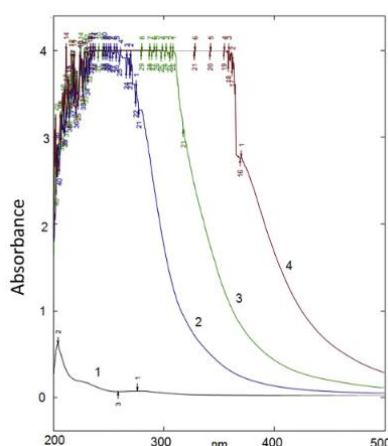
Figure 5: Absorbance spectra from 200 to 500 nm for: 1) reference glycerol, 2) adsorbed glycerol, 3) neutralized glycerol, and 4) crude glycerol (Domingos et al., 2019).

This approximation suggests that the purified glycerol contains residual impurities, primarily evidenced by the yellowish coloration of the final product (Domingos et al., 2019). The presence of these impurities likely accounts for the higher recovery of water observed during the polymerization of adsorbed, distilled, and reference glycerol, in a 1:2 ratio (Figure 4). This correlation highlights the influence of impurity levels on the reaction dynamics and water yield during the polymerization process.

Therefore, the water produced during the reaction results from the aggregation of glycerol and adipic acid monomers, which involves the breaking of hydroxyl (OH^-) and hydrogen (H^+) radicals, leading to the formation of water upon their combination. These findings align with those reported in the literature by Garti et al. (1981) and Brioude et al. (2007), as well as more recent studies by Zhang et al. (2018) and Kumar et al. (2021), who investigated polymer production from glycerol and evaluated reaction conversions based on the volume of condensed water recovered.

Furthermore, the analysis of Figures 2, 3, and 4 allows us to conclude that the mass ratio between glycerol and the reagent (adipic acid) significantly influences the quality of the produced polymers. Higher volumes of recovered water indicate a more extensive aggregation of monomers within the polymer's molecular structure, as illustrated in Figure 6. This relationship underscores the critical role of stoichiometric ratios in optimizing polymerization efficiency and polymer quality, as highlighted by recent advancements in polymerization techniques and reaction kinetics (Silva et al., 2020; Li et al., 2022).
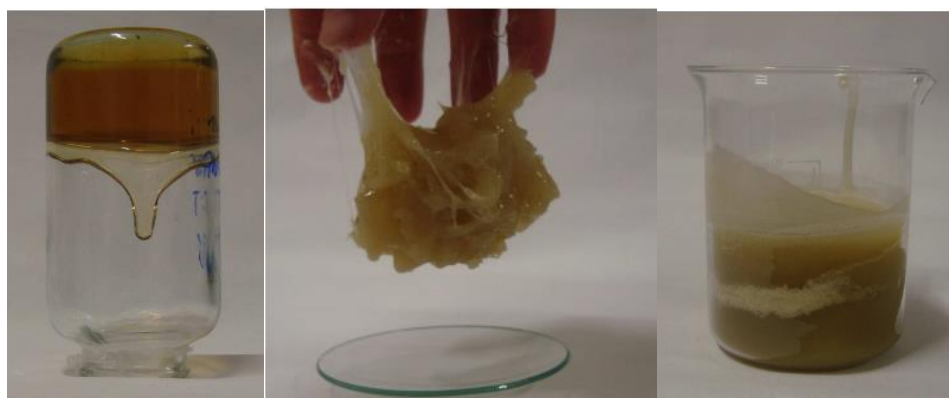
Figure 6. Polymer produced with adsorbed glycerol at the ratio: a) 1:1, b) 1:1.5, and c) 1:2

The results presented in Figure 6 show an increase in the viscosity of the produced glycerol with a decrease in the molar ratio between glycerol and adipic acid, forming a polymer with high resistance and strong adhesion to the surface of the conditioning container.

3.2. Characterization of the Produced Polymer

The polymers produced in the experimental tests, as depicted in Figures 2, 3, and 4, were characterized using infrared spectroscopy (Figure 7) within the 400–4000 cm⁻¹ range to identify the functional groups present. Figure 7 shows the spectra of adsorbed glycerol and the polymers produced with adsorbed glycerol under four different scenarios. These scenarios correspond to glycerol-to-adipic acid molar ratios of 1:0.75, 1:1, 1:1.5, and 1:2, respectively. The analysis of these spectra provides insights into the structural changes and functional group interactions that occur during polymerization, highlighting the influence of stoichiometric ratios on the final polymer properties.
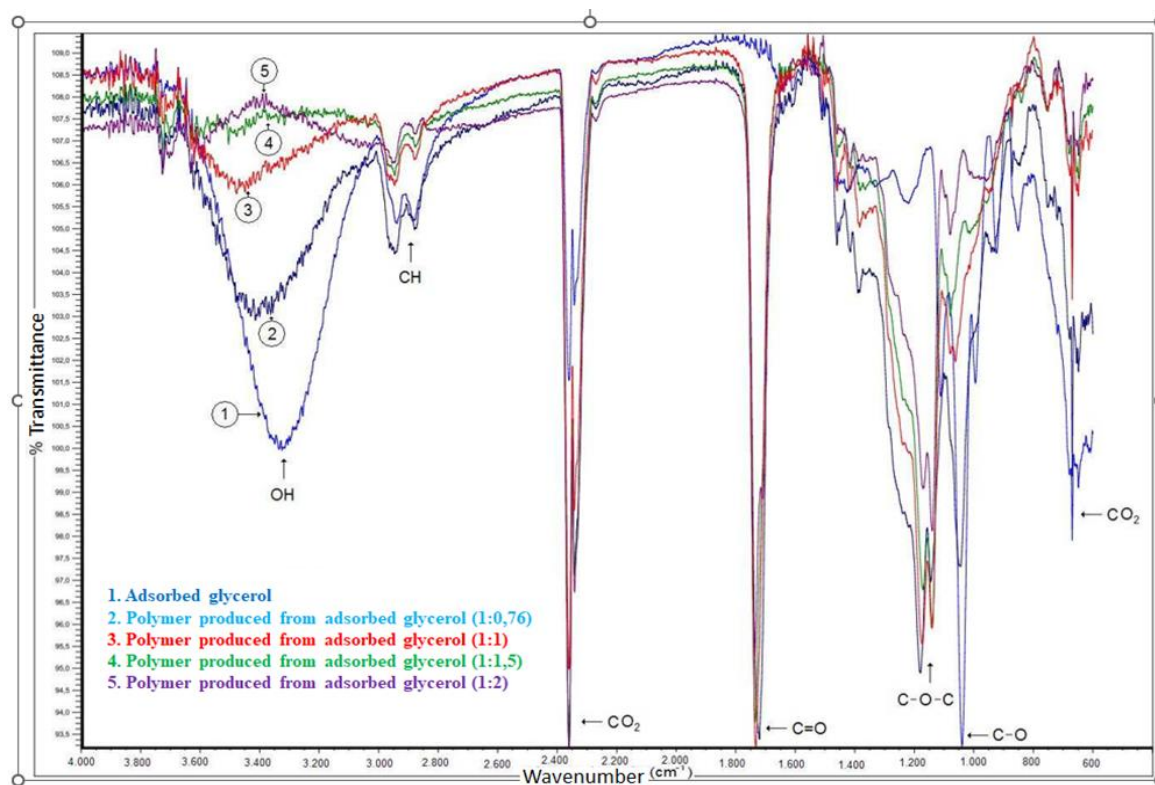

Figure 7. Infrared scan spectrum of adsorbed glycerol compared with the produced polymer

The evidence of polymer formation by polycondensation is identified by the band of the consumed hydroxyl group, which leads to the formation of water during polymerization, with an increase in the molar ratio of adsorbed glycerol to adipic acid and the consequent formation of the ester group. Additionally, there is an increase in the bands at the wavelengths corresponding to C=O, C–O–C, and C–H, characteristic of esters that constitute the polymers obtained from biomass (glycerol from biodiesel production).

These results are consistent with the findings of Zhang et al. (2018) and Kumar et al. (2021), who synthesized a polyester from glycerol and phthalic acid using glycerol-to-phthalic acid molar ratios of 1:1, 1:1.5, and 1:2. These ratios correspond to OH-to-COOH molar ratios of 1.5:1, 1:1, and 0.75:1, respectively. A decrease in the molar ratios results in a reduction of unreacted hydroxyl (OH) groups and an increase in unreacted carboxyl (COOH) groups, reflecting the stoichiometric influence on the polymerization process. Zhang et al. (2018) and Kumar et al. (2021) have further validated these findings, emphasizing the critical role of stoichiometric control in optimizing polymerization efficiency and polymer properties.

Additionally, two bands unrelated to any functional group were observed in the spectra. These bands are attributed to interference caused by dissolved carbon dioxide in the material, with approximate bands appearing between 2325 cm^{-1} and 2360 cm^{-1}, as well as a distinct signal at 667 cm^{-1}. These artifacts are common in infrared spectroscopy and do not correspond to the chemical structure of the polymer. Recent advancements in spectroscopic analysis, as highlighted by Zhang et al. (2018) and Kumar et al. (2021), have improved the identification and interpretation of such spectral interferences, ensuring more accurate characterization of polymer structures. Furthermore, studies by Silva et al. (2020) have demonstrated the application of advanced spectroscopic techniques to minimize these interferences, enhancing the reliability of polymer characterization in complex systems.
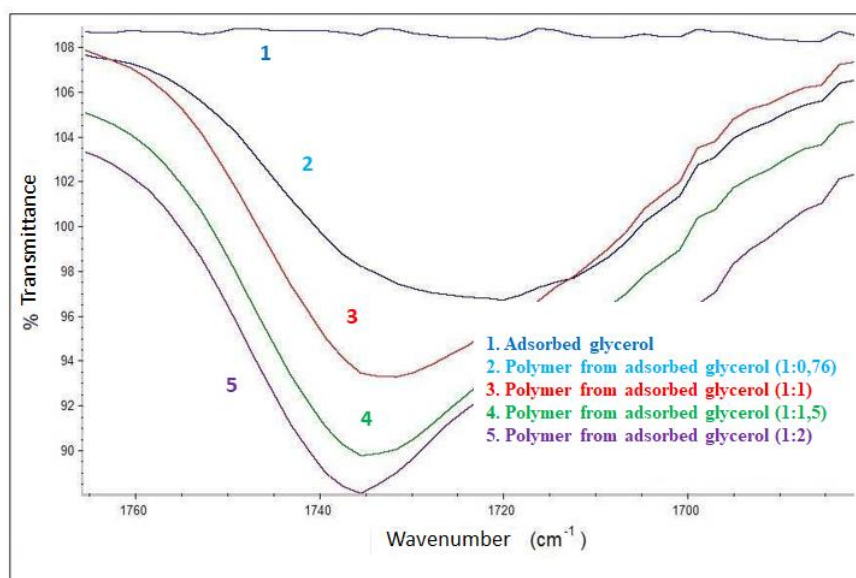

Figure 8. Highlight of the IR spectrum in the ester group band (1670–1760 cm^{-1})

According to Calderon et al. (2023), the main characteristic of polyglycerol adipic is forming ester bonds from the reaction of alcohol and carboxylic acid groups. The carbonyl group of the ester bonds can be identified by the absorption at 1730–1720 cm^{-1}. The remaining alcohol groups can be observed

at the absorption at 3600–3000 cm^{-1}, confirming the increased formation of ester bonds at higher reaction temperatures and supporting the observed OH number, acid number, and viscosity behaviors. The authors confirm that increasing O–H transmittance and decreasing phthalic acid C–H transmittance occur as the OH molar ratio increases. This observation aligns with the behavior of the OH number and acid number as the OH ratio increases. The decrease in phthalic acid C–H transmittance is due to the lower acid content as the OH ratio increases, showing a decrease in transmittance as the OH molar ratio increases, confirming that lowering the available acid groups for the reaction reduces the formation of ester bonds.

3.3. Life Cycle Assessment of Residual Glycerol

The use of residual glycerol as a raw material for polymer production is an environmentally sustainable alternative when analyzed in comparison to fossil-derived polymers, especially considering the increasing biodiesel production rates, which generate a significant amount of residual glycerol. Based on this principle, it is possible to quantify and compare the environmental impacts associated with using residual glycerol from biodiesel production for polymer synthesis, in comparison to conventional fossil-based polymers such as polyethylene and polypropylene. This allows for the establishment of a scientific foundation for adopting residual glycerol as a raw material, with the potential to reduce the environmental impacts of the polymer industry.

For this analysis, the functional unit adopted is the production of 1 kg of polymer from residual glycerol, considering the environmental impact throughout the entire life cycle, from raw material extraction to final polymer production. The system boundaries include all stages of the product's life cycle, such as obtaining residual glycerol as a byproduct of biodiesel production, transportation to the polymerization unit, the polymerization process itself, energy usage in the process, and the necessary auxiliary materials such as catalysts and solvents. The life cycle of the produced polymer is considered up to the production of the final product. The disposal or recycling of the polymer is not addressed in this evaluation.

Thus, the compilation of a Life Cycle Inventory (LCI) is an essential stage that involves quantifying the inputs and outputs of the process, encompassing raw materials, energy flows, and waste generated. The LCI incorporates the analysis of typical processes used to produce polymers from residual glycerol.

Approximately, 1 kg of residual glycerol generates 0.9 kg of polymer, considering 0.1 kg of process losses and byproducts, as the polymerization process involves dibutyl phthalate as catalysts and adipic acid as a reagent, and the conversion is not complete. The use of dibutyl phthalate as a catalyst and adipic acid as a non-toxic solvent helps minimize environmental impacts. In this process, both electrical and thermal energies are consumed, as the reactor operates at temperatures above 160 °C, with energy efficiency considered a crucial factor in determining the environmental impact.

The transportation of residual glycerol from biodiesel production facilities to processing units, along with the associated CO_2 emissions from transport, is considered. The polymerization of residual glycerol involves chemical reactions to form polymer chains, with energy consumption (thermal or electrical) and the generation of byproducts such as wastewater and gaseous effluents. CO_2 emissions resulting from the consumption of electrical and thermal energy during the polymerization process are quantified based on the energy sources used. Process waste includes non-recoverable solvents,

contaminated catalysts, and liquid effluents, and the proper management of such waste is essential to minimize environmental impacts.

The results show that the use of residual glycerol as a raw material for polymer production is an environmentally favorable alternative compared to fossil-derived polymers, especially in terms of reducing carbon footprint and using renewable resources. However, impacts related to energy consumption and chemical waste management require more in-depth critical analyses, as using residual glycerol and adopting more efficient polymerization processes and renewable energy sources can significantly reduce global environmental impacts. To achieve this, the implementation of cleaner technologies and improvements in energy efficiency are essential steps to maximize environmental benefits. Additionally, a circular economy model, where residual glycerol is efficiently utilized to generate value and mitigate the environmental impacts associated with its disposal, is an opportunity for further exploration. Sustainable catalysts and solvents, as well as polymer recycling, are areas that demand more research and development.

Therefore, the life cycle assessment of using residual glycerol for polymer production presents significant potential for reducing environmental impacts, especially by replacing fossil-derived polymers. The adoption of greener processes, renewable energy sources, and less toxic catalysts are crucial conditions to maximize environmental benefits and ensure that polymer production from residual glycerol is truly sustainable.

4. Conclusions

Based on the analysis of the results presented in this work, it is possible to conclude that:

i.   Purified glycerol can be characterized by spectrophotometry and chromatography, and used for the production of polymers, whose characteristics were evaluated in this work;

ii. The methodology of polycondensation polymerization of purified glycerol represents a significant advancement for harnessing the potential of glycerol residues produced in biodiesel production units;

iii. The polymers produced from reference, adsorbed, and distilled glycerol in different molar ratios of glycerol/adipic acid show adequate quality and potential for scaling up this process, utilizing the potential of these residues for the chemical industry;

iv. Characterizing the polymers by infrared spectroscopy in the wavelength range of 400–4000 cm^{-1} confirms the formation of functional groups related to the poly (adipic polyglycerol) polymer formed.

Competing Interest Statement

The authors declare that there are no competing interests related to the research, authorship, or publication of this manuscript. No financial, personal, or professional relationships, whether direct or indirect, exist that could inappropriately influence the work presented in this study. The authors further confirm that they have adhered to ethical guidelines in conducting and presenting the research, ensuring that the results and conclusions drawn are unbiased and free from any conflict of interest.

Author Contributions

The authors of this article contributed proportionally to the development of this work, with the first and last authors assuming greater responsibility in the proposed studies, conducted within the scope

of the Master's dissertation in Chemical Engineering at the Regional University of Blumenau, Brazil.

References

Andrade, C. T., Coutinho, F. M. B., Dias, M. L., Lucas, E. F., Oliveira, C. M. F., & Tabak, D. (2001). *Dicionário de Polímeros*. Editora Interciência.

Al-Haimi, A. A. N. M., Luo, W., Fu, J., Zhu, S., Yehia, F., & Wang, Z. (2024). Optimization of crude glycerol purification for enhanced commercial value. *Journal of Sustainable Chemistry, 15*(3), 245–260. https://doi.org/ 10.1002/jctb.7718

Attarbachi, T., Kingsley, M. D., & Spallina, V. (2023). New trends on crude glycerol purification: A review. *Fuel, 340*, 127485. https://doi.org/10.1016/j.fuel.2023.127485

Aziz, I., Sulistina, R. C., Hendrawati, N., & Adhani, L. (2018). Purification of crude glycerol from acidification using tea waste. *IOP Conference Series: Earth and Environmental Science, 175*, 012010. https://doi.org/10.1088/1755-1315/175/1/012010

Barros, A. A. C., Wust, E., & Meier, H. F. (2008). Estudo da viabilidade técnico-científica da produção de biodiesel a partir de resíduos gordurosos [Evaluate the waste fatty acid by scientific and technical study to obtain biodiesel]. *Engenharia Sanitária e Ambiental, 13*(3), 255–262. https://doi.org/10.1590/S1413-41522008000300003

Barros, A. A. C. (2022). Evaluation of extractive distillation using efficiency correlation and experimental data: Avaliação da destilação extrativa usando a correlação de eficiência e dados experimentais. *Studies in Engineering and Exact Sciences, 3*(4), 737–754. https://doi.org/10.54021/seesv3n4-012

Brioude, M. M., Guimarães, D. H., Fiúza, R. P., Prado, L. A. S. A., Boaventura, J. S., & José, N. M. (2007). Synthesis and characterization of aliphatic polyesters from glycerol, by-product of biodiesel production, and adipic acid. *Materials Research, 10*(4), 335–339. https://doi.org/10.1590/S1516-14392007000400003

Cai, T., Li, H., Zhao, H., & Liao, K. (2013). Purification of crude glycerol from waste cooking oil-based biodiesel production by orthogonal test method. *China Petroleum Processing and Petrochemical Technology, 15*(1), 48–53.

Calderon, M. J. P., Dumancas, G. G., Gutierrez, C. S., Lubguban, A. A., Alguno, A. C., Malaluan, R. M., & Lubguban, A. A. (2023). Producing polyglycerol polyester polyol for thermoplastic polyurethane application: A novel valorisation of glycerol, a byproduct of biodiesel production. *Heliyon, 9*(9), e19491. https://doi.org/10.1016/j.heliyon.2023.e19491

Chol, C. G., Dhabhai, R., Dalai, A. K., & Reaney, M. (2018). Purification of crude glycerol derived from biodiesel production process: Experimental studies and technoeconomic analyses. *Fuel Processing Technology, 178*, 78–87. https://doi.org/10.1016/j.fuproc.2018.05.023

Colombo, K., Ender, L., & Barros, A. A. C. (2017). The study of biodiesel production using CaO as a heterogeneous catalytic reaction. *Egyptian Journal of Petroleum, 26*(2), 341–349. https://doi.org/10.1016/j.ejpe.2016.05.006

Colombo, K., Ender, L., Santos, M. M., & Barros, A. A. C. (2019). Production of biodiesel from soybean oil and methanol, catalyzed by calcium oxide in a recycle reactor. *South African Journal of Chemical Engineering, 28*, 19–25. https://doi.org/10.1016/j.sajce.2019.02.001

Ciriminna, R., Pina, C. D., Rossi, M., & Pagliaro, M. (2014). Understanding the glycerol market. *European Journal of* Lipid *Science and Technology, 116*(10), 1432–1439. https://doi.org/10.1002/ejlt.201400229

Da Silva, G. P., Mack, M., & Contiero, J. (2009). Glycerol: A promising and abundant carbon source for industrial microbiology. *Biotechnology Advances, 27*(1), 30–39. https://doi.org/10.1016/j.biotechadv.2008.07.006

Dhabhai, R., Ahmadifeijani, E., Dalai, A. K., & Reaney, M. (2016). Purification of crude glycerol using a sequential physico-chemical treatment, membrane filtration, and activated charcoal adsorption. *Separation and Purification Technology, 168*, 101–106. https://doi.org/10.1016/j.seppur.2016.05.030

Domingos, A. M., Pitt, F. D., & Barros, A. A. C. (2019). Purification of residual glycerol recovered from biodiesel production. *South African Journal of Chemical Engineering, 29*(1). https://doi.org/10.1016/j.sajce.2019.06.001

European Biodiesel Board (EBB). (2023a). *Joint Position on Energy Taxation Directive (ETD) Revision*. Retrieved from https://ebb-eu.org/wp-content/uploads/2023/05/EU-Biofuels-Chain-and-EBA-joint-position-on-ETD-revision.pdf

European Biodiesel Board (EBB). (2023a). *EBB Statistical Report 2023*. Retrieved from https://ebb-eu.org/wp-content/uploads/2024/03/EBB_Statistical_Report2023-Final.pdf

Frey, H., & Haag, R. (2002). Dendritic polyglycerol: A new versatile biocompatible material. *Reviews in Molecular Biotechnology, 90*(3–4), 257–267. https://doi.org/10.1016/S1389-0352(01)00063-0

Gabriel, K. C. P., Barros, A. A. C., & Correia, M. J. N. (2015). Study of molar ratio in biodiesel production from palm oil. *International Association for Management of Technology, IAMOT Conference*, Cape Town, South Africa, 434–442.

Gabriel, K., Santos, M. M., Adriano, J., Marques, J., Lemos, M., Muachia, A., & Barros, A. A. C. (2019). Anhydrous bio-ethanol produced from Elaeis Guineensis palm wine for use as a biodiesel feedstock. *South African Journal of Chemical Engineering, 29*(1), 10–16. https://doi.org/10.1016/j.sajce.2019.03.002

Garti, N., Aserin, A., & Zaidman, B. (1981). Polyglycerol ester: Optimization and techno-economic evaluation. *Journal of the American Oil Chemists' Society, 58*(9), 878–883. https://doi.org/10.1007/BF02672963

Gerpen, J. V. (2005). Biodiesel processing and production. *Fuel Processing Technology, 86*(10), 1097–1107. https://doi.org/10.1016/j.fuproc.2005.01.004

Goldbach, A., Meier, H. F., Wiggers, V., Chiarello, L. M., & Barros, A. A. C. (2022). Combustion performance of bio-gasoline produced by waste fish oil pyrolysis. *Chemical Industry and Chemical Engineering Quarterly, 28*, 1–8. https://doi.org/10.2298/CICEQ200810010G

Gupta, A., et al. (2023). Sustainable approaches for glycerol utilization in biodiesel production: Challenges and opportunities. *Energy Conversion and Management, 276*, 116543. https://doi.org/10.1016/j.enconman.2022.116543

Habaki, H., Hayashi, T., Sinthupinyo, P., & Egashira, R. (2019). Purification of glycerol from transesterification using activated carbon prepared from Jatropha shell for biodiesel production. *Journal of Environmental Chemical Engineering, 7*(5), 103303. https://doi.org/10.1016/j.jece.2019.103303

International Energy Agency (IEA). (2023a). *Biodiesel and renewable fuel production: By-product management*. Retrieved from [insert link if available].

International Energy Agency (IEA). (2023b). *The role of glycerol in renewable energy and sustainable industrial processes*. Retrieved from [insert link if available].

Jewur, S. S. (1984). Conversão catalítica do etanol. *Química Nova, 7*(2), 67–79. Retrieved from https://typeset.io/pdf/conversao-catalitica-do-etanol-23rxdpxqnb.pdf

Kalvelage, P. M. S., Albuquerque, A. A., Barros, A. A. C., & Bertoli, S. L. (2017). (Vapor + Liquid) Equilibrium for mixtures ethanol + biodiesel from soybean oil and frying oil. *International Journal of Thermodynamics, 20*, 159–164. https://doi.org/10.5541/eoguijt.337160

Kumar, L. R., Yellapu, S. K., Tyagi, R. D., & Zhang, X. (2019). A review on variation in crude glycerol composition, bio-valorisation of crude and purified glycerol as carbon source for lipid production. *Bioresource Technology, 293*, 122155. https://doi.org/10.1016/j.biortech.2019.122155

Kumar, S., et al. (2021). Sustainable polymers from renewable resources: Role of stoichiometric control in polymerization. *ACS Sustainable Chemistry & Engineering, 9*(4), 1785–1798. https://doi.org/10.1021/acssuschemeng.0c08567

Liu, Y., et al. (2023). Recent developments in glycerol-based polyesters for sustainable materials. *Polymer Engineering and Science, 63*(5), 836–844. https://doi.org/10.1002/pen.26245

Li, X., et al. (2022). Recent progress in glycerol-based polymers: Catalytic strategies and environmental benefits. *Polymer Reviews, 62*(3), 456–489. https://doi.org/10.1080/15583724.2021.1995172

Mota, C. J. A., Da Silva, C. X. A., & Gonçalves, V. L. C. (2009). Gliceroquímica: Novos produtos e processos a partir da glicerina de produção de biodiesel. *Química Nova, 32*(3), 639–648. https://doi.org/10.1590/S0100-40422009000300008

Mota, C. J. A., et al. (2017). Recent advancements in glycerol valorization for bio-based products. *Green Chemistry, 19*(2), 419–432. https://doi.org/10.1039/C6GC02384A

Nanda, M., Yuan, Z., Qin, W., Poirier, M. A., & Xu, C. (2014). Purification of crude glycerol using acidification: Effects of acid types and product characterization. *Austin Journal of Chemical Engineering, 1*(1), 1004. Retrieved from https://austinpublishinggroup.com/chemical-engineering/fulltext/ace-v1-id1004.php

Nasir, N. F., Mirus, M. F., & Ismail, M. (2017). Purification of crude glycerol from transesterification reaction of palm oil using direct method and multistep method. *IOP Conference Series: Materials Science and Engineering, 243*, 012015. https://doi.org/10.1088/1757-899X/243/1/012015

OECD/FAO. (2023a). *OECD-FAO Agricultural Outlook 2023-2032*. Retrieved from [insert link if available].

OECD/FAO. (2023b). *Global shift toward renewable feedstocks in the chemical industry*. Retrieved from [insert link if available].

Oliveira, C. F., et al. (2020). Technological innovations for glycerol purification and applications in the biodiesel industry. *Chemical Engineering Journal, 391*, 123456. https://doi.org/10.1016/j.cej.2020.123456

Pitt, F. D., Boing, D., & Barros, A. A. C. (2011). Desenvolvimento histórico, científico e tecnológico de polímeros sintéticos e de fontes renováveis. *Revista da Unifebe, 9*(18). Retrieved from https://periodicos.unifebe.edu.br/index.php/RevistaUnifebe/article/view/47/38

Quispe, C. A. G., Coronado, C. J. R., & Carvalho, J. A. (2013). Glycerol: Production, consumption, prices, characterization, and new trends in combustion. *Renewable and Sustainable Energy Reviews, 27*, 475–493. https://doi.org/10.1016/j.rser.2013.06.017

Raman, A. A. A., Tan, H. W., & Buthiyappan, A. (2019). Two-step purification of glycerol as a value-added byproduct from the biodiesel production process. *Frontiers in Chemistry, 7*, 1–9. https://doi.org/10.3389/fchem.2019.00774

Rahman, M. M., et al. (2022). Recent trends in glycerol purification and utilization: A comprehensive review. *Renewable and Sustainable Energy Reviews, 156*, 111987. https://doi.org/10.1016/j.rser.2021.111987

Rahmanulloh, A., & Osinski, J. (2023). *Biofuels Annual*. United States Department of Agriculture (USDA), Foreign Agriculture Service. Public Distribution, September 2023. ID2023-0018. Jakarta, Indonesia.

Santos, R. G., et al. (2021). Advances in glycerol purification techniques for enhanced biodiesel production efficiency. *Fuel Processing Technology, 213*, 106678. https://doi.org/10.1016/j.fuproc.2020.106678

Silva, J. M., et al. (2021). Valorization of crude glycerol from biodiesel production: A review of recent advances. *Journal of Environmental Management, 280*, 111769. https://doi.org/10.1016/j.jenvman.2020.111769

Silva, R., et al. (2020). Optimization of glycerol polymerization for sustainable polymer

production. *Journal of Cleaner Production, 260*, 121045. https://doi.org/10.1016/j.jclepro.2020.121045

Silva, A. L., Santos, A. P., Silveira, M. B., Gonçalves, A. D. S., & Barros, A. A. C. (2025). Barriers to implementing reverse logistics in companies: A systematic literature review. *Study in Multidisciplinary Reviewer*, *6*(1), 1–22. DOI: 10.55034/smrv6n1-004.

Shinde, S. S., et al. (2021). Advancements in catalysts for ethanol dehydration: A review. *Industrial & Engineering Chemistry Research, 60*(8), 3382–3400. https://doi.org/10.1021/acs.iecr.0c06234

Tomatis, M., Zilli, M., & Pavan, F. (2024). Environmental and economic impacts of glycerol oversupply from biodiesel production. *Journal of Cleaner Production, 450*, 139876. https://doi.org/10.1016/j.jclepro.2023.139876

Virt, M., & Arnold, U. (2022). Effects of oxymethylene ether in a commercial diesel engine. *Cognitive Sustainability, 1*(3). https://doi.org/10.55343/cogsust.20

Wang, H., et al. (2023). Kinetic and mechanistic insights into glycerol polymerization for biodegradable polymers. *Chemical Engineering Journal, 451*, 138752. https://doi.org/10.1016/j.cej.2022.138752

Wolfson, A., Litvak, G., Dlugy, C., Shotland, Y., & Tavor, D. (2009). Employing crude glycerol from biodiesel production as an alternative green reaction medium. *Industrial Crops and Products, 30*(1), 78–81. https://doi.org/10.1016/j.indcrop.2009.02.003

Wu, D., et al. (2020). Green synthesis of polyglycerol and its potential applications. *Green Chemistry, 22*(11), 3451–3460. https://doi.org/10.1039/D0GC00987A

Wu, Z., et al. (2022). Functionalized biopolymers for advanced applications in biocompatible and biodegradable materials. *Biomacromolecules, 23*(4), 1234–1245. https://doi.org/10.1021/acs.biomac.1c01456

Zhang, L., et al. (2020). Renewable alcohols as feedstocks for bio-based chemicals and fuels: A review of ethanol, butanol, and other alcohol-based catalysts. *Renewable and Sustainable Energy Reviews, 130*, 1099–1115. https://doi.org/10.1016/j.rser.2020.109915

Zhang, S., et al. (2023). Optimization of glycerol polymerization with green catalysts for sustainable production. *Sustainable Chemistry & Engineering, 11*(4), 543–552. https://doi.org/10.1021/acssuschemeng.2c06345

Zhang, Y., et al. (2018). Advances in glycerol-based polymers: Synthesis and applications. *Green Chemistry*, *20*(5), 1023–1035. https://doi.org/10.1039/C7GC03502A

Yang, X., et al. (2012). Explores glycerol as a feedstock for bio-based chemicals and polymers. *[Journal/Book Title]*, *[Volume]*(Issue), [Page Range]. [DOI/Publisher].

Zeleme, A. K., & Barros, A. A. C. (2022). Biodiesel production using reactive distillation column based on intensification processes. In T. Ohyama (Ed.), *Soybean – Recent Advances in Research and Applications* (Chapter 13). IntechOpen. DOI: 10.5772/intechopen.101928

Zöldy, M., & Baranyi, P. (2023). The cognitive mobility concept. *Infocommunications Journal*, *15*(SP), 35–40. DOI: 10.36244/ICJ.2023.SI-IODCR.6

Zoldy, M., Csete, M. S., Kolozsi, P. P., Bordas, P., & Torok, A. (2022). Cognitive sustainability. *Cognitive Sustainability*, *1*(1). DOI: 10.55343/cogsust.7